DEVELOPMENT OF REPORTER GENES FOR *IN VIVO* IMAGING OF *Staphylococcus aureus*

ROCHELLE MARIE LAMB, BSc.

Thesis submitted to the University of Nottingham for the degree of Master of Philosophy

JUNE 2010

ABSTRACT

S. aureus is an opportunistic pathogen with an extensive host range, and is the etiologic agent of a wide variety of human diseases, with the ability to promote disease in most human tissues. A repertoire of virulence factors expressed during colonization and infection all contribute to the success of *S. aureus* as a pathogen. *S. aureus* is not classically considered as an intracellular pathogen, yet accumulating scientific evidence has demonstrated that this organism has intracellular survival strategies, with the ability to become internalised by, and persist within, a wide range of non-professional eukaryotic phagocytes. This phenomenon has been shown to be linked to the expression of genes under the regulation of the *S. aureus* quorum sensing system, *agr*. Specifically, *S. aureus* has been shown to breach the host-membrane bound endosome within which it is situated upon internalisation, a process which has been hypothesised to rely upon a switch in gene expression due to the accumulation of the *agr* signalling peptide within the endosome.

Many *in vitro* imaging modalities have been designed to investigate further the mechanisms behind *S. aureus* internalisation. However, *in vivo* systems such as bioluminescence and fluorescence reporter genes are limited by various factors including light extinction, restricting investigations to those using small animals. Additionally, as fundamentally two-dimensional modalities, useful anatomical information is minimal in these imaging techniques. At present few imaging modalities exist which enable

the non-invasive *in vivo* detection of bacterial reporter gene expression while offering detailed anatomical information. This study aimed to address the need to develop reporter systems for the non-invasive *in vivo* tracking systems for the monitoring of infectious disease processes, in the context of using such a technology to investigate further the genes involved in the process of *S. aureus* internalisation, and more specifically, endosomal escape.

Although it is clear that *agr* regulated genes have a role in endosomal escape of internalised *S. aureus*, it is not fully clear which genes specifically are important. A number of haemolysin genes are under the control of the *agr* system, all of which have the ability to disrupt eukaryotic cell membranes. A β-haemolysin mutant was constructed in this study to use in conjunction with existing α-, δ- and γ-haemolysin mutants in *in vitro* internalisation assays. Initial experiments indicated a role for α-haemolysin in the endosomal escape of internalised *S. aureus*. The use of an *in vivo* reporter gene system would allow for further analysis of the role of haemolysins in endosomal escape, in addition to providing detailed anatomical information.

MRI bacterioferritin (BFR) reporter genes with inducible or constitutive promoters, the *bfr* gene and the *lux* operon, were constructed and evaluated in *S. aureus*. The reporter gene was shown to be translated *in vitro*, with the expression of functional BFR which collected iron. However, ICP-MS data revealed relatively low levels of BFR. Pilot *in vivo* studies

were carried out to confirm the potential of the reporter gene for studying specific aspects of staphylococcal disease. Experiments tracking bioluminescence in a mouse tumour model demonstrated expression of the MRI reporter genes, suggesting that bacterioferritin should be successfully synthesised *in vivo*. However, due to plasmid instability *in vivo* and the relatively low levels of iron present in *S. aureus* samples as determined by ICP-MS, the tumours in this study were not scanned by MRI.

ACKNOWLEDGEMENTS

I would like to thank Rasmus Jensen, Dr. Saara Qazi and Dr. Alan Cockayne for their help and support in and out of the lab. Dr. Phil Hill for his unwavering support, positivity and kindness, in addition to his supervision and input. Prof. Paul Williams for his supervision and input. My friends and family for their continuing support and advice. The University of Nottingham and the MRC for funding.

LIST OF CONTENTS

LIST OF ABBREVIATIONS

BFR	bacterioferritin
GFP	green fluorescent protein
RFP	red fluorescent proteins
PET	positron emission tomography
SPECT	single photon emission computed tomography
MRI	magnetic resonance imaging
RF pulse	radiofrequency electromagnetic pulse
MDM	magnetic dipole moment
SPIONs	superparamagnetic iron-oxide nanoparticles
MRSA	methicillin-resistant *Staphylococcus aureus*
CA-MRSA	community-acquired methicillin-resistant *Staphylococcus aureus*
VRSA	vancomycin-resistant *Staphylococcus aureus*
agr	accessory gene regulator
AIP	autoinducing peptide
LB	Luria-Bertani
BHI	Brain Heart Infusion
TSB	Tryptic Soy Broth
DMEM	Dulbecco modified Eagle medium
PCR	polymerase chain reaction
PBS	phosphate buffered saline
OD_X	optical density at Xnm
Amp^R	ampicillin resistant

Cm^R	chloramphenicol resistant
Km^R	kanamycin resistant
Erm^R	erythromycin resistant
UV	ultraviolet
ddH_2O	double distilled water
bp	base pairs
ECL	enhanced chemiluminescence
ICP-MS	inductively coupled plasma mass spectrometry
MALDI-MS	matrix-assisted laser desorption/ionization mass spectrometry
RBS	ribosome binding site

LIST OF TABLES

LIST OF FIGURES

FIGURE 3.2: Bioluminescence as relative light units (RLU) divided by optical density (OD) of *S. aureus* RN6390 pUNK1 Sa P_{S10}-dual-term (●), pUNK1 Bs P_{S10}-dual-term (●) and pUNK1 P_{xylA}-dual-term (●). This data relates to the left y axis. Absorbance of *S. aureus* RN6390 pUNK1 Sa P_{S10}-dual-term (▲), pUNK1 Bs P_{S10}-dual-term (▲) and pUNK1 P_{xylA}-dual-term (▲) is also shown. This data relates to the right y axis. Results represent the mean value of 3 data points for each reading.

FIGURE 3.3: pUNK1 P_{S10}-bfr-luxterm.

FIGURE 3.4: Bioluminescence measured from growth of *S. aureus* pUNK P_3-bfr-luxterm in the presence of varying concentrations of promoter inducer (AIP) and inhibitor ((Ala^5)AIP-1). Results represent single readings.

FIGURE 3.5: Bioluminescence measured from growth of *S. aureus* pUNK P_{ahpC}-bfr-luxterm in the presence of varying concentrations of NaCl (M). Results represent single readings.

FIGURE 3.6: SDS-PAGE gel of *S. aureus* harbouring expression vectors pUNK1 P_{S10}-bfr-luxterm, pUNK1 P_{ahpC}-bfr-luxterm and pUNK1 P_3-bfr-luxterm. Cultures were grown with supplements of promoter inducers and inhibitors where appropriate. Red arrows indicate the suspected BFR protein, and black arrows indicate a lack of this band in the specified samples.

FIGURE 3.7: Western blot of *S. aureus* pUNK1 P_{S10}-bfr-luxterm and *S. aureus* pUNK1 P_3-bfr-luxterm treated with anti-BFR antibody. Positive control (+) *E. coli* pUNK1 P_{xylA}-dual-term, negative control (-) *S. aureus* RN6390. Figure shows **(A)** ponceau stain after blotting and **(B)** western developed for 800 seconds. Arrows indicate bands representing the BFR protein.

FIGURE 3.8: SDS-PAGE gel of *S. aureus* pUNK1 P_{S10}-bfr-luxterm and *S. aureus* pUNK1 P_3-bfr-luxterm indicating bands sent for sequencing within the red boxes.

FIGURE 3.9: Sequencing results represented as a Probability Based Mowse Score where the protein score is -10*Log(P), where P is the probability that the observed match is a random event. Protein scores greater than 81 are significant ($p<0.05$). **(A)** Results for band excised from SDS-PAGE gel of *S. aureus* pUNK1 P_3-bfr-luxterm sample and **(B)** results for band excised from SDS-PAGE gel of *S. aureus* pUNK1 P_{S10}-bfr-luxterm sample.

FIGURE 3.10: pUNK1 P_{S10}-bfd/bfr-luxterm.

FIGURE 3.11: Pellets from the centrifugation of 1ml culture of *E. coli* harbouring **(A)** pUNK1 P_{S10}-dual-term, **(B)** pUNK1 P_{S10}-bfd-luxterm, **(C)** pUNK1 P_{S10}-bfr-luxterm and **(D)** pUNK1 P_{S10}-bfd/bfr-luxterm.

FIGURE 4.8: Agarose gel electrophoresis showing PCR products from PCR of genomic DNA from *S. aureus* RN6390 and a putative *S. aureus* RN6390 *hlb* mutant, and pTS1-Dest *hlb* plasmid DNA, using primers specific for the regions outside of the regions used to construct the pTS1-Dest *hlb* plasmid and primers specific for regions outside of the *hlb* gene which were used to construct the pTS1-Dest *hlb* plasmid.

FIGURE 4.9: Schematic diagram showing the annealing sites for the hlb up F' and ery R' primers, of *S, aureus* RN6390, pTS1-Dest *hlb* and a Δ*hlb*. The black line represents the *S. aureus* RN6390 genome and the blue line represents the pTS1-Dest *hlb* backbone. Primers in grey text would not yield product due to lack of an annealing site.

FIGURE 4.10: Schematic diagram showing the annealing sites for the ery F' and hlb down R' primers, of *S, aureus* RN6390, pTS1-Dest *hlb* and a Δ*hlb*. The black line represents the *S. aureus* RN6390 genome and the blue line represents the pTS1-Dest *hlb* backbone. Primers in grey text would not yield product due to lack of an annealing site.

FIGURE 4.11: Agarose gel electrophoresis showing PCR products from PCR of genomic DNA from *S. aureus* RN6390 and a putative *S. aureus* RN6390 *hlb* mutant, and pTS1-Dest *hlb* plasmid DNA, using primers specific for the *erm* cassette and primers specific for regions outside of the *hlb* gene which were used to construct the pTS1-Dest *hlb* plasmid.

FIGURE 4.12: Schematic diagram showing the annealing sites for the hlb up F' and pTS1 R' primers, of *S, aureus* RN6390, pTS1-Dest *hlb* and a ∆*hlb*. The black line represents the *S. aureus* RN6390 genome and the blue line represents the pTS1-Dest *hlb* backbone. Primers in grey text would not yield product due to lack of an annealing site.

FIGURE 4.13: Schematic diagram showing the annealing sites for the pTS1 up F' and hlb down R' primers, of *S, aureus* RN6390, pTS1-Dest *hlb* and a ∆*hlb*. The black line represents the *S. aureus* RN6390 genome and the blue line represents the pTS1-Dest *hlb* backbone. Primers in grey text would not yield product due to lack of an annealing site.

FIGURE 4.14: Agarose gel electrophoresis showing PCR products from PCR of genomic DNA from *S. aureus* RN6390 and a putative *S. aureus* RN6390 *hlb* mutant, and pTS1-Dest *hlb* plasmid DNA, using primers specific for the backbone of the pTS1-Dest *hlb* cassette and primers specific for regions outside of the *hlb* gene which were used to construct the pTS1-Dest *hlb* plasmid.

FIGURE 4.15: Schematic diagram showing the annealing sites for the hlb outside up F' and hlb outside down R' primers, of *S. aureus* RN6390, pTS1-Dest *hlb* and a ∆*hlb* with excised *erm* cassette. The black line represents the *S. aureus* RN6390 genome and the blue line represents the pTS1-Dest *hlb* backbone. Primers in grey text would not yield product due to lack of an annealing site.

FIGURE 4.16: Schematic diagram showing the annealing sites for the hlb up F' and ery R' primers, of *S. aureus* RN6390, pTS1-Dest *hlb* and a ∆*hlb* with excised *erm* cassette. The black line represents the *S. aureus* RN6390 genome and the blue line represents the pTS1-Dest *hlb* backbone. Primers in grey text would not yield product due to lack of an annealing site.

FIGURE 4.17: Agarose gel electrophoresis showing PCR products from PCR of genomic DNA from *S. aureus* RN6390 and the *S. aureus* RN6390 *hlb* mutant, and pTS1-Dest *hlb* plasmid DNA, using primers specific for regions outside of the regions used to construct the pTS1-Dest *hlb* plasmid and primers specific for regions outside of the *hlb* gene which were used to construct the pTS1-Dest *hlb* plasmid.

FIGURE 4.18: Schematic diagram showing the annealing sites for the ery F' and hlb down R' primers, of *S. aureus* RN6390, pTS1-Dest *hlb* and a ∆*hlb* with excised *erm* cassette. The black line represents the *S. aureus* RN6390 genome and the blue line represents the pTS1-Dest *hlb* backbone. Primers in grey text would not yield product due to lack of an annealing site.

FIGURE 4.19: Schematic diagram showing the annealing sites for the hlb up F' and hlb down R' primers, of *S. aureus* RN6390, pTS1-Dest *hlb* and a ∆*hlb* with excised *erm* cassette. The black line represents the *S. aureus* RN6390 genome and the blue line represents the pTS1-Dest *hlb*

backbone. Primers in grey text would not yield product due to lack of an annealing site.

FIGURE 4.20: Agarose gel electrophoresis showing PCR products from PCR of genomic DNA from *S. aureus* RN6390 and the *S. aureus* RN6390 *hlb* mutant, and pTS1-Dest *hlb* plasmid DNA, using primers specific for regions outside of the *hlb* gene which were used to construct the pTS1-Dest *hlb* plasmid and primers specific for the *erm* cassette.

FIGURE 4.21: Cell Invasion Assay

Bioluminescence as relative light units (RLU) divided by optical density (OD) of *S. aureus* RN6390 harbouring pSB2030 *S. aureus* RN6390 harbouring pSB2035. For comparison, different scales are used to represent data relating to growth (left y axis) and *agr* expression (right y axis) to compensate for variations in promoter strength. Results represent the mean value of 6 data points for each reading.

FIGURE 4.22: Cell Invasion Assay

Fluorescence normalised for growth of *S. aureus* RN6390 and *S. aureus* RN6390 Δ*hla*, both harbouring pMK4 P_{xylA}-gfp-term Results represent the mean value of 3 data points for each reading.

FIGURE 5.1: Photos overlaid with luminescence images of mice inoculated with *S. aureus* harbouring pUNK1 P_{S10}-dual-term. Images show

luminescence 1, 2 and 3 days post-inoculation. Order of mice does not remain the same for each picture.

FIGURE 5.2: Photos overlaid with luminescence images of mice inoculated with *S. aureus* harbouring pUNK1 P_{S10}-bfr-luxterm. Images show luminescence 2 and 3 days post-inoculation. Order of mice does not remain the same for each picture.

FIGURE 5.3: Photos overlaid with luminescence images of mice inoculated with *S. aureus* harbouring pUNK1 P_3-bfr-luxterm. Images show luminescence 1 day post-inoculation.

FIGURE 5.4: Viable cell counts from the livers, spleens and tumours of one mouse from each test group. Mice were inoculated with *S. aureus* pUNK1 P_{S10}-dual-term (1 on the graph), *S. aureus* pUNK1 P_{S10}-bfr-luxterm (2 on the graph) or *S. aureus* pUNK1 P_3-bfr-luxterm (3 on the graph).

FIGURE 5.5: Confocal microscopy showing colonisation of a tumour removed from a mouse inoculated with *S. aureus* pUNK1 P_{S10}-bfr-luxterm. Actin was stained red to visualise tumours and *S. aureus* was labelled using FITC (A2, B2, C2 and D2). Images were then overlaid (A1, B1, C1 and D1). Labelled *S. aureus* can be seen with (A2) and without (B2) background correction. C1 shows the same tumour as in A1 and B1, but without anti-Protein A antibody. D1 shows a tumour from a mouse with no *S. aureus* inoculation.

FIGURE 6.1: Diagram showing a potential stem loop in the mRNA sequence of the intergenic region between the *bfd* and *bfr* genes. The red highlights the RBS of the *bfr* gene and the blue highlights the end of the *bfd* gene.

1.0: INTRODUCTION

1.1: Non-Invasive *in vivo* Molecular Imaging

The use of animal models to monitor microbial pathogenesis is fundamental to the investigation of host-pathogen interactions during disease processes. Conventional methods necessitated the euthanisation of experimental animals at various time points for analysis of colonisation sites and microbial quantities (Hutchens, M. and Luker, G.D., 2007). Our understanding of infectious diseases has been greatly facilitated by such methods, but more recently, a range of non-invasive *in vivo* molecular imaging techniques have been developed, which can be described as having a direct or indirect strategy. Direct imaging involves use of probe-target interactions to analyse endogenous genes and molecules via interactions with target epitopes or enzymes. Indirect imaging strategies are much more complex. One example of indirect imaging that is becoming increasingly popular is reporter gene imaging. This typically involves a reporter gene, a reporter probe and imaging systems capable of visualising the probe (Blasberg, 2002; Serganova *et al.*, 2006).

Such novel non-invasive *in vivo* molecular imaging techniques can be used to achieve the temporal monitoring of both eukaryotic gene expression, and also microbial disease progression, offering functional information regarding microbial gene expression. Broadly speaking, these

techniques can be categorised as optical imaging, nuclear imaging and magnetic resonance imaging modalities (Serganova *et al*., 2006).

1.1.1: Non-Invasive Optical *in vivo* Imaging

Optical imaging uses bioluminescence and fluorescence to monitor molecular and biological processes. This can be achieved through the use of endogenous reporters, for example genetically modified target cells or recombinant bacteria transformed with bioluminescent or fluorescent reporter genes, or through use of exogenous probes which can target specific cell types (Hickson, 2009). This imaging technique is implemented widely in *in vitro* studies, including those analysing bacterial infection processes, due to its safety, low cost and ease of use relative to other imaging modalities (Leevy *et al*., 2007). However, optical imaging has also been implemented to some extent in *in vivo* investigations.

1.1.1.1: Fluorescence

Fluorescence is created when emission of a photon is triggered by the molecular absorption of another photon at a shorter wavelength (Leevy *et al*., 2007). Fluorescence reporters have been successfully implemented in various *in vivo* studies, for example in the imaging of *E. coli* expressing green fluorescent protein (GFP) in the gastrointestinal tract of mice (Zhao *et al*., 2001). However, their use *in vivo* is limited for a number of reasons. Firstly, the light produced from fluorescent reporter genes is attenuated and scattered by surrounding tissues *in vivo*. This problem is further exacerbated by the endogenous autofluorescence of tissues creating

significant background emission. However, the latter issue has been somewhat improved by the development of a variety of GFP mutants which emit photons at all colours in the visible spectrum (Leevy *et al*., 2007). Of particular importance are red fluorescent proteins (RFP), which avoid much of the autofluorescence problems, and also penetrate tissues more effectively, making them useful in the imaging of larger animals. Recently, this characteristic of RFP has been exploited in the development of infrared fluorescent proteins (Shu *et al*., 2009).

1.1.1.2: Bioluminescence

Bioluminescence is created by the generation of visible light by the enzymatic action of luciferases causing oxidation of luciferin substrates (Serganova *et al*., 2006). In this way, light intensity can be directly related to the amount of luciferase, and subsequently, the gene of interest within the reporter gene system, being expressed. Unlike fluorescence, background tissue emission of light is very low, minimising any effects on the specificity and sensitivity of this technique. Due to such advantages, bioluminescence has been implemented in a variety of studies. Using a novel modified operon, Francis *et al*. (2000) were able to tag *Staphylococcus aureus* strains with bioluminescence reporter genes, allowing the assessment of antibiotic efficacy *in vivo*. Bioluminescence reporter systems have also been employed to determine the colonization dynamics of *Citrobacter rodentium* in mice (Wiles *et al*., 2004) and the replication of *Listeria monocytogenes* within murine gall bladders (Hardy *et al*., 2004).

However, despite the benefits of low cost, high throughput and the functional data that this optical imaging modality facilitates, various limitations exist which minimise the scope of its use. As with fluorescence, light extinction is unavoidable, with bioluminescence being decreased by as much as 10 fold per cm depth, due to penetration of overlying tissues, organ pigmentation, fur and scattering of light, thus limiting the technique to use in small animals. Importantly, as a fundamentally two-dimensional modality, useful anatomical information is minimal, with difficulties separating light output from closely located anatomical locations, and resolution limitations.

1.1.2: Non-Invasive Nuclear *in vivo* Imaging

Various successful non-invasive nuclear *in vivo* imaging systems exist with the potential for use in bacterial disease tracking. Single photon emission computed tomography (SPECT) has been implemented in the imaging of bacterial infections in mice via detection of a radiolabelled thymidine kinase substrate (Bettegowda *et al*., 2005). Positron emission tomography (PET) is used extensively in the clinic as a non-invasive imaging modality, with much importance in the staging of cancer. This technology has been successfully used to image the endogenous expression of reporter genes thanks to the development of complimentary radiolabelled probes and micro-PET scanners for use with small animals (Blasberg, 2002; Herschman, 2003). However, despite the relatively high sensitivity of nuclear imaging methods, resolution limitations restrict the detail of the anatomical information yielded from such a technique, and so reduce its

suitability as a candidate for a bacterial tracking imaging modality (Blasberg, 2002; Ray *et al*., 2004; Cohen *et al*., 2007).

1.1.3: Non-Invasive Magnetic Resonance *in vivo* Imaging

1.1.3.1: Magnetic Resonance Imaging

The following information was assembled with reference to an online MRI tutorial package (www.mri-tutorial.com).

Magnetic resonance imaging (MRI) is an imaging modality that measures the response of hydrogen molecules to a perturbation in a magnetic field. The body is composed largely of water molecules, each of which contains two hydrogen atoms and one oxygen atom. All nuclei that are electrically charged demonstrate a phenomenon called spin, in that they spin around their axis, and as such hydrogen nuclei demonstrate spin. This movement of the nuclei creates a magnetic field which can be measure like a mathematical vector, with an amplitude and a direction, and is referred to as the magnetic dipole moment (MDM).

Simply speaking, an MRI scanner consists of a large magnet which creates a very stable and powerful magnetic field, the direction of which is termed the z axis. When a subject is inside an MRI scanner, the MDM of the hydrogen nuclei align in the direction of the magnetic field, along the z axis. The nuclei also begin to precess, whereby there is a change in the direction of the axis around which the spin is occurring. Once the subject

is inside the MRI scanner, a radiofrequency electromagnetic pulse (RF pulse) is applied perpendicular to the z axis. This causes the MDM of the nuclei to 'tip' in the direction of the x-y plane, altering their alignment relative to the z axis (Figure 1.1).

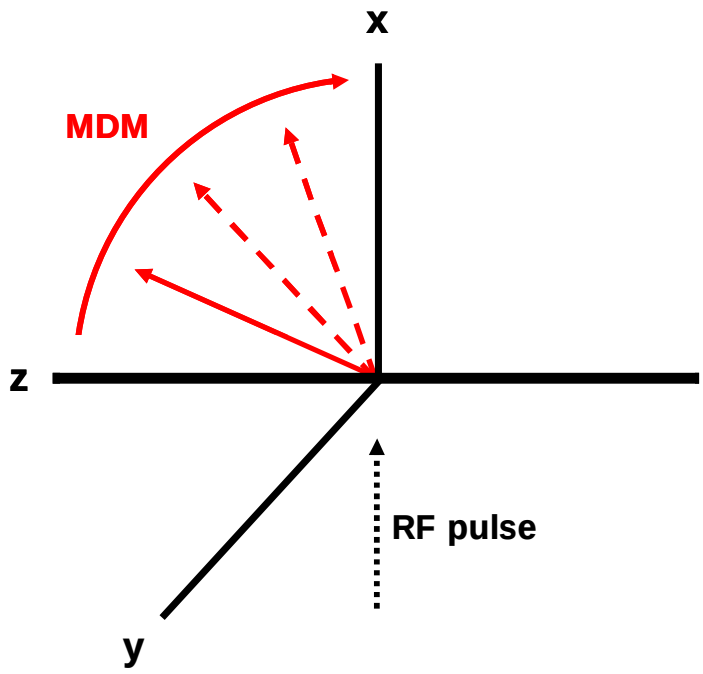

FIGURE 1.1: Diagram adapted from www.mri-tutorial.com depicting the z axis, x-y plane and direction of tip of MDM upon application of the RF pulse.

This 'tipping' generated by the RF pulse increases the energy state of the nuclei. As the MDM of the nuclei return to their original orientation, this energy is released. This process is termed relaxation, the rate of which is the parameter which is measured in MRI.

Relaxation rates can be measured as either T1 or T2 relaxation rates. Before the RF pulse is applied, the MDM amplitude is maximal in the z axis, whereas after the RF pulse has been applied, it is maximal in the x-y plane, due to 'tipping'. During relaxation, therefore, two parameters can be measured; the re-growth of the amplitude along the z axis, or the T1 relaxation rate, and the decay of amplitude in the x-y plane, or the T2 relaxation rate. Nuclei within different tissues have different T1 and T2 relaxation rates, providing the contrast on MR images which allows for the detailed anatomical information yielded from this imaging technique.

1.1.3.2: Contrast

As described above, MRI contrast is created due to differing relaxation rates within different body tissues causing varying signal strengths to be detected. These varying signal strengths are due to the fact that at any given moment after an RF pulse has been applied, nuclei within different tissues are at different stages of relaxation, with varying levels of MDM amplitude in the z axis and x-y plane.

To achieve maximal contrast between different tissues, the RF pulse sequence can be altered to allow one of these contrast mechanisms to be emphasized. T1 weighted signals are achieved when differences between MDM amplitudes in the z axis are maximised, whereas T2 weighted signals are achieved when differences between MDM amplitudes in the x-y plane are maximised. To augment contrast between different tissues

further, contrast agents, typically chosen for their magnetic properties, can be administered.

1.1.3.3: Magnetic Resonance Imaging as a Tool for Non-Invasive *in vivo* Imaging

MRI is widely used as a clinical diagnostic tool due to its non-invasive nature and high quality three-dimensional spatial resolution, generating detailed anatomical information. These factors have made MRI an exciting prospect in the non-invasive imaging of *in vivo* gene expression, through the use of MRI reporter genes that can modulate MRI contrast. This has been achieved in a number of ways using various MRI gene expression strategies.

Firstly, the use of metal-complexed MRI agents which are chemically modified by the enzymatic activity of beta-galactosidase has been documented (Louie *et al*., 2000). The need for exogenous administration of the contrast material, however, creates issues with barriers to delivery and clearance of the agent (Cohen *et al*., 2005). More recently, endogenous reporters have been developed to overcome this problem, including chemical-exchange saturation transfer (CEST) agents. Nuclei can maintain their magnetic orientation through chemical reactions. If RF radiation was applied to an agent proton, it would raise to a higher energy state, which causes the nuclei to convert to a different chemical state. This energy is then transferred to water by the exchange of protons, thus affecting the amplitude of the MR signal (Ward *et al*., 2000). The MRI

contrast achieved in this case can be switched on and off (Gilad *et al*., 2007). A recent advance describes the use of naturally occurring proteins found in magnetotactic bacteria. Specifically, the use of *magA*, a gene involved in iron sequestration within magnetotatic bacteria, as an MRI reporter has been shown to achieve MRI contrast due to the *in vivo* synthesis of magnetic iron-oxide nanoparticles (Zurkiya *et al*., 2008). These so called magnetosome proteins affect the MRI signal in a similar way to superparamagnetic iron-oxide nanoparticles (SPIONs). SPIONs are particles of iron oxide with superparamagnetic properties, causing them to acquire large magnetic moments when placed in an external magnetic field. However, the relatively large size of these particles creates issues with fast clearance (Ma *et al*., 2006). Additionally, the need for delivery of the contrast agent creates further complications. Finally, proteins involved in iron homeostasis have also been used, for example, ferritins, which are described in detail in the next section.

These recent advances in the use of MRI in gene expression analysis have made it an exciting candidate for the development of a technology that enables the non-invasive *in vivo* detection of bacterial reporter gene expression while offering detailed anatomical information. Few imaging modalities exist which can offer such prospects. As such, bacterial MRI reporter genes would be a valuable tool in the future discovery of key aspects of microbial pathogenesis. Of further importance regarding the development of such a reporter gene system is the prospect of a reduction

in the number of experimental animals used in studies due to the potential for the temporal analysis of the same individual subject (Lyons, 2005).

1.2: Bacterioferritin as an MRI Reporter

1.2.1: Ferritins

Ferritins comprise a superfamily of ubiquitous iron-storage proteins which are highly conserved throughout most organisms including animals, plants and bacteria (Andrews *et al*., 1992). The role of ferritins is the storage of iron in its non-toxic form, Fe^{3+}, which is oxidised from Fe^{2+} at ferroxidase centres within the ferritin molecule. They are also involved in protection from free radical synthesis by sequestering iron within a central cavity (Harrison *et al*., 1996).

Ferritins synthesised by different organisms share a similar structure, forming endogenous nanoparticles assembled from a 24 protein subunit shell that encloses an iron-oxide core capable of storing up to 4500 iron atoms in the form of crystalline ferrihydrite (Carrondo, 2003). Three types of ferritin have been discovered in bacteria, including the haem containing bacterioferritins (BFR), for example BFR from *Escherichia coli*. The haem within bacterioferritins is situated between pairs of the 24 monomers which associate as dimers (Carrondo, 2003). Two haem-free ferritins also exist; an archetypal ferritin, for example *ftn*, and a structurally different, dodecameric, Dps-like ferritin, for example that of *Listeria innocua* (Ilari *et*

al., 2000; Chiancone *et al*., 2004). *S. aureus* has various genes involved in the global regulation of intracellular iron concentrations, including those that encode for the Fur, PerR and Zur proteins. In addition, *S. aureus* also has genes which encode a number of iron storage proteins; *ftnA* which encodes for a ferritin, Ftn, and *mrgA* which encodes for a ferritin-like Dps homologue, MrgA (Horsburgh *et al*., 2001).

1.2.2: The use of Ferritins as MRI Reporters *in vivo*

The ferrihydrite core of ferritins confers superparamagnetic properties which affect the T1 and T2 relaxation rates of water (Vymazal *et al*., 1998). This results in the darkening of T_2-weighted MRI causing contrast that is easily imaged (Gossuin *et al*., 2004). Consequently, ferritins are ideal candidates for the development of endogenous MRI reporters, eliminating the need for delivery of the contrast agent, and have been used as such in various studies employing human ferritins as MRI reporters in eukaryotic cells. Genove *et al*. (2005) demonstrated imaging of virus-transduced mouse neurons and glia *in vivo* in a time-lapse fashion over several weeks. Imaging of gene expression in C6 glioma tumours and transgenic mice has also been achieved (Cohen *et al*., 2005; Cohen *et al*., 2007).

The use of such MRI reporter genes that can modulate MRI contrast are of great scientific value in the development of a non-invasive *in vivo* tracking system for microbial disease, as the additional anatomical information yielded by MRI in conjunction with the functional data related to gene expression would confer numerous advantages to this imaging modality in

the monitoring of infectious disease processes. Recently, this has been achieved by use of an *E. coli* bacterioferritin reporter system which allowed the imaging of tumour colonisation by *E. coli*. This tumour targeting behaviour demonstrates not only an exciting use for MRI reporters in the therapeutic monitoring of cancer treatments but also an ideal platform upon which to develop the use of MRI reporters in bacterial disease processes (Hill *et al*., manuscript in preparation).

1.3: *Staphylococcus aureus*

1.3.1: Background

Staphylococcus aureus, of the Micrococcaceae family, is a spherical, Gram-positive bacterium which grows in grape-like clusters. Species of the genus *Staphylococcus* are ubiquitous commensals of humans, and furthermore, *S. aureus* is found naturally inhabiting the skin and mucous membranes of a high proportion of healthy humans. In fact, approximately 20% of the population is estimated to be persistently colonized with *S. aureus*, and 60% of the population are intermittent carriers (Kluytmans *et al.*, 1997).

S. aureus is an opportunistic pathogen with an extensive host range, and is the etiologic agent of a wide variety of human diseases, with the ability to promote disease in most human tissues. A repertoire of virulence factors expressed during colonization and infection, including cell wall

components, toxins and enzymes, all contribute to the success of *S. aureus* as a pathogen. Infections associated with *S. aureus* include superficial skin infections and more serious diseases such as toxic shock syndrome and endocarditis. It is also often associated with long-term and persistent infections, frequently recurring after seemingly successful treatment (Alexander and Hudson, 2001).

The threat posed by this persistent organism is further augmented by its ability to develop antimicrobial resistance. The prevalence of antibiotic resistant strains of *S. aureus* has increased with the introduction of novel therapies, resulting in the development of methicillin-resistant *Staphylococcus aureus* (MRSA). Methicillin was introduced in 1961 in an attempt to control strains of *S. aureus* already possessing genes encoding resistance to many β-lactam antibiotics (Schito, 2006). Nonetheless, resistance to methicillin was documented soon after its introduction (Hiramatsu *et al.*, 2001). This resistance results from the action of an acquired penicillin-binding protein, PBP2a, which is encoded by a gene of nonstaphylococcal origin, the *mecA* gene (de Jonge and Tomasz, 1993; Berger-Bachi and Rohrer, 2002).

A major concern regarding MRSA is the discovery of its involvement in a number of infections in non-healthcare settings (Schito, 2006). Such infections are referred to as community-acquired (CA) MRSA infections, which occur in healthy community-dwelling individuals with no established risk factors for MRSA acquisition (Maltezou and Giamarellou, 2006).

The current line of therapy relied upon for the treatment of MRSA is the use of glycopeptides, commonly vancomycin. However, fully vancomycin-resistant *S. aureus* (VRSA) strains have now been discovered due to acquisition of a foreign *vanA* gene (Courvalin, 2006; Schito, 2006).

1.3.2: Virulence

S. aureus strains have a remarkably wide range of virulence factors which have been usefully categorised by Franklin and Lowy (1998), and their variety reflects the significance of *S. aureus* as an important pathogen in humans. Firstly, the peptidoglycan cell wall its self has endotoxin like activity, stimulating the release of a range of host inflammatory mediators.

An array of surface proteins contributes to *S. aureus* pathogenicity via various mechanisms. Some proteins function as adhesins, facilitating bacterial adhesion to endothelial cells. Many of these proteins are able to bind to components of the extracellular matrix facilitating their colonisation in host tissue, for example the fibrinonectin binding proteins, clumping factors, collagen binding proteins, elastin binding proteins and protein A (Hauck and Ohlsen, 2006). In addition to binding molecules in the extracellular matrix, protein A is able to bind the Fc region of human immunoglobulin proteins conferring antiphagocytic effects.

S. aureus also produce toxins with differing actions such as haemolysins, exfoliative toxins, pyrotoxigenic superantigens, Panton-Valentine leukocidin and enterotoxins, some of which are known to be responsible

for the symptoms of specific diseases within humans. Of recent concern is the emergence of highly virulent CA-MRSA and MSSA strains which express the Panton-Valentine leukocidin, an enzyme that creates pores in the cell membrane of leukocytes (Shallcross *et al.*, 2009).

In order to aid infection spread, *S. aureus* produces various enzymes such as proteases, hyaluronidases and lipases, which allow breakthrough into adjacent tissues areas to facilitate spread of infection. Other important enzymes include those responsible for antimicrobial resistance, as discussed previously.

Finally, *S. aureus* possess various systems allowing them to exploit the host environment for their own survival. One such example is the iron-responsive surface determinant (Isd) system which enables the uptake of iron in the form of haem-iron, from which the iron can then be liberated (Grigg *et al.*, 2010).

1.3.3: Quorum Sensing and Virulence Gene Regulation

Apart from the toxins responsible for directly causing disease, such as α-haemolysin or toxic shock syndrome toxin, no *S. aureus* virulence factor has been shown to have the capability of causing disease on its own (Fournier and Philpott, 2005). To establish infection, therefore, coordination of the expression of several virulence genes must take place. These virulence factors, along with other extracellular proteins involved in enabling adaptation to the environment, are the accessory proteins, and

the regulation of their expression is achieved primarily via two interconnected modes of regulation; response to cell density and response to external stimuli (Novick and Jiang, 2003).

1.3.3.1: Response to Cell Density

It has been suggested that during early growth, *S. aureus* surface protein genes are expressed at high levels, due to their roles in facilitating attachment to host cells and protecting bacterial cells from the host immune response. Later on in infection, a transition point occurs and exoprotein genes are expressed whilst surface protein expression is downregulated (Shompole *et al.*, 2003). This switch in gene expression allows the bacteria to colonize the host and reach sufficient population densities before the production of virulence factors, thus increasing the chances of establishing a successful infection. In *S. aureus* this switch in gene expression is known to be regulated by quorum sensing, a cell density dependent gene expression regulatory system in bacteria (Peng *et al.*, 1988). Quorum sensing regulated expression of virulence factor genes is thought to give bacteria a selective advantage over host defences, and so often plays an important role in the pathogenesis of the bacterium, as is the case in *S. aureus* (Smith and Iglewski, 2003).

The best-studied two-component signal transduction system in *S. aureus* is the accessory gene regulator (*agr*) quorum sensing system. Various studies involving animal models, using *S. aureus agr* mutants, have shown that virulence of *S. aureus* is reduced when quorum sensing is impaired,

proving its role in the pathogenesis of *S. aureus* in some diseases (Abdelnour *et al.*, 1993; Gillaspy *et al.*, 1995).

1.3.3.2: Response to External Stimuli

In addition to quorum sensing, a variety of other virulence gene regulation systems have been discovered in *S. aureus*. Other two-component signal transduction systems in addition to *agr* play a large role in allowing a change in virulence gene expression in response to environmental stimuli, and include *sae*, *srr* and *arl*. *S. aureus* also possesses an alternative sigma factor σ^B which is activated by environmental stress and energy depletion. Finally, various transcription factors control transcription of various extracellular proteins, and include the SarA homologues, SarS, SarT and Rot (Novick, 2003).

1.3.4: *S. aureus* Haemolysins

Some of the proteins regulated by the *agr* quorum sensing system belong to the *S. aureus* haemolysin group of toxins. *S. aureus* produces four haemolysins: α-, β-, γ- and δ-haemolysin.

α-haemolysin is a self-assembling, channel-forming exotoxin with a molecular weight of 33kDa produced by many *S. aureus* strains. It is toxic to many mammalian cells, and is characterised by its ability to lyse erythrocytes, being predominantly active against rabbit erythrocytes (Dinges *et al.*, 2000). α-haemolysin is secreted as a water-soluble monomer which binds with host cell membranes and consequently

penetrates the lipid bilayer. The monomer then oligomerises to form a membrane-inserted cylindrical heptamer with a 1nm to 2nm pore capable of lysing the eukaryotic cell (Bhakdi and Tranum-Jensen, 1991). This is due to the efflux of K^+ and other small molecules, and the influx of Na^+, Ca^{2+} and other small molecules, causing osmotic swelling of the erythrocyte and eventual lysis. α-haemolysin is encoded by the *hla* gene and is transcribed under control of the previously described *agr* system (Dinges *et al.*, 2000).

S. aureus β-haemolysin is highly haemolytic for sheep erythrocytes but not rabbit erythrocytes, and is designated the "hot-cold" haemolysin due to an enhancement in haemolytic activity by incubation below 10°C after treatment at 37°C. The *hlb* gene encodes a 330-amino-acid polypeptide with a predicted molecular weight of 39kDa. A 34 residue signal sequence is cleaved from this polypeptide upon secretion, giving the mature protein with a molecular weight of approximately 35kDa. Like α-haemolysin, β-haemolysin is also up regulated after the exponential phase (Dinges *et al.*, 2000).

γ-haemolysin is a bicomponent toxin composed of two separate polypeptides which act synergistically causing damage to neutrophils, macrophages and many varieties of mammalian erythrocytes (Taylor and Bernheimer, 1974; Dinges *et al.*, 2000). Despite the structure of γ-haemolysin, the *hlg* locus actually comprises three genes, *hlgA*, *hlgB* and *hlgC*, whereby it is postulated that *hlgB* and *hlgC* are cotranscribed and

hlgA is separately expressed (Cooney *et al.*, 1993). Each of the three genes encodes a protein, HlgA, HlgB and HlgC, which, in their mature form, have molecular weights of 32kDa, 32.5kDa and 34kDa respectively (Dinges *et al.*, 2000). HlgA has previously been called the γ_1 component of the toxin, and HlgC, the γ_2 component. These components share 70% residue identity, and approximately 30% identity with HlgB (Cooney *et al.*, 1993). Similar to Panton-Valentine leukocidin, γ-haemolysin is made up of an S and an F component (for slow- and fast-eluting proteins in an ion-exchange column), and it is thought that it is the S subunit that is important for mediating an inflammatory response within the host, leading to suggestions that the S subunit is responsible for the initial binding to host cell membranes (Dinges *et al.*, 2000).

δ-haemolysin is a 26-amino-acid peptide capable of causing damage to erythrocytes and other mammalian cells, and is made by 97% of *S. aureus* strains. This toxin forms an α-helix with regions of hydrophobicity and hydrophilicity, leading to suggestions regarding mechanisms of action that δ-haemolysin acts as a surfactant to disrupt the cell membrane (Dinges *et al.*, 2000). δ-haemolysin production is controlled by *agr*, and δ-haemolysin itself is coded for by RNAIII, which acts as mRNA for the *hld* gene (Janzon *et al.*, 1989).

1.3.5: *S. aureus* as an Intracellular Organism

S. aureus is not classically considered as an intracellular pathogen, yet accumulating scientific evidence has demonstrated that this organism has

intracellular survival strategies, with the ability to become internalised by, and persist within, a wide range of non-professional eukaryotic phagocytes; in fact, studies show that *S. aureus* is ingested by human and mouse osteoblasts (Ellington *et al.*, 1999; Jevon *et al.*, 1999), human umbilical vein endothelial cells (Menzies and Kourteva, 1998), bovine mammary epithelial cells (Bayles *et al.*, 1998; Qazi *et al.*, 2001), chick fibroblasts (Alexander and Hudson, 2001) and human keratinocytes (Kintarak *et al.*, 2004). Furthermore, internalisation of *S. aureus in vivo* into chick osteoblasts has been reported (Reilly *et al.*, 2000). In some cases this internalization appears to be mediated by cell surface-localized proteins including fibronectin binding proteins (Lammersa *et al*., 1999; Ahmed *et al*., 2001). Extracellular proteins have also been implicated; Haggar *et al*. (2003) demonstrated a role for an extracellular protein, extracellular adherence protein (Eap), which can rebind to the surface of *S. aureus* whilst also binding a variety of plasma protein including fibronectin and fibrinogen. Eap was infact shown to play a role in *S. aureus* adhesion and ultimately internalisation into eukaryotic cells, with Eap deficient mutant strains being internalised to a lesser extent than the wild type. Moreover, exogenously added Eap enhanced internalisation, whilst anti-Eap antibodies prevented internalisation of various *S. aureus* strains.

Staphylococci are renowned for their capability to cause persistent infections in both humans and animals. The mechanisms employed to achieve such long-term colonization remain unknown. Nonetheless, the

now widely reported phenomenon of *S. aureus* internalisation and intracellular survival has led to hypotheses regarding the role of this internalisation in chronic recurrent staphylococcal diseases and persistent infections, drawing similarities with the benefits that this mode of colonization has for classic facultative intracellular organisms. This theory is supported by evidence of an intracellular reservoir of *S. aureus* in the nasal mucosa of patients with recurrent *S. aureus* rhinosinusitis (Clement *et al.*, 2005).

1.4: MultiSite Gateway® Technology

MultiSite Gateway® Technology allows the simultaneous cloning of multiple DNA fragments in a defined order and orientation through use of site-specific recombination. MultiSite Gateway® donor vectors have two specific *att* sites flanking a cassette containing the *ccd*B gene and a chloramphenicol resistance gene (Cm-*ccd*B cassette). The *ccd*B gene allows for negative selection due to the inhibition of growth of *E. coli* caused by the *ccd*B protein, and the chloramphenicol resistance gene allows for counterselection. Polymerase Chain Reaction (PCR) products with flanking *att* sites can be used in BP recombination reactions to generate entry clones, whereby the Cm-*ccd*B cassette in the MultiSite Gateway® donor vector is replaced by the PCR product. In a similar manner, three entry clones containing, for example, a promoter, a gene of interest and a terminator, respectively, can be used in an LR

recombination reaction with a MultiSite Gateway® destination vector also containing two specific *att* sites flanking the Cm-*ccd*B cassette, to simultaneously transfer the three DNA fragments into the destination vector.

This technology is possible due to the specificity of the *att* sites; *att*B sites will recombine only with their cognate *att* sites, enabling the DNA fragments to be incorporated into a donor vector in a particular orientation, and subsequently into a destination vector in a specific order. To this end, different donor vectors are available with different *att* sites. This system is illustrated in Figure 1.2 and Figure 1.3.

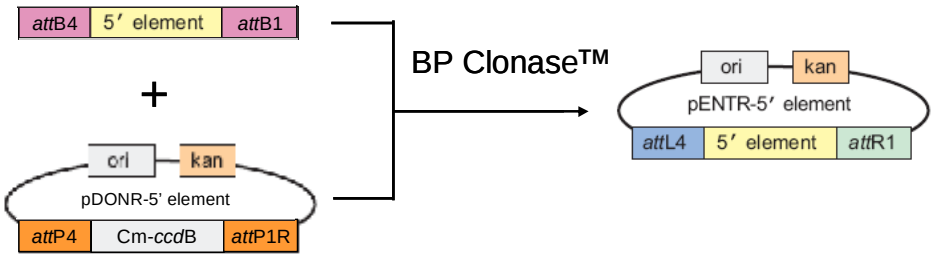

FIGURE 1.2: BP Recombination Reaction

Recombination of an *att*B substrate, in this example an *att*B PCR product, with an *att*P substrate, in this example a donor vector with *att*P sites found on pDONR P4-P1R, to create an *att*L and *att*R containing entry clone for use in MultiSite Gateway® Three-Fragment Vector Construction. The reaction is catalyzed by BP Clonase™ II enzyme mix, a mixture of the λ Integrase (Int) and *E. coli* Integration Host Factor (IHF) proteins (Invitrogen).

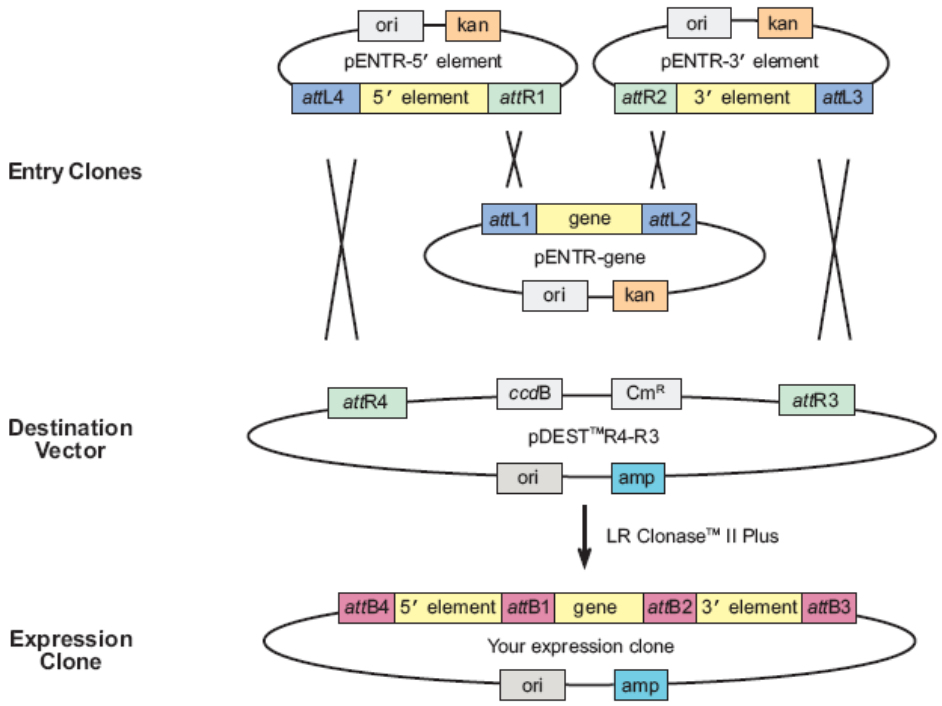

FIGURE 1.3: LR Recombination Reaction

Recombination of *att*L and *att*R containing entry clones with each other and an *att*R containing destination vector to create an *att*B containing expression clone. The reaction is catalyzed by LR Clonase™ II Plus enzyme mix, a mixture of the λ Int and Excisionase (Xis) proteins, and the *E. coli* IHF protein (Invitrogen).

1.5: Aims and Objectives

This aims of this study are based upon the need to develop reporter systems for the non-invasive *in vivo* tracking systems for the monitoring of infectious disease processes, in addition to the investigation of *S. aureus* haemolysin mutants both *in vitro* and through use of the developed

reporter system. To achieve these aims, the following objectives were formulated:

1. To construct and evaluate *in vitro* an MRI bacterioferritin reporter gene for *S. aureus*.
2. To evaluate the *S. aureus* MRI bacterioferritin reporter gene *in vivo* in an established mouse model.
3. To construct a β-haemolysin mutant in *S. aureus* using Gateway® technology for the *in vitro* analysis of the involvement of *agr* regulated gene products in endosomal escape.
4. To evaluate the *S. aureus* haemolysin mutants in conjunction with the MRI reporter in a specific disease model.

2.0: MATERIALS AND METHODS

2.1: Bacterial Strains and Plasmids

TABLE 2.1: Bacterial strains and plasmids used in this study.

Organism/Plasmid	Description	Source or Reference
Strain		
E. coli TOP10	*E. coli* cloning isolate, *recA*, *endA* genotype	Invitrogen
E. coli One Shot® *ccd*B Survival™ T1 Phage-Resistant Cells	Derivative of TOP10 strain, resistant to the *ccd*B gene product, *ton*A genotype to confer resistance to T1 and T5 phage	Invitrogen
S. aureus RN4220	Restriction deficient *agr* mutant, derivative of 8325-4	Kreiswirth *et al*., 1983
S. aureus RN6390	*agr*+ laboratory strain, derivative of 8325-4	Peng *et al*., 1988
S. aureus 8325-4	Wild-type strain, cured of prophages and plasmids	Novick, 1967
Plasmid		
pSB2030	P_{xylA}-*gfp3opt-luxABCDE* inserted into pGC4 backbone, Amp^R, Cm^R	Qazi *et al*., 2001
pSB2035	P_3 amplified by PCR from *S. aureus* 8325-4, exchanged with P_{xylA} from pSB2030, Amp^R, Cm^R	Qazi *et al*., 2001
pSB3010	3 fragment expression cassette in pMK4, *xylR*P_{xylA}:*luxABCDE*:rrnBT_1T_2	Perehinec *et al*., 2007

pSB3016	3 fragment expression cassette in Gateway® destination vector pDEST-pTS1, P_{xylRA}:*intC*:rrnBT_1T_2, Amp^R, Cm^R	Hill laboratory collection
pDONR P4-P1R	Gateway® entry vector, *att*P1R and *att*P4 sites to clone *att*B4 and *att*B1 flanked PCR products, Km^R, Cm^R, *ccd*B+	Invitrogen
pDONR P221	Gateway® entry vector, *att*P1 and *att*P2 sites to clone attB1 and attB2 flanked PCR products, Km^R, Cm^R, *ccd*B+	Invitrogen
pDONR P2R-P3	Gateway® entry vector, *att*P2R and *att*P3 sites to clone *att*B2 and *att*B3 flanked PCR products, Km^R, Cm^R, *ccd*B+	Invitrogen
pTS1-Dest +lac	Gateway® destination vector, *att*R4 and *att*R3 sites for recombination with entry clones in a Multisite Gateway® LR reaction, contains temperature sensitive replicon, Amp^R, Cm^R, *ccd*B+	Hill laboratory collection
pDEST-pUNK1	pUNK1 containing *att*R4 and *att*R3 sites for recombination with entry clones in a Multisite Gateway® LR reaction, Erm^R, Cm^R, *ccd*B+	Perehinec *et al*., 2007

pDONR P4-P1R::*hlb* up	Gateway® entry vector, *hlb* upstream region amplified by PCR with incorporated *att* sites and cloned into pDONR P4-P1R by BP recombination reaction, Km^R	This study
pDONR P221 ery PhiC	Gateway® entry vector, *att*L1 and *att*L2 sites flanking Erm^R gene, Km^R	Hill laboratory collection
pDONR P2R-P3::*hlb* down	Gateway® entry vector, *hlb* downstream region amplified by PCR with incorporated *att* sites and cloned into pDONR P2R-P3 by BP recombination reaction, Km^R	This study
pTS1-Dest *hlb*	pTS1-Dest +lac backbone with *hlb* upstream region, Erm^R gene and *hlb* downstream region inserted via LR recombination reaction with entry clones pDONR P4-P1R::*hlb* up, pDONR P221 ery PhiC and pDONR P2R-P3::*hlb* down, Erm^R, Cm^R, Amp^R	This study
pDONR P4-P1R Sa P_{S10}	Gateway® entry vector, *S. aureus* S10 promoter amplified by PCR with incorporated *att* sites and cloned into pDONR P4-P1R by BP recombination reaction, Km^R	Hill laboratory collection

pDONR P4-P1R Bs P_{S10}	Gateway® entry vector, *B. subtilis* S10 promoter amplified by PCR with incorporated *att* sites and cloned into pDONR P4-P1R by BP recombination reaction, Km^R	Hill laboratory collection
pDONR P4-P1R P_3	Gateway® entry vector, *S. aureus* P_3 promoter amplified by PCR with incorporated *att* sites and cloned into pDONR P4-P1R by BP recombination reaction, Km^R	Hill laboratory collection
pDONR P4-P1R P_{ahpC}	Gateway® entry vector, *S.* aureus P_{ahpC} promoter amplified by PCR with incorporated *att* sites and cloned into pDONR P4-P1R by BP recombination reaction, Km^R	Hill laboratory collection
pDONR P221 dual	Gateway® entry vector, *gfp-luxABCDE* amplified by PCR with incorporated *att* sites and cloned into pDONR P221 by BP recombination reaction, Km^R	Hill laboratory collection
pDONR P221 bfd	Gateway® entry vector, *E. coli bfd* gene amplified by PCR with incorporated *att* sites and cloned into pDONR P221 by BP recombination reaction, Km^R	This study

pDONR P221 bfr	Gateway® entry vector, *E. coli* *bfr* gene amplified by PCR with incorporated *att* sites and cloned into pDONR P221 by BP recombination reaction, Km^R	Hill laboratory collection
pDONR P221 bfd/bfr	Gateway® entry vector, *E. coli* *bfd* and *bfr* gene amplified by PCR with incorporated *att* sites and cloned into pDONR P221 by BP recombination reaction, Km^R	This study
pDONR P2R-P3 term	Gateway® entry vector, $rrnBT_1T_2$ amplified by PCR with incorporated *att* sites and cloned into pDONR P2R-P3 by BP recombination reaction, Km^R	Hill laboratory collection
pDONR P2R-P3 luxterm	Gateway® entry vector, *luxABCDE* and $rrnBT_1T_2$ amplified by PCR with incorporated *att* sites and cloned into pDONR P2R-P3 by BP recombination reaction, Km^R	This study
pMK4 P_{xylA}-gfp-term	pMK4 backbone with P_{xylA}, *gfp* and $rrnBT_1T_2$, Amp^R, Cm^R	Hill laboratory collection
pUNK1 P_{xylA}-dual-term	pDEST-pUNK1 backbone with P_{xylA}, *gfp-luxABCDE* and $rrnBT_1T_2$ inserted via LR recombination reaction with entry clones pDONR P4-P1R P_{xylA}, pDONR P221 dual and pDONR P2R-P3 term, Erm^R	Hill laboratory collection

pUNK1 Sa P_{S10}-dual-term	pDEST-pUNK1 backbone with *S. aureus* P_{S10}, *gfp-luxABCDE* and $rrnBT_1T_2$ inserted via LR recombination reaction with entry clones pDONR P4-P1R Sa P_{S10}, pDONR P221 dual and pDONR P2R-P3 term, Erm^R	This study
pUNK1 Bs P_{S10}-dual-term	pDEST-pUNK1 backbone with *B. subtilis* P_{S10}, *gfp-luxABCDE* and $rrnBT_1T_2$ inserted via LR recombination reaction with entry clones pDONR P4-P1R Bs P_{S10}, pDONR P221 dual and pDONR P2R-P3 term, Erm^R	This study
pUNK1 P_{S10}-bfd-luxterm	pDEST-pUNK1 backbone with *S. aureus* P_{S10}, *E. coli bfd* and *luxABCDE*-$rrnBT_1T_2$ inserted via LR recombination reaction with entry clones pDONR P4-P1R Sa P_{S10}, pDONR P221 bfd and pDONR P2R-P3 luxterm, Erm^R	This study
pUNK1 P_{S10}-bfr-luxterm	pDEST-pUNK1 backbone with *S. aureus* P_{S10}, *E. coli bfr* and *luxABCDE*-$rrnBT_1T_2$ inserted via LR recombination reaction with entry clones pDONR P4-P1R Sa P_{S10}, pDONR P221 bfr and pDONR P2R-P3 luxterm, Erm^R	This study

pUNK1 P_{S10}-bfd/bfr-luxterm	pDEST-pUNK1 backbone with *S. aureus* P_{S10}, *E. coli bfd-bfr* and *luxABCDE*-rrnBT_1T_2 inserted via LR recombination reaction with entry clones pDONR P4-P1R Sa P_{S10}, pDONR P221 bfd/bfr and pDONR P2R-P3 luxterm, Erm^R	This study
pUNK1 P_3-bfr-luxterm	pDEST-pUNK1 backbone with *S. aureus* P_3, *E. coli bfr* and *luxABCDE*-rrnBT_1T_2 inserted via LR recombination reaction with entry clones pDONR P4-P1R P_3, pDONR P221 bfr and pDONR P2R-P3 luxterm, Erm^R	This study
pUNK1 P_3-bfd/bfr-luxterm	pDEST-pUNK1 backbone with *S. aureus* P_3, *E. coli bfd-bfr* and *luxABCDE*-rrnBT_1T_2 inserted via LR recombination reaction with entry clones pDONR P4-P1R P_3, pDONR P221 bfd/bfr and pDONR P2R-P3 luxterm, Erm^R	This study
pUNK1 P_{ahpC}-bfr-luxterm	pDEST-pUNK1 backbone with *S. aureus* P_{ahpC}, *E. coli bfr* and *luxABCDE*-rrnBT_1T_2 inserted via LR recombination reaction with entry clones pDONR P4-P1R P_{ahpC}, pDONR P221 bfr and pDONR P2R-P3 luxterm, Erm^R	This study

2.2: Chemical Reagents

All of the general chemicals used in this study were obtained from Sigma Aldrich unless otherwise stated.

2.3: Growth Media

2.3.1: Luria-Bertani Medium

Luria-Bertani (LB) broth was prepared using 10g tryptone (Oxoid), 5g yeast extract (Difco) and 5g sodium chloride made up to 1L with distilled water. The solution was then sterilised by autoclaving.

LB agar was prepared as above with the addition of 1.5% (w/v) Number 1 Bacteriological Agar (Oxoid).

2.3.2: Brain Heart Infusion

Brain Heart Infusion (BHI) broth (Oxoid) was prepared as described by the manufacturer. The solution was sterilised by autoclaving.

BHI agar was prepared as above with the addition of 1.5% (w/v) Number 1 Bacteriological Agar (Oxoid).

2.3.3: Tryptic Soy Broth

Tryptic Soy Broth (TSB) (Oxoid) was prepared as described by the manufacturer. The solution was sterilised by autoclaving.

TSB agar was prepared as above with the addition of 1.5% (w/v) Number 1 Bacteriological Agar (Oxoid).

2.3.4: LK Medium

LK broth was prepared using 10g tryptone (Oxoid), 5g yeast extract (Difco) and 7g potassium chloride made up to 1L with distilled water. The solution was then sterilised by autoclaving.

LK top agar was prepared as above with the addition of 0.75% (w/v) agar (Difco). LK-citrate agar was prepared as above with the addition of 1% (w/v) Number 1 Bacteriological Agar (Oxoid) and 0.05% (w/v) Na citrate.

2.3.5: SMMP50

SMMP50 medium was made up from 5.5 parts SMM buffer (1M sucrose, 0.04M maleic acid, 0.04M magnesium chloride, pH 6.5), 4 parts 7% (w/v) Penassay broth and 0.5 parts 10% (w/v) bovine serum albumin. The SMM buffer and Penassay broth (Difco) were mixed and autoclaved and then the bovine serum albumin was filter sterilised and added to the sterile mixture.

2.4: Supplements

Growth medium was supplemented with the following antibiotics, where appropriate, at the given concentrations, unless otherwise stated:

Ampicillin (Amp):	100μg ml^{-1}
Chloramphenicol (Cm):	30μg ml^{-1} (Gram-negative organisms)
	5μg ml^{-1} (Gram-positive organisms)
Kanamycin (Km):	50μg ml^{-1}
Erythromycin (Erm):	150μg ml^{-1} (Gram-negative organisms)
	5μg ml^{-1} (Gram-positive organisms)

2.5: Growth Conditions

Liquid cultures were grown aerobically in LB overnight at 37°C with gentle agitation at 200rpm unless otherwise stated. Agar plates were incubated statically overnight at 37°C unless otherwise stated.

Growth of bacterial cultures in liquid medium was monitored by optical density at 600nm (OD_{600}) using a Pharmacia Novaspec II Spectrophotometer.

2.6: DNA Manipulations

2.6.1: Genomic DNA Purification

Genomic DNA purification was carried out using DNeasy Blood and Tissue Kits (Qiagen) according to the manufacturer's instructions.

2.6.2: Plasmid Preparation

Plasmid DNA preparation was carried out using QIAprep Spin Miniprep Kits (Qiagen) according to the manufacturer's instructions. For *S. aureus* plasmid preparation, 5µl of lysostaphin (5mg ml^{-1} solution suspended in ddH_2O) was added with the first buffer step (250µl Buffer P1) and incubated at 37°C for 30 minutes.

2.6.3: Restriction Digests

Cleavage of DNA with restriction enzymes (Promega) was performed according to 'Current Protocols in Molecular Biology' (Ausubel *et al*., 2000).

2.6.4: Construction of Entry Clones

The PCR primers used in the construction of DNA fragments to be inserted into Gateway® entry clone vectors are described in Table 2.2 and were supplied by Sigma-Genosys Ltd. Gateway® BP Clonase™ Enzyme Mix (Invitrogen) was used according to the manufacturer's instructions.

2.6.5: LR Recombination Reactions

Gateway® LR Clonase™ Enzyme Mix (invitrogen) was used according to the manufacturer's instructions.

2.6.6: PCR Clean Up

Purification of DNA fragments from PCR was achieved using a Zymoclean™ Gel DNA Recovery Kit (Zymo Research), according to the manufacturer's instructions.

2.7: Agarose Gel Electrophoresis

Agarose gels were prepared in 1 x TAE (40mM Tris Acetate, 2mM EDTA, pH8.5) at a concentration of 0.8% (w/v) agarose. Ethidium bromide was added to a final concentration of 10μg ml^{-1}. Samples were loaded with 5μl Blue/Orange 6x loading Dye (Promega). Gels were run in 1 x TAE buffer at 80V and DNA was then visualised using an ultraviolet (UV) transilluminator.

2.8: Polymerase Chain Reaction

2.8.1: Primers

TABLE 2.2: List of primers used in this study. Red text indicates Gateway® *att* sites. Blue text indicates incorporated restriction sites.

Primer Name	Nucleotide Sequence (5'-3')	Restriction/ *att* Sites
hlb up F'	GGGG ACA ACT TTG TAT AGA AAA GTT GGT TTA AAC TCT ATC ATG CTT CAG TAC TG	*att*B4 forward, *Pme*I
hlb up R'	GGGG ACT GCT TTT TTG TAC AAA CTT GCA TTA TCA CTC CTT TTA TAT AGC	*att*B1 reverse
hlb down F'	GGGG ACA GCT TTC TTG TAC AAA GTG GTG CTC AAC TAA CTA ATA ACT TG	*att*B2 forward
hlb down R'	GGGG ACA ACT TTG TAT AAT AAA GTT GGT TTA AAC CTG AGA AGA ATC TTG ATG GTG	*att*B3 reverse, *Pme*I
hlb outside up F'	CCG ATA CCT CTA TCA TGC TTC	N/A
hlb outside down R'	GTT AGC ACT ATC GAC TAC TTT C	N/A
bfd F'	GGGG ACA AGT TTG TAC AAA AAA GCA GGC TAA GGA GGA ATA AAA AAT GTA CGT TTG TCT TTG TAA TGG TAT CAG C	*att*B1 forward
bfd R'	GGGG ACC ACT TTG TAC AAG AAA GCT GGG TTT ATG CGG ACT CCT TAA ACT CCG	*att*B2 reverse
bfr R'	GGGG ACC ACT TTG TAC AAG AAA GCT GGG TCT CAA CCT TCT TCG CGA ATC	*att*B2 reverse
pTS1 F'	GCT CAC TCA TTA GGC ACC	N/A

pTS1 R'	GTA ACA TCT GAC CGA GAT T	N/A
ery F'	GCC ATA AAC TAT CAT ATC TTC	N/A
ery R'	GAT CCG AGC TTA TCG ATT TCG	N/A
luxA F'	GGGG ACA GCT TTC TTG TAC AAA AG GAG GAC TCT CTA TGA AAT TTG GAA AC	*att*B2 forward
term R'	GGGG ACA ACT TTG TAT AAT AAA GTT GTT TAA ACT GGC AGT TTA TGG CGG GC	*att*B3 reverse, *Pme*I
Sa S10 F'	GGGG ACA ACT TTG TAT AGA AAA GTT GTT TAA ACC GTT CTT ATG ACT AAT TAT ATA G	*att*B4 forward, *Pme*I
Bs S10 F'	GGGG ACA ACT TTG TAT AGA AAA GTT GTT TAA ACT CGA AAC AGT ATT ATC AAG AAC	*att*B4 forward, *Pme*I

2.8.2: General PCR Parameters

All PCR reactions were performed in a Hybaid PCR Express Thermo (Hybaid, Ashford, UK) thermal cycler. Unless stated otherwise, reactions were performed in 50µl volumes with GoTaq DNA Polymerase. Briefly, on ice, 1µl of each primer (from 100µM stock), 100ng template, 1µl dNTP mix (to a final concentration of 10mM of each dNTP), 4µl MgCl (to a final concentration of 2mM), 10µl of 5 x buffer and 0.25µl GoTaq DNA Polymerase were mixed. The reaction was made up to a final volume of 50µl with sterile distilled water. Reaction parameters were as follows:

Initial Denaturation	95°C	2 minutes

30 cycles of:

Denature	95°C	30 seconds
Anneal	48-65°C	30 seconds
Extend	72°C	1 minute/kb of PCR product
Final Extension	72°C	10 minutes

2.8.3: AccuPrime™ Taq DNA Polymerase

Some PCR reactions were performed using AccuPrime™ Taq DNA Polymerase (Invitrogen) due to the length of the expected PCR products. AccuPrime™ Taq DNA Polymerase is a high-fidelity DNA polymerase which is effective over a wide range of target sizes. Briefly, on ice, 1µl of each primer (from 10µM stock), 100ng genomic DNA template or 10ng plasmid DNA template, 5µl of 10 x AccuPrime buffer and 0.2µl AccuPrime™ Taq DNA Polymerase were mixed. The reaction was made up to a final volume of 50µl with sterile distilled water. Reaction parameters were as follows:

Initial Denaturation	94°C	2 minutes

30 cycles of:

Denature	94°C	30 seconds
Anneal	48-65°C	30 seconds
Extend	68°C	1 minute/kb of PCR product
Final Extension	68°C	10 minutes

2.9: Transfer of Plasmid DNA into Bacterial Cells

2.9.1: Dialysis of DNA, BP and LR Reactions

DNA was dialysed against water using 0.025µm (13mm) dialysis filters (Millipore). A petri dish containing deionised water was used, and the filter was allowed to float on the surface with the shiny side facing upwards. 10µl DNA was pipetted onto the filter and left to dialyse for 30 minutes.

2.9.2: Preparation of Electrocompetent *E. coli*

E. coli from an overnight culture grown aerobically at 37°C with gentle agitation at 200rpm, in 20ml LB broth was used to inoculate 1L sterile LB broth (1:100). This culture was grown as described above until an OD_{600} of 0.5 was reached. The rest of the protocol was carried out on ice. Bacterial cells were harvested by centrifugation (4,000 x *g*, 4°C, 15 minutes) and then washed with 1L cold water. The cell suspension was then centrifuged as before, washed with 500ml cold water, and further centrifuged before washing with 20ml 10% glycerol. The suspension was centrifuged a final time, as before, and resuspended in 1ml 10% glycerol. 40µl aliquots were transferred to eppendorf tubes and frozen rapidly in liquid nitrogen before storage at -80°C.

2.9.3: Electroporation of Plasmid DNA into *E. coli*

10µl dialysed DNA was added to 40µl of electrocompetent cells, mixed on ice until the cells were fully thawed, and then transferred to a pre-chilled 2mm gap gene pulser electroporation cuvette (Biorad). A single pulse of

2.5kV (200Ω) was delivered to the cuvette using a Biorad Gene Pulser. Immediately after the pulse 1ml LB broth was added, and the cell suspension was incubated statically at 37°C for 1 hour before plating onto the appropriate selective agar and incubation overnight at 37°C.

2.9.4: Preparation of Electrocompetent *S. aureus*

An overnight culture of *S. aureus* grown aerobically at 37°C with gentle agitation at 200rpm was diluted 1:50 into TSB, and grown aerobically at 37°C until an OD_{600} of 0.3-0.8 was reached. Bacterial cells were harvested by centrifugation (8,000 x *g*, 10 minutes) and washed with an equal volume of 500mM sucrose. The cell suspension was then centrifuged as before, resuspended in 0.5 volume of 500mM sucrose and incubated on ice for 15-30 minutes. The suspension was centrifuged a final time, as before, and resuspended in 0.1 volume of 500mM sucrose. 40µl aliquots were transferred to eppendorf tubes and stored at -80°C.

2.9.5: Electroporation of Plasmid DNA into *S. aureus*

10µl dialysed DNA was added to 40µl of electrocompetent cells, mixed on ice until the cells were fully thawed, and then transferred to a pre-chilled 2mm gap gene pulser electroporation cuvette (Biorad). A single pulse of 2.5kV (100Ω) was delivered to the cuvette using a Biorad Gene Pulser. Immediately after the pulse 1ml SMMP50 medium was added, and the cell suspension was incubated statically at 37°C for 3 hours before plating onto the appropriate selective agar.

All plasmid DNA for electroporation into *S. aureus* RN6390 was first electroporated into *S. aureus* RN4220, a restriction negative strain capable of accepting *E. coli* DNA. Plasmid DNA was then isolated from *S. aureus* RN4220 as described in section 2.6.2 of Materials and Methods before electroporation into *S. aureus* RN6390.

2.9.6: Phage Transduction

The donor strain was grown overnight at 37°C aerobically in LB broth and used to inoculate a 10ml solution consisting of 5ml LB broth and 5ml phage buffer (1mM $MgSO_4$, 4mM $CaCl_2$, 50mM Tris-HCl pH7.8, 5.9g/L NaCl and 1g/L gelatin) until the solution appeared slightly turbid. 100µl phage 11 was then added, before 10 minutes incubation at room temperature. The solution was then incubated at 30°C shaking at 50rpm for approximately 4 hours, or until complete lysis had occurred and the solution appeared clear. The lysate was then filter sterilised.

The recipient strain was grown overnight at 37°C aerobically in 20ml LK broth. The culture was then centrifuged (5,000 x *g*) for 10 minutes and resuspended in 1ml LK broth. 500µl of these cells were then mixed with 1ml LK broth, 10mM $CaCl_2$ and 500µl phage lysate, before static incubation at 37°C for 25 minutes, followed by aerobic incubation at 37°C for 15 minutes. 1ml ice cold 0.02M Na citrate was then added and incubated on ice for 5 minutes. The solution was then centrifuged as above and all supernatant was removed, before resuspension in 1ml ice cold 0.02M Na citrate. The solution was then incubated on ice for 2 hours

and plated onto LK-citrate plates containing the relevant selective antibiotic at 1/33 the concentration normally used. Plates were incubated at 37°C for 1.5 hours. Plates were then overlaid with 5ml LK top agar containing the relevant selective antibiotic at x6 the concentration normally used. Plates were then incubated at 37°C for 48 hours.

2.10: Protein Visualisation using SDS-PAGE

2.10.1: Preparation of Cell Lysates from *E. coli*

10ml overnight culture at an OD_{600} of 0.5 were harvested by centrifugation and resuspended in 250µl 2 x SDS PAGE sample buffer (1g SDS, 10ml Glycerol, 10ml β-Mercapto Ethanol, 4ml 1M Tris-HCl pH 6.8, and a small amount of Bromophenol Blue, made up to total volume of 100ml with water). The cell suspension was boiled for 5 minutes and then centrifuged (13,000 x *g*, 5 minutes). 15µl of the suspension was loaded per lane of a 15% (w/v) polyacrylamide gel.

2.10.2: Preparation of Cell Lysates from *S. aureus*

10ml overnight culture at an OD_{600} of 0.5 were harvested by centrifugation and resuspended in 500µl 80µg ml^{-1} lysostaphin in phosphate buffered saline (PBS). The cell suspension was incubated at 37°C for 30 minutes. 250µl 2 x SDS PAGE sample buffer was then added and the cell suspension was boiled for 5 minutes and then centrifuged (13,000 x *g*, 5

minutes). 15µl of the suspension was loaded per lane of a mini acrylamide gel.

2.10.3: SDS-PAGE Gel Electrophoresis

Acrylamide gels were used for protein analysis by gel electrophoresis. 15% Resolving Gel was made up with 5ml Acryl-bis (30% (w/v) acrylamide:0.8% bis), 1.25ml Resolving Gel Buffer, 100µl 10% (w/v) SDS, 75µl 10% (w/v) AP, 3.2ml ddH_2O and 5µl Temed. Approximately 2cm Stacking Gel (750µl 30% Acryl-bis, 1.5ml Stacking Gel Buffer, 60µl 10% SDS, 150µl 10% ammonium persulfate, 3ml ddH_2O and 6µl Temed) was then poured on top of the resolving gel with a comb in place to create wells.

Gels were run in running buffer (3.03g Tris, 1g SDS and 14.4g glycine in 1L water) at 200V.

Resolving Gel Buffer:

> 3M Tris-HCl (pH 8.8), 36.3g Tris and 48ml 1M HCl mixed and made up to total volume of 100ml with water.

Stacking Gel Buffer:

> 0.5M Tris-HCl (pH 6.8), 6g Tris dissolved in 40ml ddH2O, titrated to pH 6.8 with 1M HCl and made up to total volume of 100ml with water.

2.10.4: Coomassie Staining

Gels were stained with Coomassie Brilliant Blue solution (15ml Methanol, 10ml Acetic Acid and 0.2g Coomassie Blue made up to total volume of 100ml with water) overnight with gentle agitation before destaining with 15ml Methanol and 10ml Acetic Acid made up to total volume of 100ml with water, for approximately 1 hour. Gels were then transferred to distilled water.

2.11: Western Blotting

2.11.1: Electrophoresis

A gel/membrane sandwich was set up as shown in the diagram below:

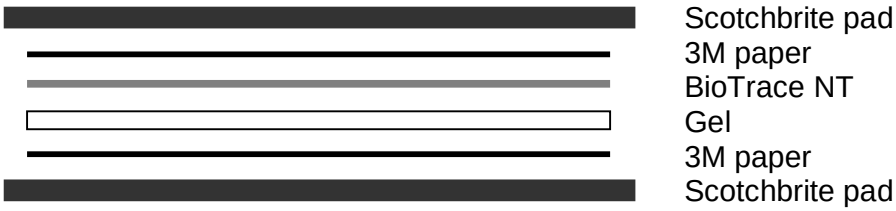

3M filter paper, blotting membrane (BioTrace NT) (PALL Life Sciences, USA) and BioRad Scotchbrite pads were all pre-soaked in blotting buffer (14.4g glycine, 3.03g Tris in 1L deionised H_2O). The sandwich was gently compressed using a pipette on its side to remove any air bubbles, before being transferred to a holder and placed in the electrophoresis tank. The tank was filled with blotting buffer and the gel was then electrophoresed at a 140mA constant current for 1.5 hours.

2.11.2: Ponceau Staining

The membrane was removed from the sandwich and stained with Ponceau S solution (Sigma) for 1 minute with gentle agitation. The membrane was then rinsed with ddH_2O until bands were visible.

2.11.3: Antibody Staining

The membrane was blocked in 20ml 5% (w/v) skimmed milk in PBS for 15 minutes at room temperature with gentle agitation before briefly rinsing three times with PBS in a tray. The membrane was then incubated in 20ml PBS with 5% (w/v) skimmed milk, 0.1% (v/v) Tween 20 and the primary antibody (polyclonal mouse-antiserum directed against bfr) at a 1:10 dilution for 1.5 hours. Washing in PBS was then repeated for 5 minutes, three times, with gentle agitation. Incubation with the secondary antibody (rabbit anti-mouse, horseradish peroxidase conjugated) at a dilution of 1:2000 was then carried out, as described above with the antibody, before washing as above.

2.11.4: Enhanced Chemiluminescence (ECL) Developing

3ml each of solutions A and B from an ECL™ Western Blotting Detection System kit (GE Healthcare) were mixed in a universal and pipetted onto the membrane in a tray. After 2-3 minutes of gentle agitation excess developer was drained off and the membrane was transferred to a clean acetate sheet and then covered with a second acetate sheet. Any air bubbles were gently removed by rubbing the top of the acetate sheet with

blue roll. The membrane was then exposed to ECL film with the protein side of the membrane towards the film.

2.12: Bacterial Mutagenesis

2.12.1: Construction of Knockout Mutants

S. aureus harbouring the temperature sensitive pTS1 mutagenesis plasmid were grown overnight statically in LB supplemented with 5µg ml^{-1} Cm and Erm at 30°C to facilitate recombination. Cultures were then diluted 10 fold in LB and 100µl volumes of 10^{-4}, 10^{-5} and 10^{-6} dilutions were plated onto LB agar supplemented with 5µg ml^{-1} Erm before incubation overnight at 42°C to promote plasmid loss. Any colonies were replica plated onto LB agar supplemented with 5µg ml^{-1} Cm and then onto LB agar supplemented with 5µg ml^{-1} Erm, before incubation overnight at 37°C. Genomic DNA purification of colonies which grew on Erm supplemented plates but not Cm supplemented plates was carried out and DNA was screened by PCR.

2.12.2: Excision of the Erm^R Gene

The *S. aureus* RN6390 Δ*hlb* was transformed with the pTS1 intC expression vector, pSB3016, and grown statically at 30°C to early log phase. Xylose was then added at a final concentration of 1% (w/v), before further incubation aerobically at 30°C for 5 hours. Cultures were then diluted 10 fold in LB and 100µl volumes of 10^{-4}, 10^{-5} and 10^{-6} dilutions

were plated onto non-selective LB agar before incubation overnight at 42°C to promote loss of the temperature sensitive pSB3016 plasmid. Any colonies were replica plated onto LB agar alone, LB agar supplemented with 5µg ml^{-1} Cm and LB agar supplemented with 5µg ml^{-1} Erm in order to detect clones which had lost both the chromosomal *erm* gene and the IntC expression vector.

2.13: Iron Quantification

2.13.1: Iron Assay

A QuantiChrom™ Iron Assay Kit (DIFE-250) (Bioassay Systems) was used for quantification of iron concentrations in cell lysates. Standards were prepared as described by the manufacturer and mixed with 50µl overnight culture at an OD_{600} of 0.5. Reagents were added as described by the manufacturer and optical density was read at 590nm. Iron concentrations were then calculated according to the manufacturer's instructions.

2.13.2: Inductively Coupled Plasma Mass Spectrometry

Iron concentration in bacterial samples was analysed by Inductively Coupled Plasma Mass Spectrometry (ICP-MS). This was carried out by Dr. Uwe Gbureck at the University of Würzburg in Germany.

2.14: Haemolysin Assay

Phenotypic confirmation of the newly transduced α- and γ-haemolysin mutants was achieved using a defibrinated rabbit blood (TCS Biosciences) assay. Bacteria were grown aerobically overnight at 37ºC in LB medium. The OD_{600} reading was taken and cells were then centrifuged (5,000 x *g*) at 4ºC. The supernatant was filter sterilised to remove any remaining bacterial cells. 50µl of supernatant was then added to 950µl of haemolysin buffer (0.145mM NaCl and 20mM $CaCl_2$) and 25µl rabbit blood, and mixed by inverting. Samples were incubated for 15 minutes at 37ºC and then centrifuged (13,000 rpm) for 1 minute in a tabletop micro litre centrifuge (Heraeus Biofuge Pico). The OD_{543} of the supernatant was then taken (1ml haemolysin buffer and 25µl rabbit blood used as blank).

Haemolysin activity was calculated as follows:

$$OD_{543} \times 1000 / OD_{600} \times 50 \times 0.5 \times 15$$

2.15: Tissue Culture and Cell Invasion Assay

2.15.1: Maintenance of Cell Line

A human respiratory tract epithelial cell line, A549, was used in all cell invasion assays. A549 cells were routinely cultured in Dulbecco modified Eagle medium (DMEM; Sigma) supplemented with 10% foetal bovine

serum (Gibco), 2mM L-glutamine, 5µg ml^{-1} insulin, 1µg ml^{-1} hydrocortisone, 100 U ml^{-1} penicillin and 100µg ml^{-1} streptomycin (Sigma). Cells were grown at 37ºC with 5% CO_2.

2.15.2: Trypsinisation of Monolayer Cultures

Confluent cells were re-seeded into new tissue culture flasks as follows. Medium was removed and cells were washed 3 times with 10ml PBS. 2ml trypsin-EDTA was then added to the flask, which was incubated at 37ºC with 5% CO_2 for 5 minutes. During this incubation period, the flask was intermittently tapped to aid detachment. 8ml fresh medium was added to the flask and cells were resuspended by flushing with a sterile pipette. 2ml of this cell suspension was then used to seed 20ml fresh medium in a fresh tissue culture flask. Flasks were then incubated at 37ºC with 5% CO_2.

2.15.3: Cell Invasion Assay

Bacteria harbouring expression vectors were grown statically overnight at 30ºC in HEPES-buffered Dulbecco modified Eagle medium (DMEM; Sigma) plus 10% (v/v) RPMI, the appropriate antibiotic and 5nM (Ala^5)AIP-1 (McDowell *et al.*, 2001). Bacteria were centrifuged (5,000 x *g*) and then washed with an equal volume fresh medium to remove the (Ala^5)AIP-1. Following a further centrifugation step (5,000 x *g*) bacteria were concentrated 10 fold in DMEM. This suspension was used to inoculate fresh invasion medium (5µg ml^{-1} chloramphenicol) to a final OD_{600} of 0.8 – 1.0.

Tissue culture cells were seeded into a 96-well tissue culture microtiter plate in DMEM (without antibiotic) and grown overnight at 37°C in 5% CO_2 to achieve monolayers. The following morning the medium was removed and replaced with fresh DMEM (HEPES buffered). Cells were then incubated for 1 hour at 37°C in 5% CO_2 before infection with 200µl of the prepared bacterial inoculum. The plate was centrifuged for 20 minutes (1,000 x *g*) to facilitate interaction of the bacteria with the eukaryotic cell surface. The plate was then incubated at 37°C for 1 hour to allow internalisation of the bacteria. For removal of external bacterial cells, tissue culture cell monolayers were washed 3 times with fresh DMEM in an automated plate washer (Cellwash, Thermo Labsystems) and monolayers were then incubated for 20 minutes at 37°C with 200µl of DMEM containing lysostaphin (10 µg ml^{-1}; Sigma). Monolayers were washed again as before, and 200µl HEPES-buffered DMEM containing lysostaphin (2 µg ml^{-1}; Sigma) was added to each well. The tissue culture plate was incubated at 37°C in a Tecan Genios Pro multifunctional detector (Perkin-Elmer Instruments), where fluorescence or bioluminescence and absorbance were monitored over a 24 hour period.

2.16: Animal Work

Female BALB/c mice were obtained from Harlan (Borchen, Germany). Five- to six-week-old female mice were injected subcutaneously with 3.3 x 10^4 murine 4T1 mammary cancer cells (ATCC: CRL-2539) re-suspended

in 100µl PBS. Bacteria were grown in 5ml of LB broth containing 5µg ml^{-1} chloramphenicol until reaching an OD_{600} of 0.4 (corresponding to approximately 2 x 10^8 CFU ml^{-1}) and washed twice in PBS. The suspension was then diluted to approximately 1 x 10^7 CFU ml^{-1} and 100µl injected into the lateral tail vein of 4T1 tumour-bearing BALB/c mice 14 days post cell implantation. Bioluminescence from the mice was monitored with a Nightowl CCD (Berthold) imaging system equipped with isoflurane anaesthesia.

All animal experiments were carried out in accordance with protocols approved by the “Regierung von Unterfranken” (Würzburg, Germany). After sacrificing the mice, organs were removed and homogenised with PBS for plating at various dilutions. Histology was performed using an anti-Protein A antibody followed by a FITC labelled secondary antibody.

3.0: CONSTRUCTION AND *IN VITRO* EVALUATION OF AN MRI REPORTER IN *S. AUREUS*

3.1: Objectives

At present few imaging modalities exist which enable the non-invasive *in vivo* detection of bacterial reporter gene expression while offering detailed anatomical information. One of the main aims of this study, therefore, is to develop such a modality by the construction and *in vitro* evaluation of an MRI bacterioferritin reporter gene for *S. aureus*.

3.2: Introduction

3.2.1: Promoters: P_3, P_{S10} and P_{ahpC}

In the *agr* quorum sensing system, two promoters, P_2 and P_3, drive expression of two divergent transcriptional units, RNAII and RNAIII, respectively. The *agrBDCA* operon encodes the proteins involved in the quorum sensing system: AgrB, AgrD, AgrC and AgrA. AgrB, the processing enzyme, is a transmembrane protein responsible for the modification of the N- and C- terminals of the propeptide, AgrD, via cleavage and condensation, resulting in the formation of the autoinducing peptide (AIP). Together, AgrC and AgrA form the two-component regulatory system. AgrC is a transmembrane histidine-protein kinase

which acts as the receptor for the AIP. Upon binding the AIP, AgrC is phosphorylated, stimulating the transcriptional activator, AgrA. AgrA in turn activates the two promoters, P_2 and P_3, causing increased transcription of the P_2 and P_3 operons at high cell densities (Yarwood and Schlievert, 2003).

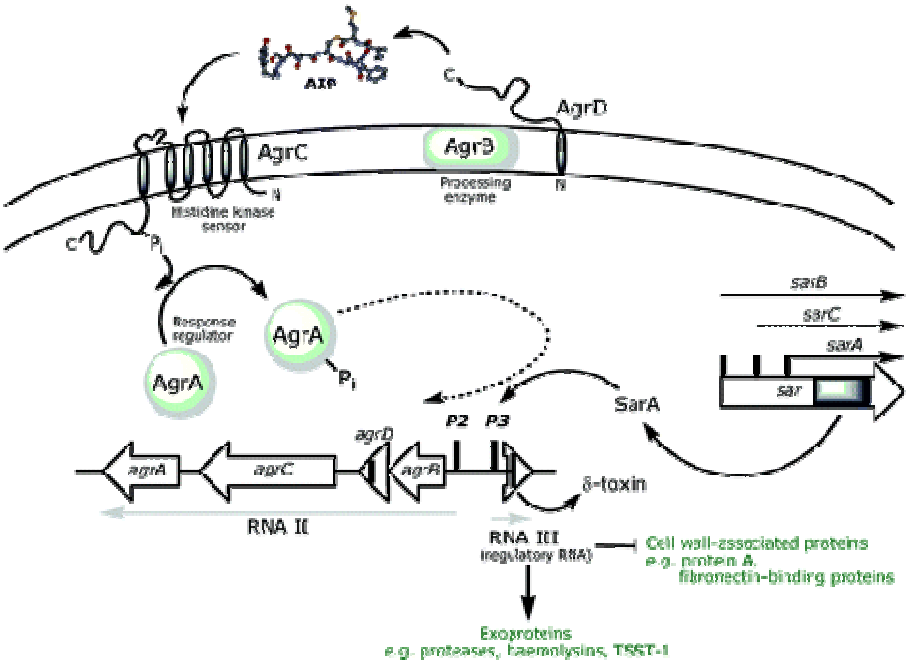

FIGURE 3.1:

Schematic representation of the Staphylococcal quorum sensing system showing the *agr* locus and its regulatory pathways (Chan *et al.*, 2004).

Activation of the P_3 promoter by AgrA causes an increase in the P_3 transcript, RNAIII, in the bacterial cell. RNAIII, the effector molecule, acts at the transcriptional level, increasing expression of secreted bacterial proteins including haemolysins and toxic-shock syndrome toxin (Yarwood and Schlievert, 2003).

The P_{S10} controls transcription of the ribosomal protein gene, *rpsJ*, within bacteria including *E. coli*, *Bacillus subtilis* and *S. aureus*. As a functional part of the 30S ribosomal subunit, the gene product, S10, is necessary for transcription to take place within the bacteria, and as such the P_{S10} can be used as a marker for growth, due to its constitutive expression during bacterial replication.

The P_{ahpC} controls transcription of the *S. aureus ahpC* gene, a homologue of the *E. coli ahpC* gene which encodes part of an alkyl hydroperoxidase reductase involved in protection from oxidative stress. In *S. aureus* the gene product shows homology with that of *E. coli* at the amino acid and secondary protein structure levels, and appears to be expressed in response to osmotic stress (Armstrong-Buisseret *et al*., 1995).

3.2.2: *E. coli* Bacterioferritin

Previous evaluation of a variety of bacterial ferritin-like proteins, namely *bfr*, *fri* and *ftn*, was carried out by Hill *et al*. (manuscript in preparation) for their potential use as MRI reporter genes in prokaryotic studies. Their investigation showed that *E. coli* BFR had the strongest effect on T2 relaxation rates. For these reasons, *E. coli* BFR was chosen as the ferritin of choice for incorporation into an *S. aureus* MRI reporter gene system.

3.2.3: The *lux* Operon

Light is naturally emitted by some bacteria due to presence of an operon consisting of five genes, the *luxCDABE* operon. A luciferase encoded by

luxAB catalyses the oxidation of $FMNH_2$ and a long-chain fatty aldehyde which is synthesised by the *luxCDE* encoded fatty acid reductase. The *lux* operon is widely used experimentally to create bioluminescence in a variety of bacterial species. However, use of the operon in this way has been largely restricted to Gram negative bacteria, since all known naturally occurring bioluminescent bacteria are also Gram negative, making expression of bioluminescence genes in genetically differing Gram positive bacteria more difficult. However, modified *lux* operons with inserted Gram positive RBS have now allowed bioluminescence to be used in Gram positive organisms at a range of temperatures without the need for an exogenous substrate, thus overcoming this issue (Francis *et al*., 2000).

3.3: Results

3.3.1: Construction and Evaluation of Expression Vectors with various Constitutive Promoters

For the construction of the MRI reporters two inducible promoters were selected, *S. aureus* P_3 and P_{ahpC}, for *in vitro* evaluation. Additionally, a constitutive promoter was also required for use in *in vivo* experiments, and as such, the *S. aureus* and *B. subtilis* P_{S10} were chosen for analysis. The *B. subtilis* P_{S10} consists of two adjacent promoter regions, increasing the likelihood that expression of genes downstream of this promoter will be transcribed constitutively during growth (Li *et al*., 1997). Two new expression vectors, pUNK1 Bs P_{S10}-dual-term and pUNK1 Sa P_{S10}-dual-

term, were constructed using the existing Gateway® entry clones, pDONR P4-P1R Bs P_{S10}, containing the *B. subtilis* P_{S10}, pDONR P4-P1R Sa P_{S10}, containing the *S. aureus* P_{S10}, pDONR P221 dual and pDONR P2R-P3 term. These entry clones were combined in LR reactions with the destination vector pDEST-pUNK1 to create pUNK1 Bs P_{S10}-dual-term and pUNK1 Sa P_{S10}-dual-term. For comparison with these new expression vectors for selection of the promoter which gives the highest levels of transcription as indicated by bioluminescence, an existing expression vector, pUNK1 P_{xylA}-dual-term was used. The *xylA* gene is involved in the regulation of expression of xylose utilization genes in *Bacillus megaterium*, and without its cognate repressor, *xylR*, is constitutively expressed in the absence of xylose (Rygus *et al.*, 1991).

All expression vectors were transformed into *S. aureus* RN4220 by electroporation with selection on LB agar supplemented with 5µg ml^{-1} Erm. Transformants were then streaked onto LB agar supplemented with 5µg ml^{-1} Erm and analysed for bioluminescence using an EG & G Berthold luminograph (LB980). Light colonies were re-plated and colonies picked for subjection to plasmid DNA preparation. This DNA was then transformed into *S. aureus* RN6390 by electroporation with selection on LB agar supplemented with 5µg ml^{-1} Erm. Again, transformants were streaked onto LB agar supplemented with 5µg ml^{-1} Erm and analysed for bioluminescence using an EG & G Berthold luminograph (LB980). Light colonies were re-plated and colonies picked for use in a growth curve. The growth curve was carried out in a Tecan Genios Pro multifunctional

detector (Perkin-Elmer Instruments), where bioluminescence and absorbance were monitored.

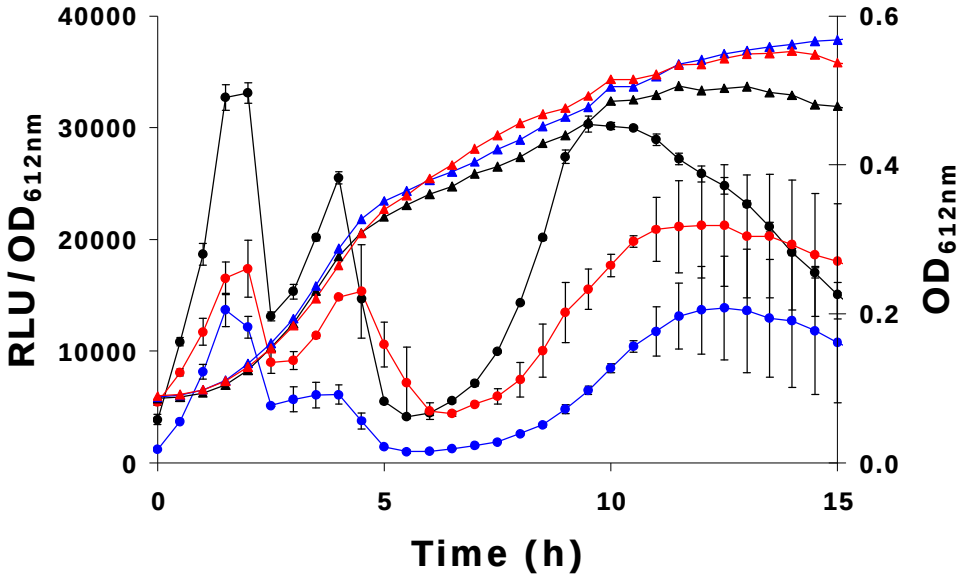

FIGURE 3.2: Bioluminescence as relative light units (RLU) divided by optical density (OD) of *S. aureus* RN6390 pUNK1 Sa P_{S10}-dual-term (●), pUNK1 Bs P_{S10}-dual-term (●) and pUNK1 P_{xylA}-dual-term (●). This data relates to the left y axis. Absorbance of *S. aureus* RN6390 pUNK1 Sa P_{S10}-dual-term (▲), pUNK1 Bs P_{S10}-dual-term (▲) and pUNK1 P_{xylA}-dual-term (▲) is also shown. This data relates to the right y axis. Results represent the mean value of 3 data points for each reading.

The growth curve illustrated in Figure 3.2 shows that, when normalised for growth, the *S. aureus* P_{S10} gives the highest levels of bioluminescence. Taken into account with the fact that Sa P_{S10} is a native *S. aureus* promoter, this promoter was chosen for the MRI reporter constructs. From this point onward this promoter will be referred to as P_{S10} as opposed to Sa P_{S10}.

3.3.2: Construction of pUNK1 P_{S10}-bfr-luxterm, pUNK1 P_3-bfr-luxterm and pUNK1 P_{ahpC}-bfr-luxterm for use as MRI Reporters in *S. aureus*

Primers were designed to amplify the *lux* cassette along with a downstream terminator sequence (rrnBT_1T_2) which occur in succession in an existing vector, pSB3010. Specific *att*B sites were also integrated into the primers to allow for BP reactions with Gateway® entry clones. PCR was carried out with the existing vector to yield product that was then used in BP reactions to create pDONR P2R-P3 luxterm.

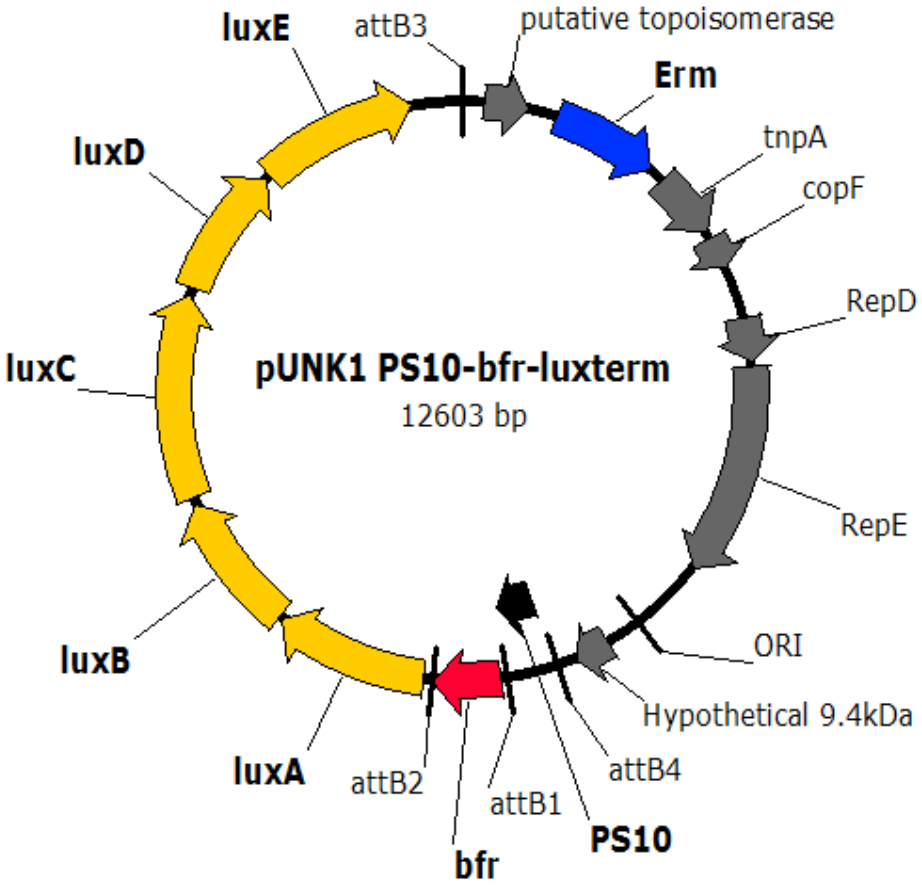

FIGURE 3.3: pUNK1 P_{S10}-bfr-luxterm.

Along with the previously existing Gateway® entry clones pDONR P4-P1R P_3, pDONR P4-P1R Sa P_{S10}, pDONR P4-P1R P_{ahpC} and pDONR P221 bfr (Table 2.1), these newly constructed entry clones were used in LR reactions with the destination vector pDEST-pUNK1 to create pUNK1 P_{S10}-bfr-luxterm, pUNK1 P_3-bfr-luxterm and pUNK1 P_{ahpC}-bfr-luxterm (Figure 3.3).

3.3.3: Evaluation of pUNK1 P_{S10}-bfr-luxterm, pUNK1 P_3-bfr-luxterm and pUNK1 P_{ahpC}-bfr-luxterm

The newly constructed pUNK1 P_{S10}-bfr-luxterm and pUNK1 P_3-bfr-luxterm plasmids were dialysed before transformation into *E. coli* TOP10 by electroporation, and selection on LB agar supplemented with 150µg ml^{-1} Erm. Transformants were then streaked onto LB agar supplemented with 150µg ml^{-1} Erm and analysed for bioluminescence using an EG & G Berthold luminograph (LB980). Light colonies were re-plated and colonies picked for plasmid DNA preparation and confirmation by restriction mapping. This DNA was then transformed into *S. aureus* RN4220, with selection on LB agar supplemented with 5µg ml^{-1} Erm, and bioluminescence screening and plasmid DNA preparation as described above. This DNA was then transformed into *S. aureus* RN6390, with selection on LB agar supplemented with 5µg ml^{-1} Erm, and bioluminescence screening, plasmid DNA preparation and confirmation by restriction mapping as described above.

3.3.3.1: Growth Curves

Growth curves were carried out to evaluate the *in vitro* transcription of the MRI reporter gene operon by analysis of bioluminescence. Additionally, *S. aureus* pUNK1 P_3-bfr-luxterm was grown with varying concentrations of the P_3 promoter inducer, AIP-1, and the promoter inhibitor, (Ala^5)AIP-1, to determine optimal conditions for promoter control (McDowell *et al.*, 2001). *S. aureus* pUNK1 P_{ahpC}-bfr-luxterm was grown with varying concentrations of NaCl, a known promoter inducer (Armstrong-Buisseret *et al.*, 1995).

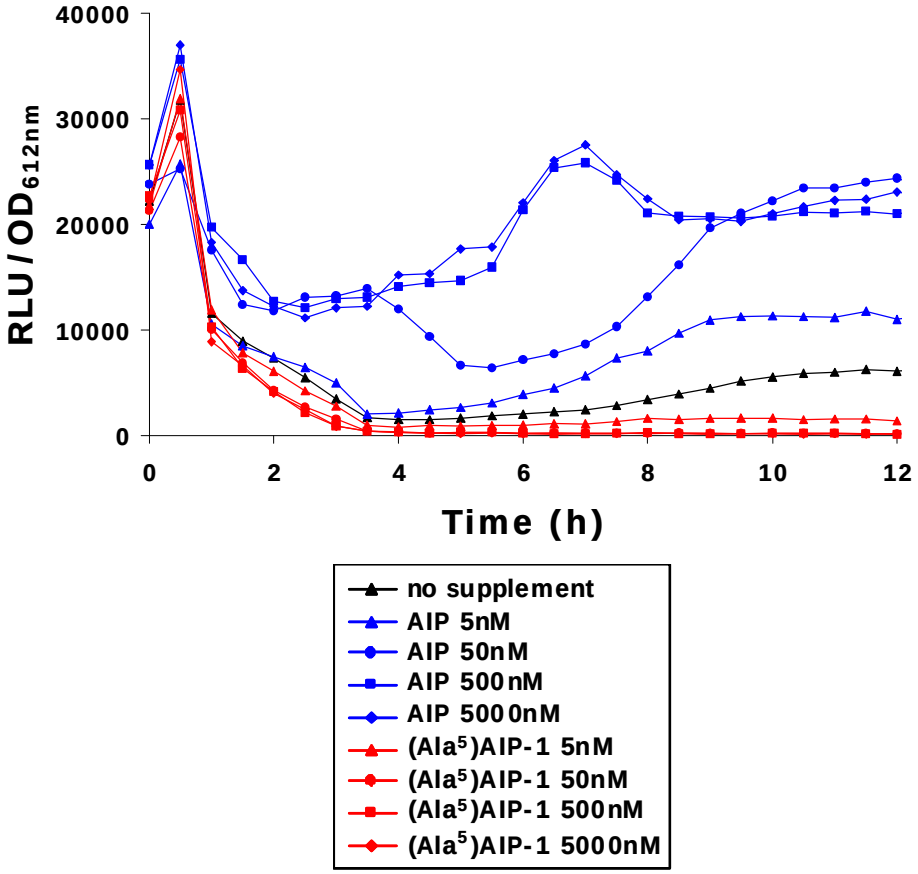

FIGURE 3.4: Bioluminescence measured from growth of *S. aureus* pUNK P_3-bfr-luxterm in the presence of varying concentrations of promoter inducer (AIP) and inhibitor ((Ala^5)AIP-1). Results represent single readings.

As is clear in Figure 3.4, the P_3 promoter is successfully induced with increasing concentrations of AIP-1. The bioluminescence readings from the pUNK1 P_3-bfr-luxterm construct also indicate transcription of the reporter system *in vitro*. Although the P_{ahpC} is also clearly induced by concentrations of NaCl between 0.4-1M (Figure 3.5), these induced levels of bioluminescence peak below 8000 RLU/OD_{600}. Comparing this to the P_3 construct, it is clear that higher levels of light can be induced in the P_3 construct, making it more suitable for *in vivo* studies where the tissue penetration of light can be a problem. It was therefore decided at this point to proceed with the two expression vectors, pUNK1 P_3-bfr-luxterm and pUNK1 P_{S10}-bfr-luxterm.

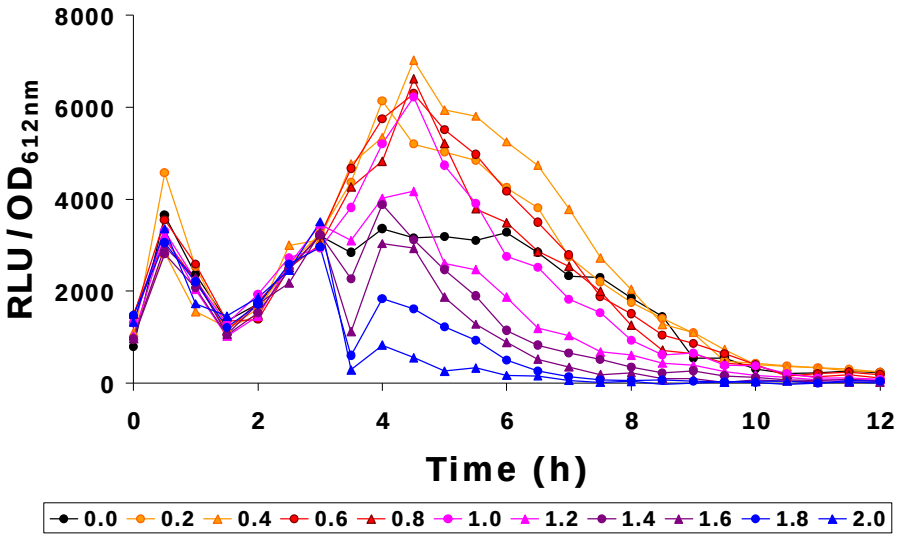

FIGURE 3.5: Bioluminescence measured from growth of *S. aureus* pUNK P_{ahpC}-bfr-luxterm in the presence of varying concentrations of NaCl (M). Results represent single readings.

3.3.3.2: SDS-PAGE of *S. aureus* Lysates from Reporter Constructs

To confirm translation of BFR, SDS-PAGE gels were carried out. Cultures of *S. aureus* harbouring the MRI reporter vectors were grown both with and without the presence of the promoter inducer, where appropriate; for the P_{ahpC} and P_3 promoters these were NaCl at 0.4M and AIP-1 at 5000nM, respectively. *S. aureus* harbouring the P_3 promoter construct was also grown in the presence of (Ala^5)AIP-1 at 5000nM, an inhibitor of the transcription of this promoter. Cell lysates were prepared from these cultures for SDS-PAGE analysis.

SDS-PAGE gels of these samples suggest that the *bfr* genes in the expression vectors are being translated (Figure 3.6). A band of the correct size for the bacterioferritin protein (~20kD) can be seen in both the *E. coli* strain alone, which will produce its own bacterioferritin, and to a heavier extent in the *E. coli* pUNK1 P_{S10}-bfr-luxterm strain. In the *S. aureus* RN6390 strain, no band is present, which is consistent with the fact that *S. aureus* does not produce its own bacterioferritin. Similarly, the control *S. aureus* RN6390 strain harbouring pUNK1 P_{S10}-dual-term, a plasmid of similar size to the *bfr* expression vectors, does not show a band. However, all of the *S. aureus* RN6390 harbouring *bfr* expression vectors show a band of equal size to those present in the *E. coli* strains. Interestingly, despite equal loading of samples in each lane, the strains grown in the presence of promoter inducers do not appear to produce any more bacterioferritin than those without inducer or indeed with inhibitor.

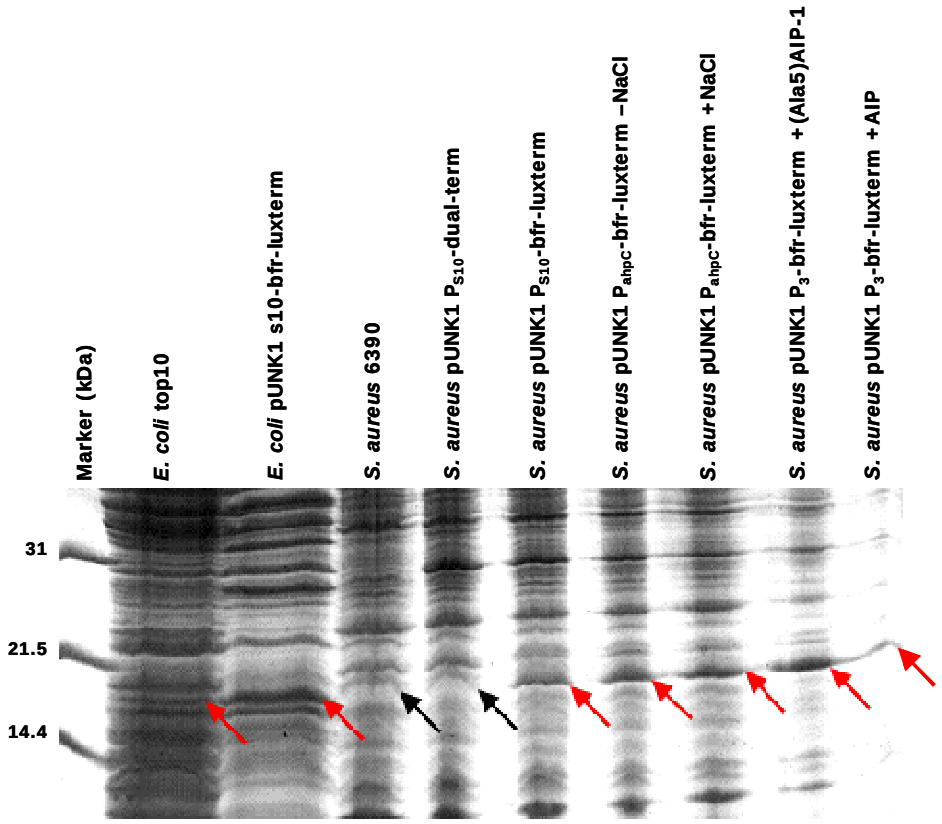

FIGURE 3.6: SDS-PAGE gel of *S. aureus* harbouring expression vectors pUNK1 P_{S10}-bfr-luxterm, pUNK1 P_{ahpC}-bfr-luxterm and pUNK1 P_3-bfr-luxterm. Cultures were grown with supplements of promoter inducers and inhibitors where appropriate. Red arrows indicate the suspected BFR protein, and black arrows indicate a lack of this band in the specified samples.

3.3.3.3: Western Blots

This work was done in conjunction with Dr. Jochen Stritzker from the University of Würzburg in Germany.

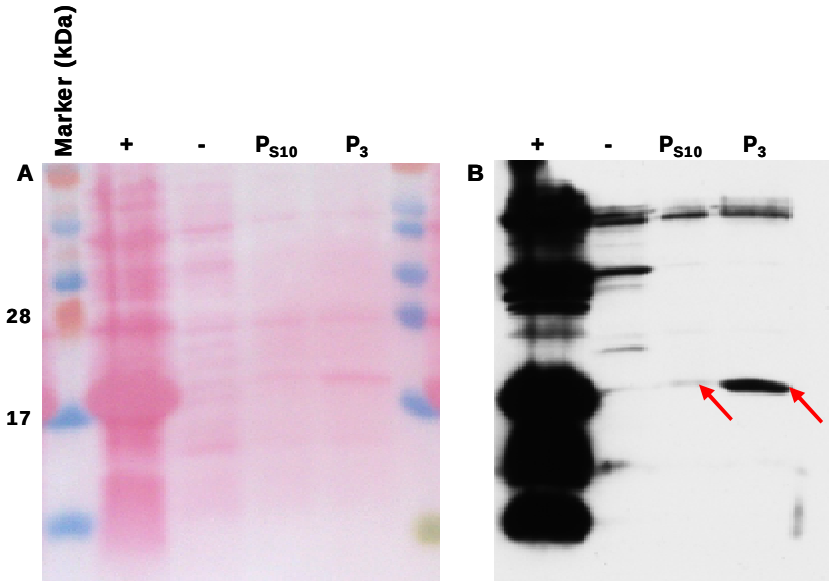

FIGURE 3.7: Western blot of *S. aureus* pUNK1 P_{S10}-bfr-luxterm and *S. aureus* pUNK1 P_3-bfr-luxterm treated with anti-BFR antibody. Positive control (+) purified *E. coli* BFR, negative control (-) *S. aureus* RN6390. Figure shows **(A)** ponceau stain after blotting and **(B)** western developed for 800 seconds. Arrows indicate bands representing the BFR protein.

Western blots were carried out to confirm that the bands seen on the SDS-PAGE gels were in fact bacterioferritin and not a different protein, which would explain the apparent lack of inducibility seen in the SDS-PAGE gels above. A primary rabbit polyclonal antibody against *E. coli* BFR was used with a horseradish peroxidise-linked secondary goat anti-rabbit antibody. The Western blot suggests that the bands seen on the SDS-PAGE gels of the correct size are bacterioferritin, indicating that the expression vectors are being translated *in vitro* (Figure 3.7)

3.3.3.4: Sequencing

Due to the cross-reactivity of the primary antibody which can be seen in Figure 3.7 B, the same samples were again used for SDS-PAGE and the suspected bacterioferritin bands were excised from the gel and sent for sequencing by matrix-assisted laser desorption/ionization mass spectrometry (MALDI-MS). The SDS-PAGE gel can be seen in Figure 3.8. Results indicated that the bands were bacterioferritin, with the top score for both samples being a match with the *E. coli* bacterioferritin protein (Figure 3.9).

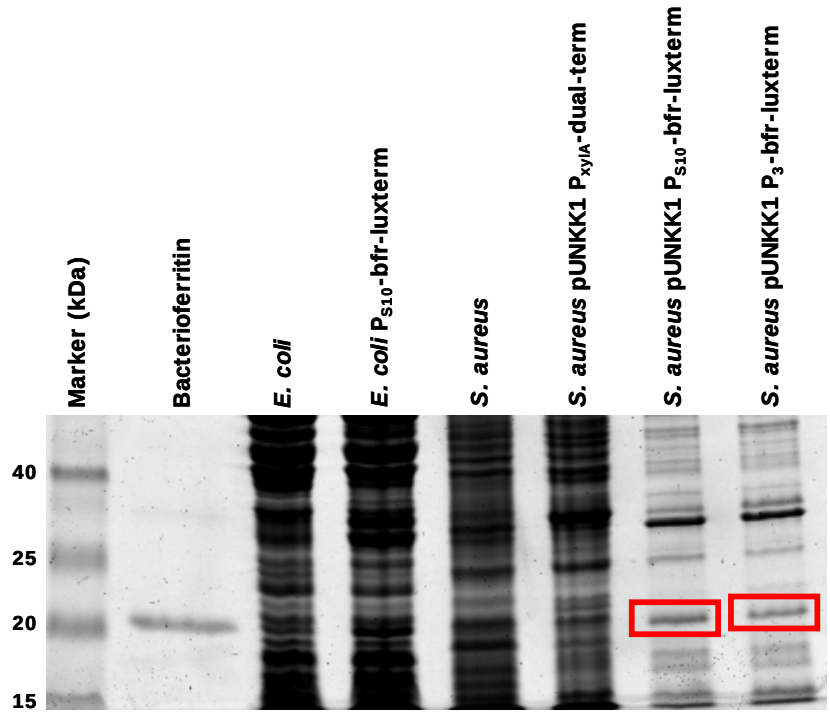

FIGURE 3.8: SDS-PAGE gel of *S. aureus* pUNK1 P_{S10}-bfr-luxterm and *S. aureus* pUNK1 P_3-bfr-luxterm indicating bands sent for sequencing within the red boxes.

Top Score: **133** for gi|16131215, bacterioferritin, iron storage and detoxification protein [Escherichia coli str. K-12 substr. MG1655]

A

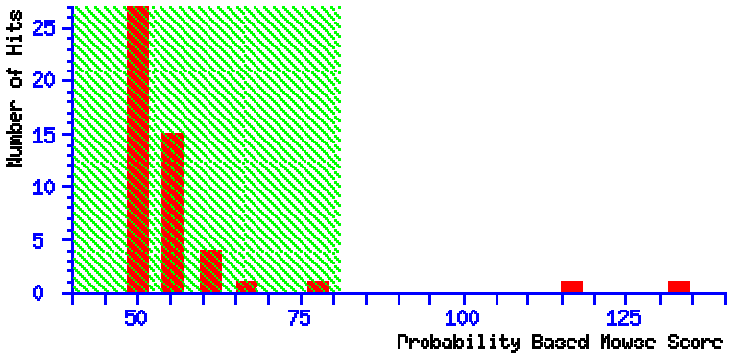

Top Score: **149** for gi|16131215, bacterioferritin, iron storage and detoxification protein [Escherichia coli str. K-12 substr. MG1655]

B

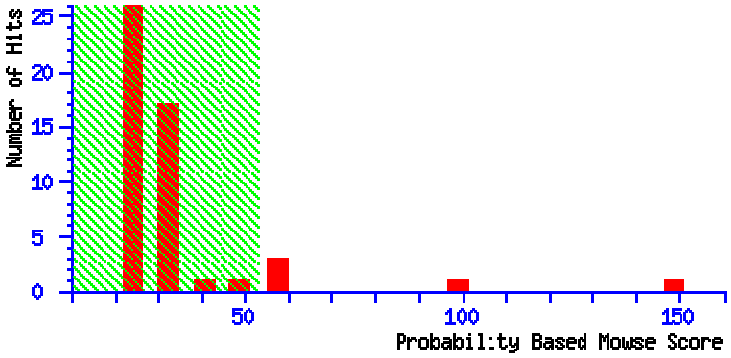

FIGURE 3.9: Sequencing results represented as a Probability Based Mowse Score where the protein score is -10*Log(P), where P is the probability that the observed match is a random event. Protein scores greater than 81 are significant ($p<0.05$). **(A)** Results for band excised from SDS-PAGE gel of *S. aureus* pUNK1 P_3-bfr-luxterm sample and **(B)** results for band excised from SDS-PAGE gel of *S. aureus* pUNK1 P_{S10}-bfr-luxterm sample.

3.3.3.5: ICP-MS

With confirmation of the successful expression of BFR, ICP-MS was carried out on the same samples to determine the amount of iron present in the bacterial cells as an indicator of the BFR function. The results showed no increase in iron concentrations within *S. aureus* RN6390 harbouring the MRI reporter vectors, suggesting that in *S. aureus* the bacterioferritin is non-functional and is not loading with iron (Table 3.1).

In the *E. coli* genome, the *bfr* gene is located downstream of a *bfd* gene, whose product, a [2Fe-2S] protein, forms a complex with BFR. Although the function of this protein is unknown, it has been hypothesised that it may participate in the iron storage function of BFR (Garg *et al*., 1996). This theory would explain the lack of function of the bacterioferritin translated in *S. aureus*, while the *E. coli* strains harbouring the MRI reporter collect more iron due to their native *bfd*.

TABLE 3.1: ICP-MS data showing iron concentration of cell lysates of *S. aureus* harbouring pUNK1 P_{S10}-dual-term and pUNK1 P_{S10}-bfr-luxterm. Figures represent single samples.

Strain	Iron (µg/L)
***S. aureus* pUNK1 P_{S10}-dual-term**	**1213**
***S. aureus* pUNK1 P_{S10}-bfr-luxterm**	**758**

3.3.4: Construction of pUNK1 P_{S10}-bfd/bfr-luxterm and pUNK1 P_3-bfd/bfr-luxterm for use as MRI Reporters in *S. aureus*

To test this hypothesis, new reporter plasmids were constructed incorporating the *bfd* gene, a potential iron loader. Primers were designed to amplify the *bfd* gene alone and the *bfd* gene along with the *bfr* gene from *E. coli*. Specific *att*B sites were also integrated into the primers to allow for BP reactions with Gateway® entry clones. PCR was carried out with *E. coli* TOP10 lysates to yield product that was then used in BP reactions to create pDONR P221 bfd and pDONR P221 bfd/bfr.

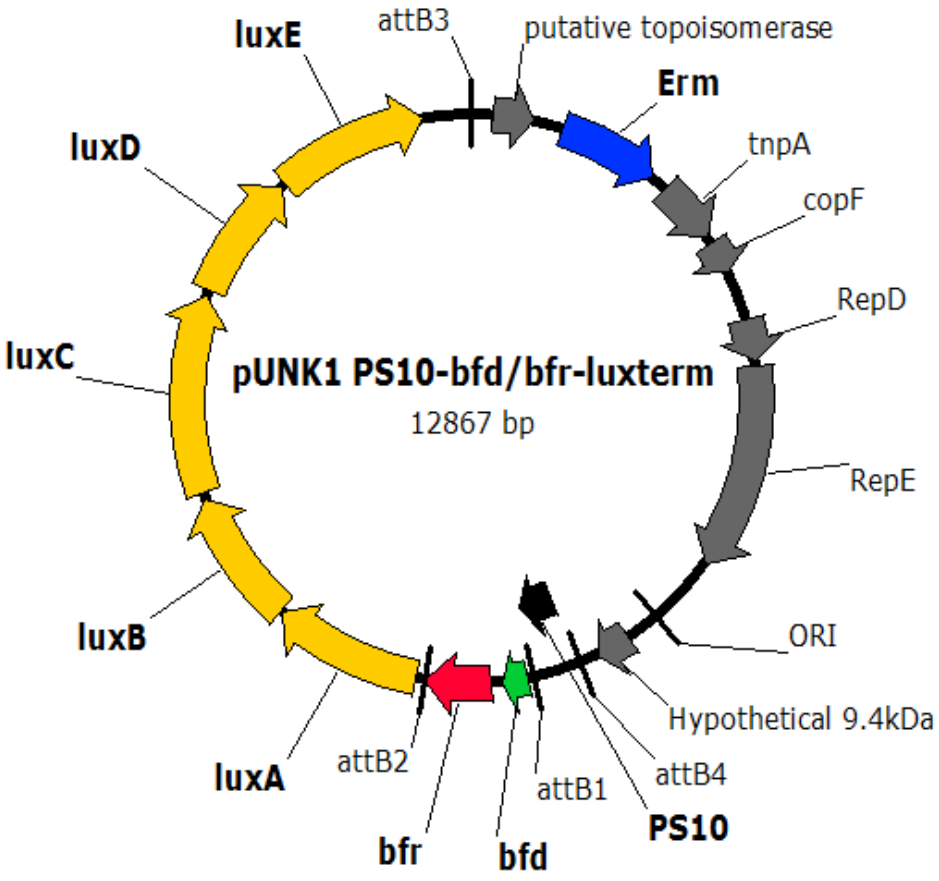

FIGURE 3.10: pUNK1 P_{S10}-bfd/bfr-luxterm

Along with the previously existing Gateway® entry clones pDONR P4-P1R P_3 and pDONR P4-P1R Sa P_{S10}, and the entry clone constructed for this study, pDONR P2R-P3 luxterm, these newly constructed entry clones were used in LR reactions with the destination vector pDEST-pUNK1 to create pUNK1 P_{S10}-bfd-luxterm, pUNK1 P_{S10}-bfd/bfr-luxterm and pUNK1 P_3-bfd/bfr-luxterm (Figure 3.10).

3.3.5: Evaluation of pUNK1 P_{S10}-bfd/bfr-luxterm and pUNK1 P_3-bfd/bfr-luxterm

The newly constructed pUNK1 P_{S10}-bfd-luxterm, pUNK1 P_{S10}-bfd/bfr-luxterm and pUNK1 P_3-bfd/bfr-luxterm plasmids were dialysed before transformation into *E. coli* TOP10 by electroporation, and selection on LB agar supplemented with 150µg ml^{-1} Erm. Transformants were then streaked onto LB agar supplemented with 150µg ml^{-1} Erm and analysed for bioluminescence using an EG & G Berthold luminograph (LB980). Light colonies were re-plated and colonies picked for subjection to plasmid DNA preparation. This DNA was then transformed into *S. aureus* RN4220, with selection on LB agar supplemented with 5µg ml^{-1} Erm, and bioluminescence screening and plasmid DNA preparation as described above. This DNA was then transformed into *S. aureus* RN6390, with further selection on LB agar supplemented with 5µg ml^{-1} Erm, bioluminescence screening and plasmid DNA preparation.

3.3.5.1: SDS-PAGE of *E. coli* and *S. aureus* Lysates from *bfr* and *bfd/bfr* Reporter Constructs

To confirm translation of bacterioferritin from the new expression vectors, SDS-PAGE gels were carried out. Cultures of *E. coli* transformed with pUNK1 P_{S10}-dual-term, pUNK1 P_{S10}-bfd-luxterm, pUNK1 P_{S10}-bfr-luxterm and pUNK1 P_{S10}-bfd/bfr-luxterm were grown and cell lysates prepared. During this process, 1ml of each sample was centrifuged to analyse pellet colour, since *E. coli* is known to change to a pink colour when BFR is expressed due to the haem molecules within the protein.

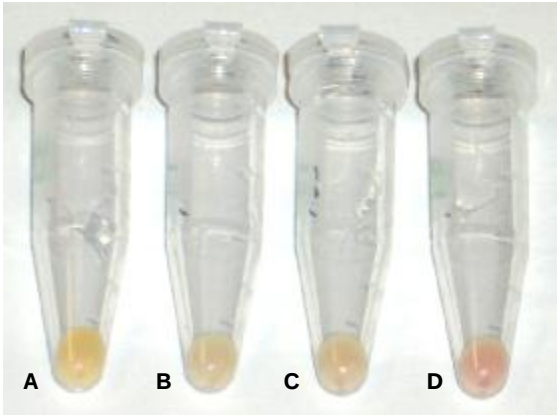

FIGURE 3.11: Pellets from the centrifugation of 1ml culture of *E. coli* harbouring **(A)** pUNK1 P_{S10}-dual-term, **(B)** pUNK1 P_{S10}-bfd-luxterm, **(C)** pUNK1 P_{S10}-bfr-luxterm and **(D)** pUNK1 P_{S10}-bfd/bfr-luxterm.

As can be seen in Figure 3.11, the *E. coli* pUNK1 P_{S10}-bfr-luxterm and pUNK1 P_{S10}-bfd/bfr-luxterm pellets are pinker in colour than the other samples, indicating that BFR is being translated *in vitro* by the new expression vectors. A pinker pellet would be expected in samples

harbouring expression vectors containing the *bfr* gene, due to increased amounts of BFR. However, the colour of the *E. coli* pUNK1 P_{S10}-bfd/bfr-luxterm pellet is significantly pinker than that of *E. coli* pUNK1 P_{S10}-bfr-luxterm, indicating that the *bfd* gene may in some way enhance translation of the *bfr* gene. If this were the case, then the deep pink colour could be attributed to the fact that this expression vector contains both the *bfd* and *bfr* genes, resulting in increased amounts of BFR production in this sample.

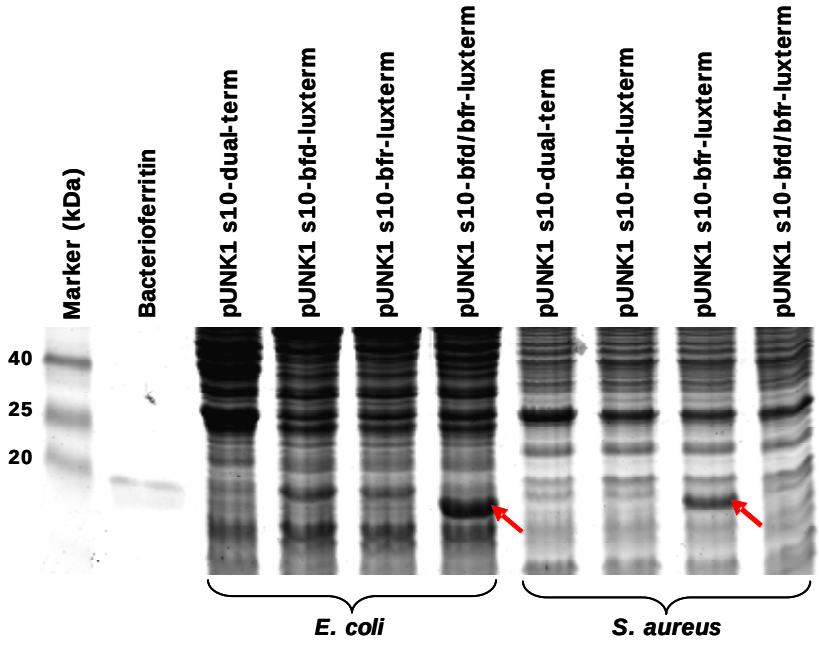

FIGURE 3.12: SDS-PAGE gel of *E. coli* and *S. aureus* RN6390 harbouring pUNK1 P_{S10}-dual-term, pUNK1 P_{S10}-bfd-luxterm, pUNK1 P_{S10}-bfr-luxterm and pUNK1 P_{S10}-bfd/bfr-luxterm. Arrows indicate the thicker bacterioferritin bands seen in the *E. coli* pUNK1 P_{S10}-bfd/bfr-luxterm sample and the *S. aureus* pUNK1 P_{S10}-bfr-luxterm sample.

To determine concentrations of bacterioferritin within each sample, cultures of *S. aureus* RN6390 harbouring the new MRI reporter vectors were also grown and were normalised to an OD_{600} of 0.5. Cell lysates prepared from these cultures were used in SDS-PAGE analysis with the *E. coli* samples.

SDS-PAGE gels of the *E. coli* samples used for pellet analysis also suggest that the pink colour seen in the pellet from centrifugation of the *E. coli* pUNK1 P_{S10}-bfd/bfr-luxterm was due to an increase in the amount of BFR, due to the thicker band seen on the gel for this sample (Figure 3.12).

Interestingly, unlike the *E. coli* samples, the *S. aureus* harbouring the pUNK1 P_{S10}-bfr-luxterm is the sample which produced the most bacterioferritin, with no visible band seen in the *S. aureus* pUNK1 P_{S10}-bfd/bfr-luxterm sample. As would be expected, the *S. aureus* pUNK1 P_{S10}-bfd-luxterm did not see any bacterioferritin synthesised as *S. aureus* does not have a bacterioferritin gene within its genome. However, it would be expected that the *bfr* gene within the expression vector pUNK1 P_{S10}-bfd/bfr-luxterm would be expressed, causing the synthesis of bacterioferritin. All samples contained the same quantity of protein so this could not explain the lack of bacterioferritin seen in the *S. aureus* pUNK1 P_{S10}-bfd/bfr-luxterm sample.

3.3.5.2: Iron Assay

Before cell lysates were prepared for SDS-PAGE analysis as described, samples of the bacterial cultures were taken and subjected to the QuantiChrom™ Iron Assay.

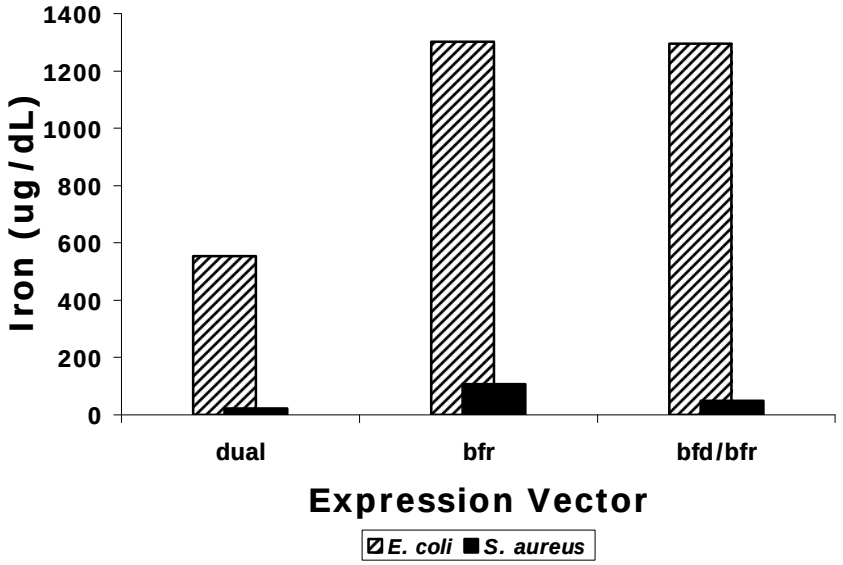

FIGURE 3.13: Iron levels of cell lysates of *S. aureus* and *E.coli* harbouring pUNK1 P_{S10}-dual-term (dual), pUNK1 P_{S10}-bfr-luxterm (bfr) and pUNK1 P_{S10}-bfd/bfr-luxterm (bfd/bfr).

As can be seen in Figure 3.13, higher concentrations of iron were present in cell lysates of *E. coli* harbouring expression vectors with the incorporated *bfr* gene, suggesting that the BFR being produced is functional and is binding iron. Presence of the *bfd* did not appear to increase iron concentrations, even with more BFR in this sample, but this could be due to sufficient gene product from the native *E. coli bfd*, and so a role for the *bfd* gene product in iron loading can not be determined from this data. In contrast to previous ICP-MS analysis of *S. aureus* strains

harbouring *bfr* expression vectors, the iron assay clearly demonstrates an almost 5 fold increase in iron concentrations in *S. aureus* pUNK1 P_{S10}-bfr-luxterm. However, although some iron appears to have been collected in the *S. aureus* pUNK1 P_{S10}-bfd/bfr-luxterm strain, it is to a much lesser extent than that seen in *S. aureus* pUNK1 P_{S10}-bfr-luxterm. Despite this, an iron loading role for *bfd* cannot be ruled out, since SDS-PAGE analysis showed that the pUNK1 P_{S10}-bfd/bfr-luxtrem plasmid does not appear to cause synthesis of large amounts of bacterioferritin. The lack of iron collection could therefore be due to a lack of bacterioferritin rather than due to the lack of iron loading.

3.3.5.3: ICP-MS

Due to the differences noted between data from the iron assay described above and the preliminary ICP-MS data carried out on the original expression vectors, ICP-MS was carried out again using the same samples prepared for the iron assay (Table 3.2).

TABLE 3.2: ICP-MS data showing iron concentration of cell lysates of *S. aureus* harbouring pUNK1 P_{S10}-dual-term and pUNK1 P_{S10}-bfr-luxterm. Figures represent single samples.

Strain	Iron (µg/L)
***S. aureus* pUNK1 P_{S10}-dual-term**	**135**
***S. aureus* pUNK1 P_{S10}-bfr-luxterm**	**174**

As with the iron assay, this data clearly shows an increase in iron concentration in *S. aureus* pUNK1 P_{S10}-bfr-luxterm, indicative of functioning BFR in this strain.

3.3.5.4: Evaluation of Plasmid Loss

In order to determine the reason for the lack of iron collection seen in the *S. aureus* pUNK1 P_{S10}-bfd/bfr-luxterm strain, the *S. aureus* samples were grown both with and without antibiotic selection to establish any potential role played by plasmid loss due to inactivation of antibiotic (Figure 3.14).

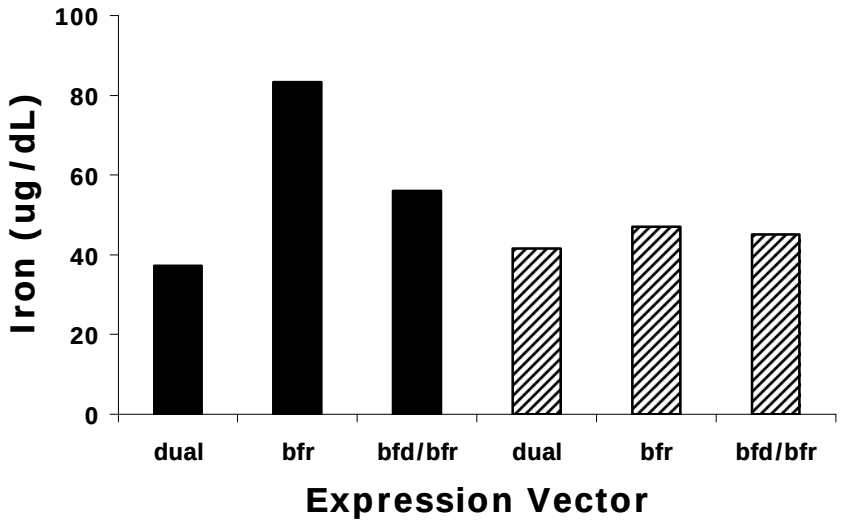

FIGURE 3.14: Iron levels in cell lysates of *S. aureus* pUNK1 P_{S10}-dual-term (dual), pUNK1 P_{S10}-bfr-luxterm (bfr) and pUNK1 P_{S10}-bfd/bfr-luxterm grown in the presence of 5μg ml^{-1} Erm (black columns) and without antibiotics (striped columns).

Some plasmid loss appears to have occurred in both *S. aureus* pUNK1 P_{S10}-bfr-luxterm and pUNK1 P_{S10}-bfd/bfr-luxterm as indicated by the

reduced iron concentrations in cell lysates from cultures grown without antibiotic present. However, SDS-PAGE analysis of the same samples suggests that despite potential plasmid loss, both strains grown with and without antibiotic selection appear to make the same quantity of protein, which implies that plasmid loss is not the cause of reduced iron collection in *S. aureus* pUNK1 P_{S10}-bfd/bfr-luxterm (Figure 3.15).

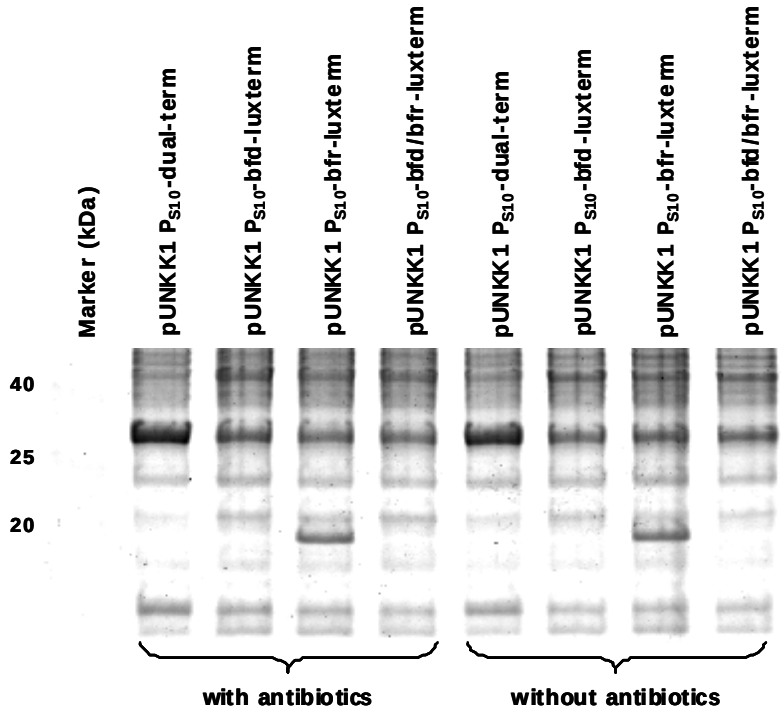

FIGURE 3.13: SDS-PAGE gel of *S. aureus* harbouring pUNK1 P_{S10}-dual-term, pUNK1 P_{S10}-bfd-luxterm, pUNK1 P_{S10}-bfr-luxterm and pUNK1 P_{S10}-bfd/bfr-luxterm grown with (5μg ml^{-1} Erm) and without antibiotic selection.

3.3.5.5: Sequencing

To ensure there were no mutations within the plasmid that may be responsible for the lack of production of BFR, a sample of the plasmid

DNA prepared from *S. aureus* RN6390 was sent for sequencing. The sequencing revealed no mutations within the plasmid, indicating that this was not a cause for the failed expression of BFR.

3.3.5.6: Bioluminescence Assays to Determine any Interference of Transcription or Translation due to *bfd* Gene

The apparent BFR expression and iron collection in the *S. aureus* pUNK1 P_{S10}-bfr-luxterm strain demonstrates the ability for the *in vivo* expression of the MRI reporter in *S. aureus*, and the functionality of the translated BFR. Taking this into account, it would appear that the *bfd* is perhaps affecting the transcription or translation of the downstream *bfr* in the pUNK1 P_{S10}-bfd/bfr-luxterm reporter.

The *bfd* gene is not native to *S. aureus* strains. It is therefore possible that this gene contains a transcription terminator sequence recognised in *S. aureus*, causing termination of transcription before the ribosome reaches the *bfr* gene. If this is the case, then no light would be seen from the *S. aureus* pUNK1 P_{S10}-bfd/bfr-luxterm due to lack of transcription of the *lux* operon downstream of the *bfr* gene. If the presence of the *bfd* gene is somehow affecting the translation of the *bfr* gene, then bioluminescence would still be expected as the genes of the *lux* operon have their own ribosome binding sites (RBS).

To test this hypothesis, light assays were carried out using *S. aureus* RN6390 samples harbouring pUNK1 P_{S10}-bfr-luxterm and pUNK1 P_{S10}-bfd/bfr-luxterm.

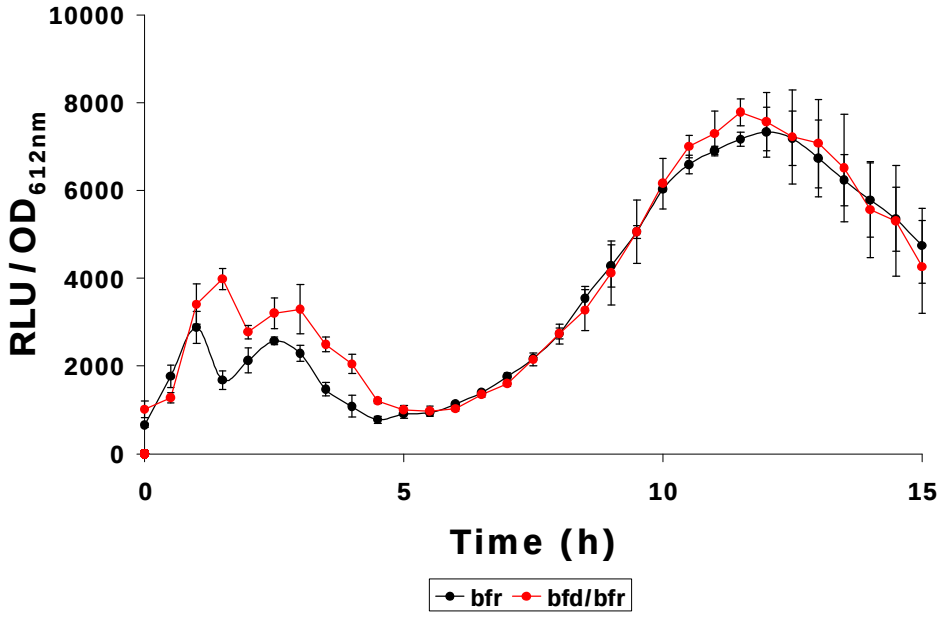

FIGURE 3.16: Bioluminesce relative to growth of *S. aureus* harbouring pUNK1 P_{S10}-bfr-luxterm and pUNK1 P_{S10}-bfd/bfr-luxterm. Results represent the mean value of 3 data points for each reading.

As can be seen in Figure 3.16, *S. aureus* pUNK1 P_{S10}-bfd/bfr-luxterm is emitting light levels similar to those from *S. aureus* pUNK1 P_{S10}-bfr-luxterm, suggesting that the *lux* operon in the *S. aureus* pUNK1 P_{S10}-bfd/bfr-luxterm reporter gene has been translated. This supports the proposal that the *bfd* gene is not stopping transcription of the *bfr* gene, but is more likely having some effect on the translation of the *bfr* gene. Furthermore, the fact that the levels of light are as high in the *S. aureus*

harbouring pUNK1 P_{S10}-bfd/bfr-luxterm as they are in the *S. aureus* harbouring pUNK1 P_{S10}-bfr-luxterm, suggests that the *bfd* gene is neither stopping nor affecting the level of transcription of the MRI reporter gene transcript.

4.0: CONSTRUCTION AND CHARACTERISATION OF A *hlb* MUTANT AND CHARACTERISATION OF EXISTING HAEMOLYSIN MUTANTS IN *S. AUREUS*

4.1: Objectives

Although it is clear that *agr* regulated genes have a role in endosomal escape of internalised *S. aureus*, it is not fully clear which genes specifically are important. A number of haemolysin genes are under the control of the *agr* system, all of which have the ability to disrupt eukaryotic cell membranes. With these factors in mind, haemolysins appear to be ideal candidates in the study of genes involved in endosomal escape of internalised *S. aureus*. One of the aims of this study, therefore, was to determine the role of *S. aureus* haemolysins in endosomal escape of internalised *S. aureus* with the intention of tracking bacterial gene expression *in vivo* using MRI expression vectors developed in this study.

4.2: Introduction

As described earlier, *S. aureus* has been shown to demonstrate intracellular survival strategies, with the ability to become internalised by, and persist within, a wide range of non-professional eukaryotic

phagocytes. Once internalisation has occurred, *S. aureus* is situated in a host membrane-bound endosome. However, *S. aureus* has been shown to have the ability to escape this endosome, residing and potentially replicating in the host cell cytoplasm (Bayles *et al.*, 1998; Wesson *et al.*, 1998). *S. aureus* replication within bovine mammary epithelial cells has been demonstrated by Qazi *et al.* (2004) using fluorescently labelled bacteria and time-lapse confocal microscopy. *S. aureus* has also been shown to replicate intracellularly within a human pulmonary epithelial cell line (Kahl *et al.*, 2000).

Although it has been shown that internalised *S. aureus* breach the endosome, the mechanisms via which this escape occurs are not well understood. Wesson *et al.* (1998) have suggested a model describing a role for *agr*-regulated quorum sensing in *S. aureus* internalisation and endosomal escape. The model proposes that before internalisation, the autoinducer peptide (AIP) levels are low, due to dilution into surrounding extracellular fluids, resulting in expression of cell-surface associated adherence factors by *S. aureus*. Expression of such factors at this stage facilitates binding of *S. aureus* to host cell surfaces, thus promoting internalisation. Once internalised, the bacteria are bound within an endosome, within which concentrations of the AIP increase, triggering *agr* expression, and subsequently production of the many exoproteins up-regulated by this quorum sensing system. It is thought that some of these exoproteins then function in endosomal escape. This model is supported by the observation that an *agr* mutant, *S. aureus* RN6911, which produces

increased levels of cell surface binding proteins and lower amounts of exoproteins, was internalised at higher efficiencies in bovine mammary epithelial cells than the wild-type strain, but was unable to replicate intracellularly (Wesson *et al*., 1998; Qazi *et al*., 2004).

4.3: Results

4.3.1: Construction of pTS1-Dest *hlb* for use in *S. aureus* Mutagenesis

Primers were designed to amplify approximately 1000bp of both the upstream and downstream regions flanking the *hlb* gene responsible for the production of β-haemolysin from *S. aureus* RN6390 genomic DNA. Specific *att*B sites were also integrated into the primers to allow for BP reactions with Gateway® entry clones. *S. aureus* RN6390 genomic DNA was used in PCR with the newly designed primers yielding product which was used in BP reactions, creating pDONR P4-P1R::*hlb* up and pDONR P2R-P3::*hlb* down (Figure 4.1 A and Figure 4.2 A). These new entry clones were transformed into *E. coli* TOP10 by electroporation with selection on LB agar supplemented with 50µg ml^{-1} Km. Transformants were then streaked onto fresh LB agar supplemented with 50µg ml^{-1} Km and colonies picked for plasmid DNA preparation and confirmation by restriction mapping.

A

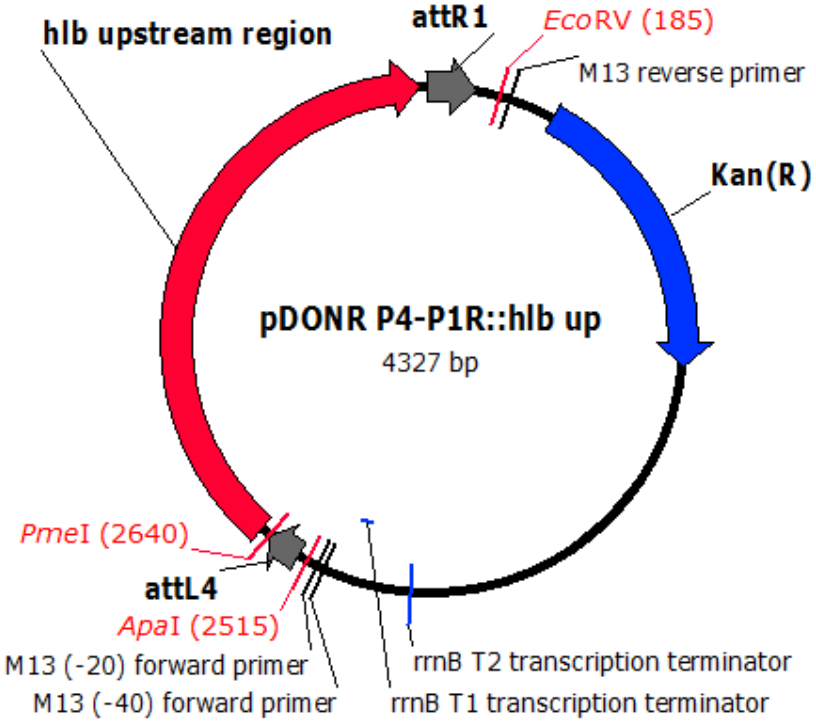

B

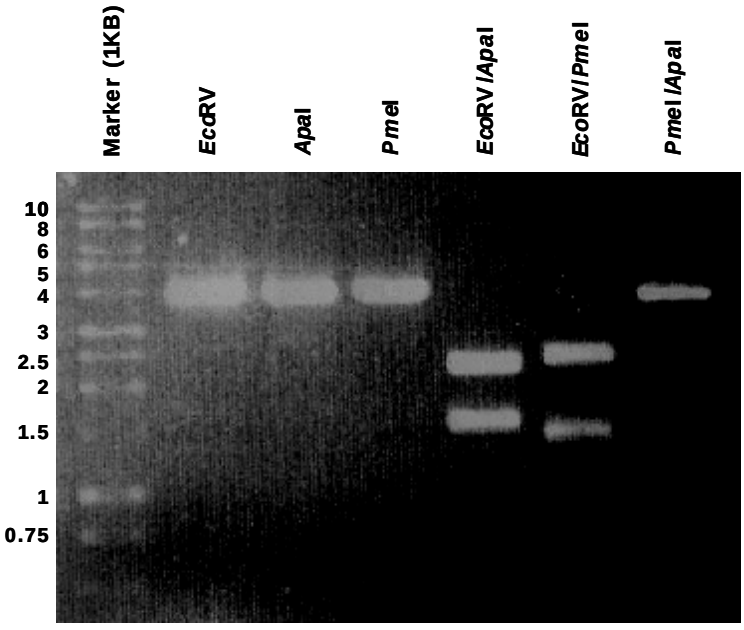

FIGURE 4.1: (A) pDONR P4-P1R::*hlb* up and **(B)** agarose gel electrophoresis of pDONR P4-P1R::*hlb* up fragments, after restriction with *Apa*I, *Eco*RV and *Pme*I.

A

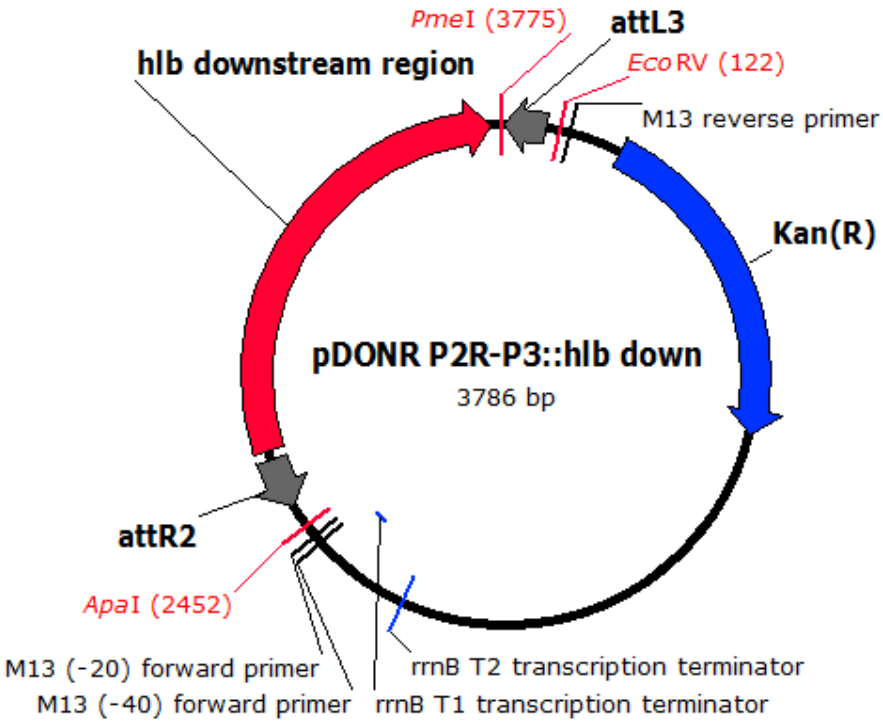

B

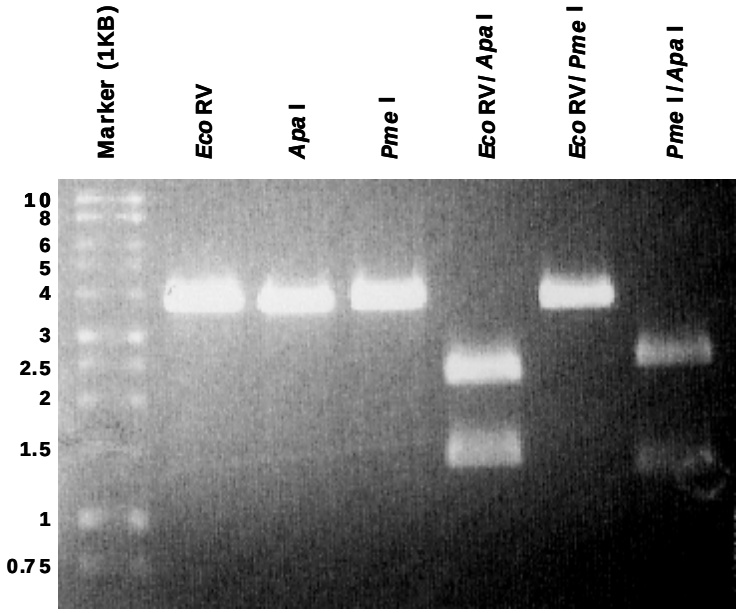

FIGURE 4.2: (A) pDONR P2R-P3::*hlb* down and **(B)** agarose gel electrophoresis of pDONR P2R-P3::*hlb* down fragments, after restriction with *Apa*I, *Eco*RV and *Pme*I.

Bands of the sizes expected after analysis of the new plasmid maps constructed using Vector NTI software (Invitrogen) were visualised on an agarose gel by electrophoresis, indicating that the BP reactions were successful (Figure 4.1 B and Figure 4.2 B).

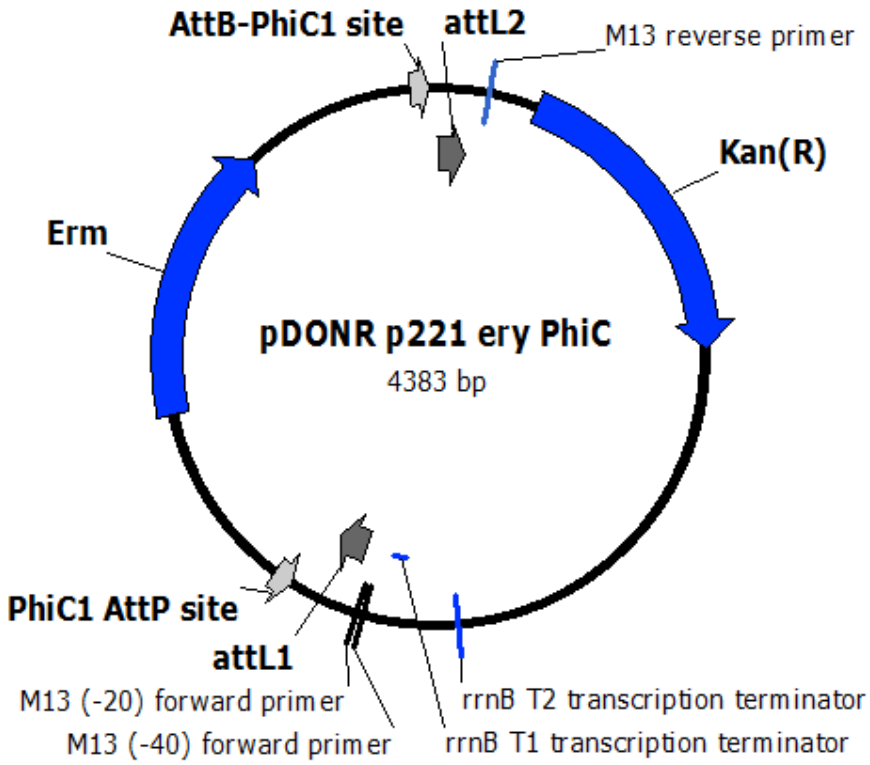

FIGURE 4.3: pDONR P221 ery PhiC

Along with pDONR p221 ery PhiC (Figure 4.3), these newly constructed entry clones were used in an LR recombination reaction with a Gateway® destination vector, pTS1-Dest +lac, to create pTS1-Dest *hlb* (Figure 4.4 A and Figure 4.5).

A

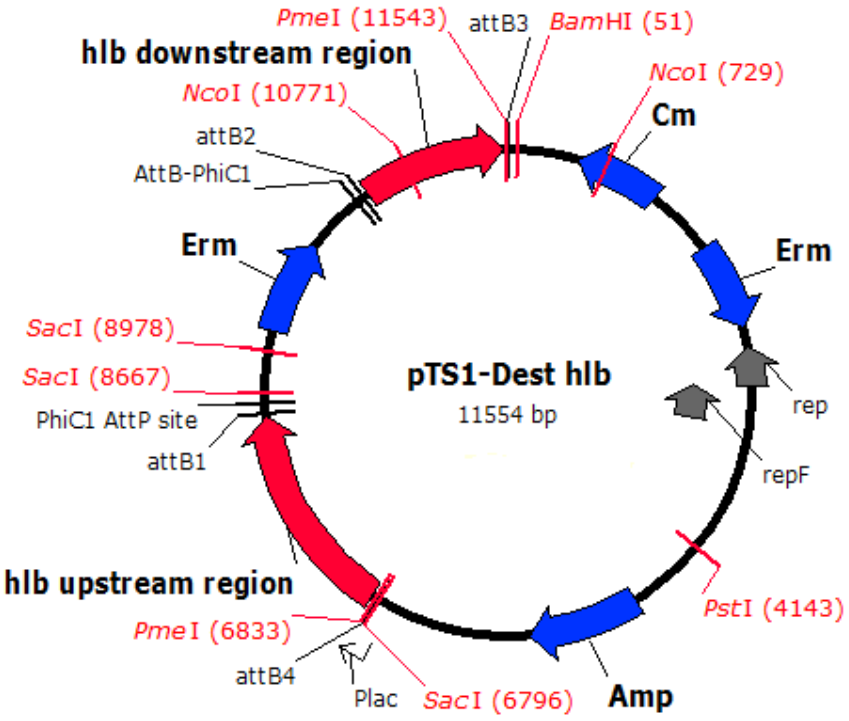

B

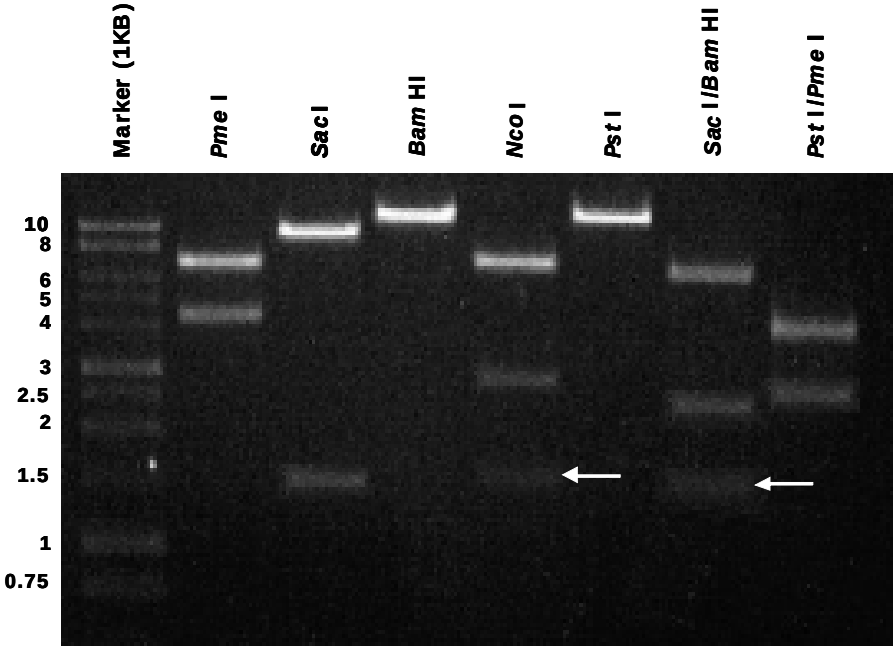

FIGURE 4.4: (A) pDTS1-Dest *hlb* and **(B)** agarose gel electrophoresis of pDTS1-Dest *hlb* fragments, after restriction with *Pme*I, *Sac*I, *Bam*HI, *Nco*I, and *Pst*I. White arrows are present to highlight less visible bands.

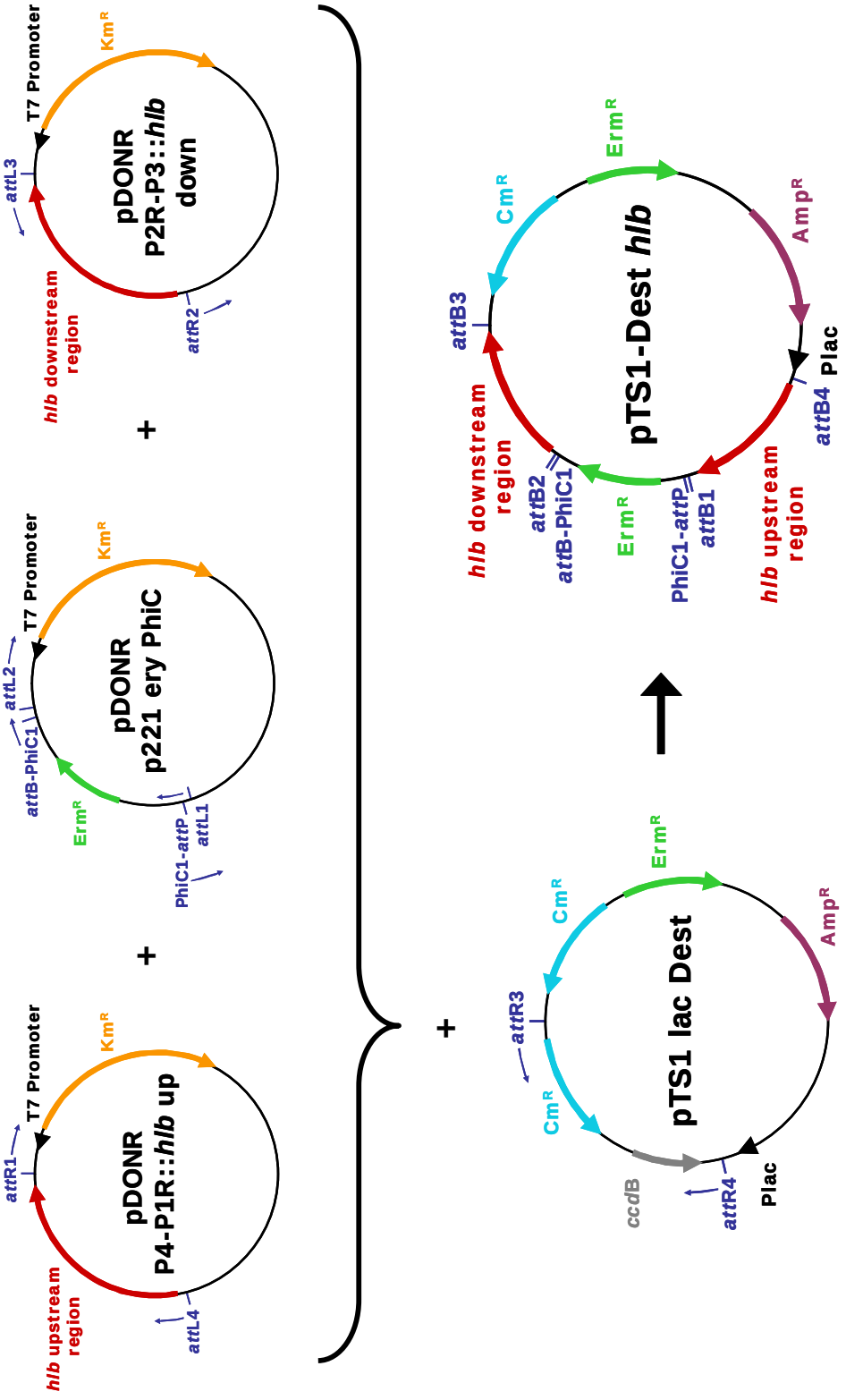

FIGURE 4.5: Schematic diagram showing the construction of pTS1-Dest *hlb* from three entry clones and a destination vector with specific *att* sites.

This new plasmid was transformed into *E. coli* TOP10 by electroporation with selection on LB agar supplemented with 100µg ml^{-1} Amp. Transformants were then streaked onto fresh LB agar supplemented with 100µg ml^{-1} Amp and colonies picked for plasmid DNA preparation and confirmation by restriction mapping.

Bands of the sizes expected after analysis of the new plasmid map constructed using Vector NTI software (Invitrogen) were visualised on an agarose gel by electrophoresis, indicating that the LR recombination reaction was successful (figure 4.4 B).

4.3.2: Mutagenesis in *S. aureus* using pTS1-Dest *hlb*

The newly constructed pTS1-Dest *hlb* was used in the mutagenesis of *S. aureus* RN6390 to create a *hlb* mutant with resistance to erythromycin. The newly constructed temperature sensitive pTS1-Dest *hlb* mutagenesis plasmid was transformed into *S. aureus* RN4220 by electroporation with selection on LB agar supplemented with 5µg ml^{-1} Erm and 5µg ml^{-1} Cm, and incubation overnight at 30°C. Transformants were then streaked onto fresh LB agar supplemented with 5µg ml^{-1} Erm and 5µg ml^{-1} Cm, incubated overnight at 30°C and colonies then picked for subjection to plasmid DNA preparation. This DNA was then transformed into *S. aureus* RN6390 by electroporation with selection on LB agar supplemented with 5µg ml^{-1} Erm and 5µg ml^{-1} Cm. Transformants were grown overnight statically in LB supplemented with 5µg ml^{-1} Erm and 5µg ml^{-1} Cm at 30°C to facilitate recombination, followed by plating on LB agar supplemented

with 5µg ml^{-1} Erm before incubation overnight at 42°C to promote plasmid loss. Any colonies were replica plated onto LB agar supplemented with 5µg ml^{-1} Cm and then LB agar supplemented with Erm and 5µg ml^{-1} before incubation overnight at 37°C. Genomic DNA purification of colonies which grew on LB agar supplemented with 5µg ml^{-1} Erm but not Cm was carried out and the DNA from these putative mutants was screened by PCR using different primers to confirm the occurrence of a double cross.

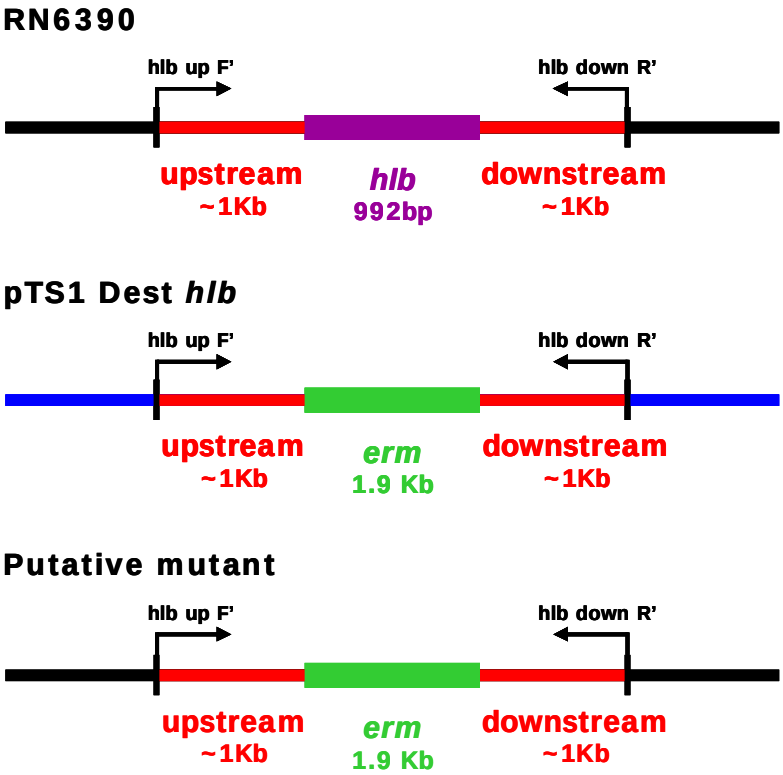

FIGURE 4.6: Schematic diagram showing the annealing sites for the hlb up F' and hlb down R' primers, of *S, aureus* RN6390, pTS1-Dest *hlb* and a Δ*hlb*. The black line represents the *S. aureus* RN6390 genome and the blue line represents the pTS1-Dest *hlb* backbone.

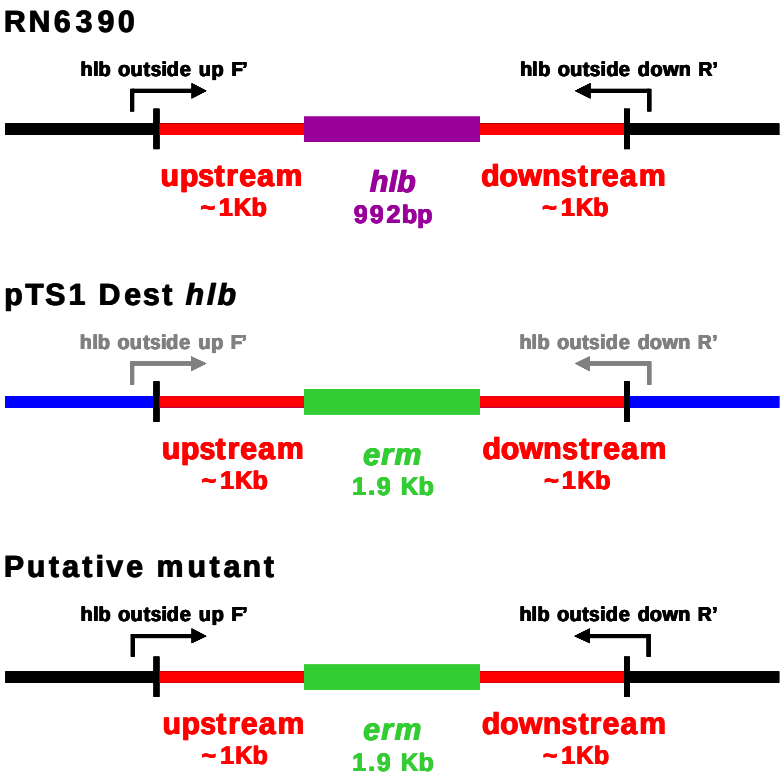

FIGURE 4.7: Schematic diagram showing the annealing sites for the hlb outside up F' and hlb outsite down R' primers, of *S, aureus* RN6390, pTS1-Dest *hlb* and a Δ*hlb*. The black line represents the *S. aureus* RN6390 genome and the blue line represents the pTS1-Dest *hlb* backbone. Primers in grey text would not yield product due to lack of an annealing site.

As can be seen in Figure 4.8, primers specific to regions outside of the 1Kb upstream and downstream regions of the *hlb* gene incorporated in the pTS1-Dest *hlb*, give no product from the plasmid, as would be expected, but show product from the wild type *S. aureus* RN6390 and the putative mutant. The band from the putative mutant however, is approximately 900bp bigger than that from RN6390, due to deletion of the 992bp long *hlb* gene and replacement with the 1.9Kb long *erm* cassette. Primers for the

hlb upstream and downstream region yield equally large bands from the plasmid and putative mutant, since the product should be of exactly the same sequence; upstream and downstream regions of *hlb* with the incorporated *erm* cassette. The *S. aureus* RN6390 shows a smaller band since the PCR product is simply the upstream and downstream regions flanking the *hlb* gene, without any inserted antibiotic marker (Figure 4.6 and Figure 4.7).

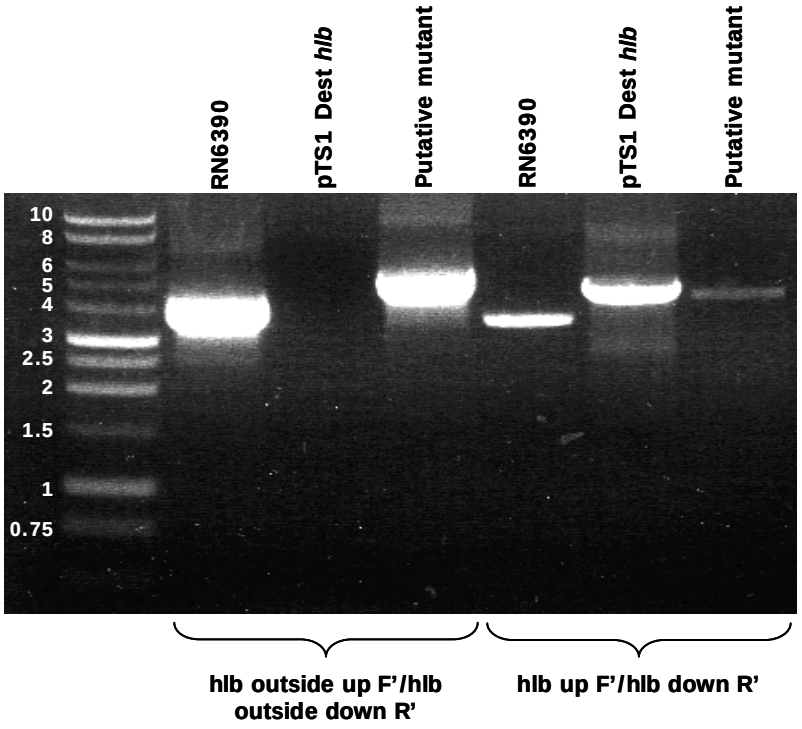

FIGURE 4.8: Agarose gel electrophoresis showing PCR products from PCR of genomic DNA from *S. aureus* RN6390 and a putative *S. aureus* RN6390 *hlb* mutant, and pTS1-Dest *hlb* plasmid DNA, using primers specific for the regions outside of the regions used to construct the pTS1-Dest *hlb* plasmid and primers specific for regions outside of the *hlb* gene which were used to construct the pTS1-Dest *hlb* plasmid.

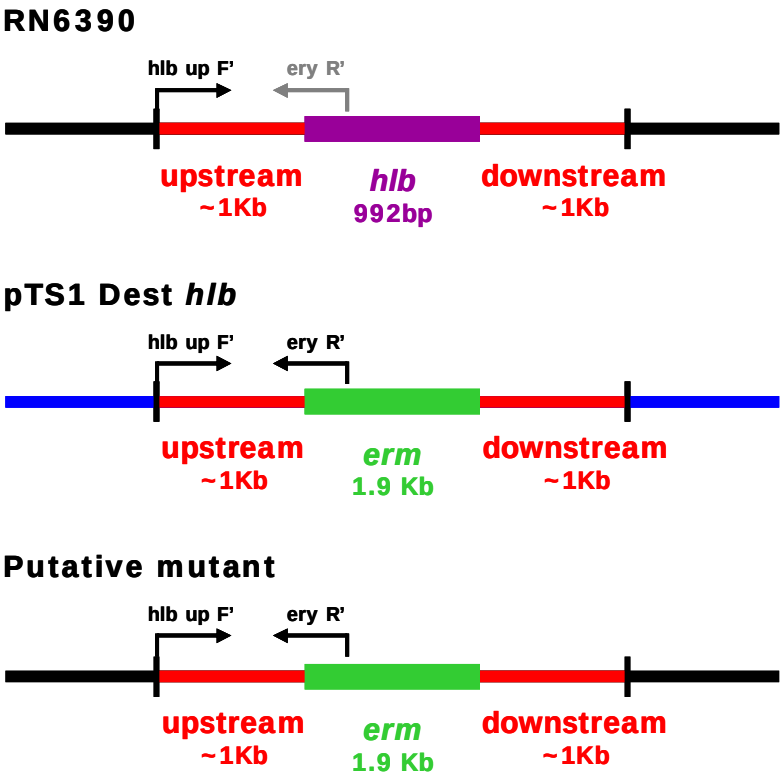

FIGURE 4.9: Schematic diagram showing the annealing sites for the hlb up F' and ery R' primers, of *S, aureus* RN6390, pTS1-Dest *hlb* and a Δ*hlb*. The black line represents the *S. aureus* RN6390 genome and the blue line represents the pTS1-Dest *hlb* backbone. Primers in grey text would not yield product due to lack of an annealing site.

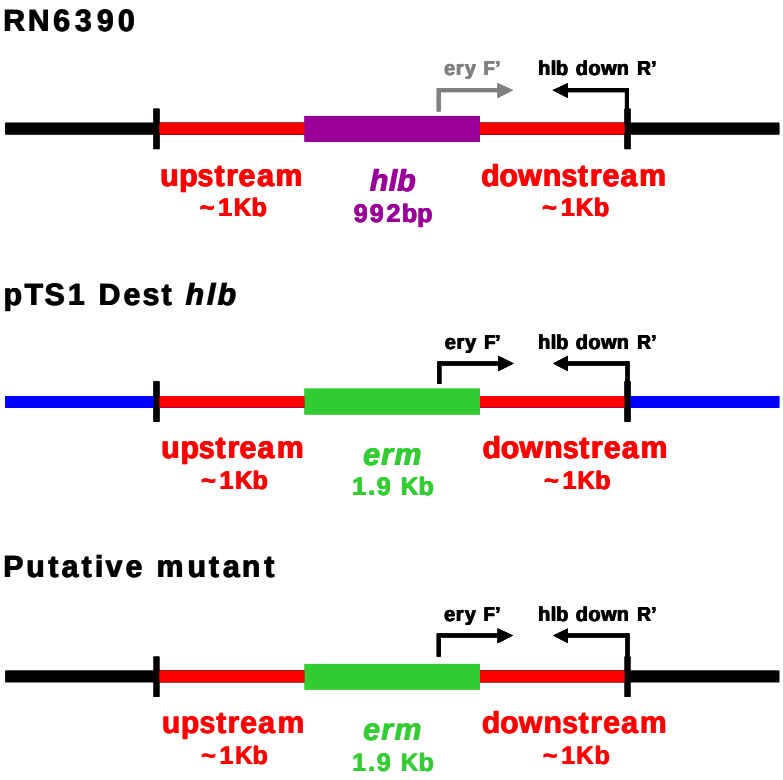

FIGURE 4.10: Schematic diagram showing the annealing sites for the ery F' and hlb down R' primers, of *S, aureus* RN6390, pTS1-Dest *hlb* and a Δ*hlb*. The black line represents the *S. aureus* RN6390 genome and the blue line represents the pTS1-Dest *hlb* backbone. Primers in grey text would not yield product due to lack of an annealing site.

Figure 4.11 shows the presence of the *erm* cassette in the putative mutant from PCR with primers within the cassette and the 1Kb upstream and downstream regions flanking the *hlb* gene. As would be expected, PCR using *S. aureus* RN6390 yields no product since there is no *erm* cassette present within the genome (Figure 4.9 and Figure 4.10).

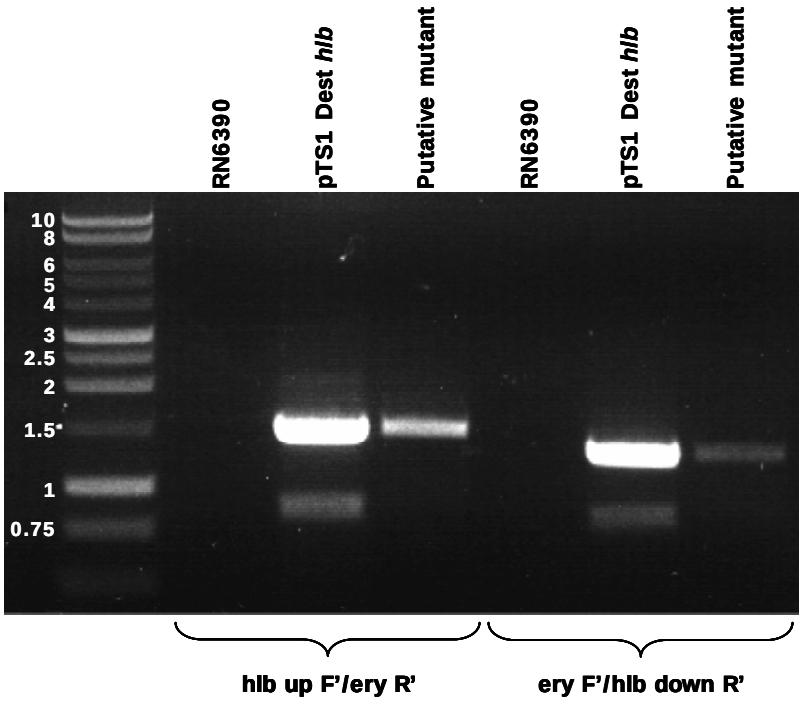

FIGURE 4.11: Agarose gel electrophoresis showing PCR products from PCR of genomic DNA from *S. aureus* RN6390 and a putative *S. aureus* RN6390 *hlb* mutant, and pTS1-Dest *hlb* plasmid DNA, using primers specific for the *erm* cassette and primers specific for regions outside of the *hlb* gene which were used to construct the pTS1-Dest *hlb* plasmid.

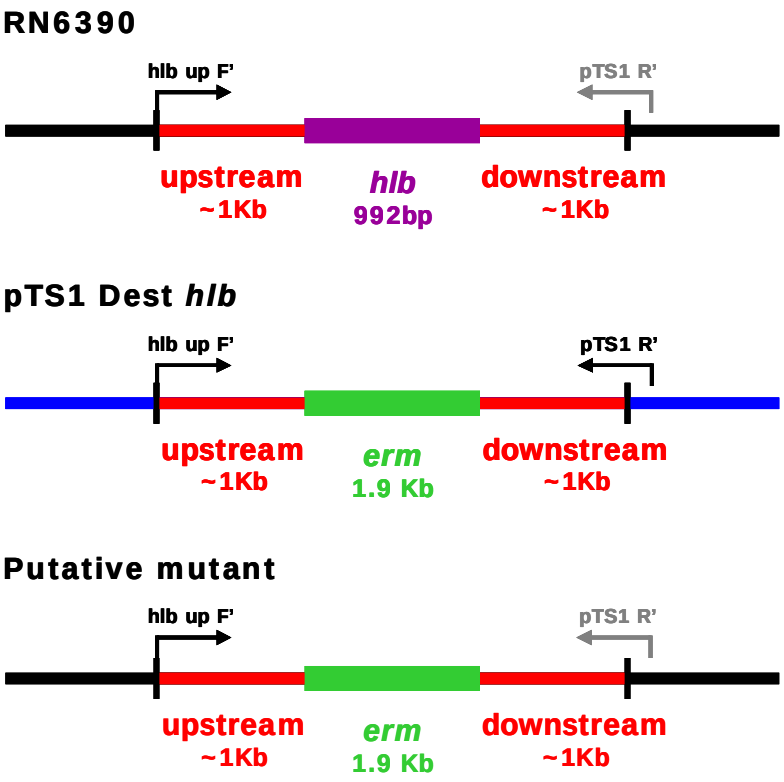

FIGURE 4.12: Schematic diagram showing the annealing sites for the hlb up F' and pTS1 R' primers, of *S, aureus* RN6390, pTS1-Dest *hlb* and a ∆*hlb*. The black line represents the *S. aureus* RN6390 genome and the blue line represents the pTS1-Dest *hlb* backbone. Primers in grey text would not yield product due to lack of an annealing site.

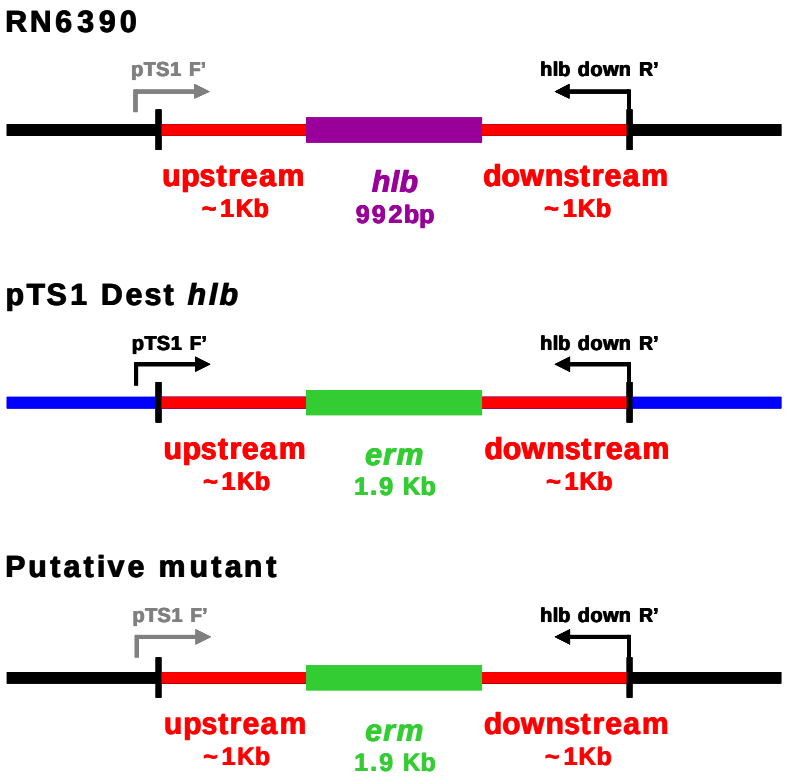

FIGURE 4.13: Schematic diagram showing the annealing sites for the pTS1 up F' and hlb down R' primers, of *S, aureus* RN6390, pTS1-Dest *hlb* and a Δ*hlb*. The black line represents the *S. aureus* RN6390 genome and the blue line represents the pTS1-Dest *hlb* backbone. Primers in grey text would not yield product due to lack of an annealing site.

Figure 4.14 confirms the loss of the pTS1-Dest *hlb* plasmid from the putative mutant, which should not have any pTS1-Dest *hlb* present if a double cross has taken place. The lack of product yielded from PCR with the pTS1 primers in the putative mutant suggests that this is the case (Figure 4.12 and Figure 4.13).

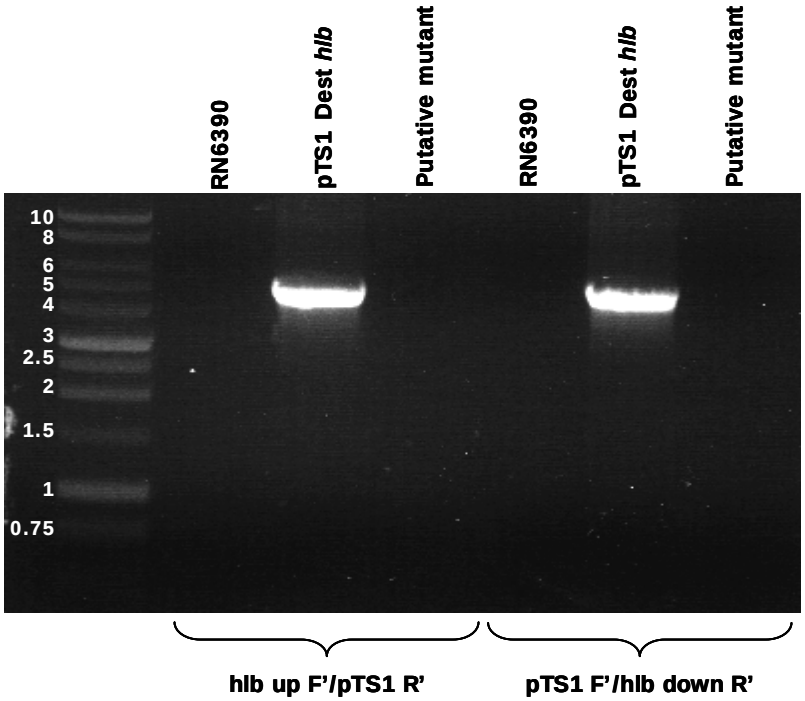

FIGURE 4.14: Agarose gel electrophoresis showing PCR products from PCR of genomic DNA from *S. aureus* RN6390 and a putative *S. aureus* RN6390 *hlb* mutant, and pTS1-Dest *hlb* plasmid DNA, using primers specific for the backbone of the pTS1-Dest *hlb* cassette and primers specific for regions outside of the *hlb* gene which were used to construct the pTS1-Dest *hlb* plasmid.

PCR with the above illustrated six pairs of primers confirms a double cross with the pTS1-Dest *hlb* plasmid and the genome of *S. aureus* RN6390. The putative mutant also demonstrates the phenotype of erythromycin resistance, indicating that the mutagenesis was successful. Further confirmation with Western blotting would be desirable before using this mutant for *in vivo* experiments.

4.3.3: Excision of *erm* Gene in *S. aureus hlb* Mutant

The *erm* gene was excised from the newly constructed mutant to facilitate the future construction of double mutants. The *S. aureus* RN6390 Δ*hlb* was transformed with the pTS1 intC expression vector, pSB3016, and xylose added to induce transcription of the expression vector. Cultures were then plated onto non-selective LB agar before incubation overnight at 42°C to promote loss of the temperature sensitive pSB3016 plasmid. Any colonies were replica plated onto LB agar alone, LB agar supplemented with 5µg ml^{-1} Cm and LB agar supplemented with 5µg ml^{-1} Erm in order to detect clones which had lost both the chromosomal *erm* gene and the IntC expression vector. Genomic DNA purification of colonies which grew on LB agar alone but not LB agar supplemented with 5µg ml^{-1} Erm or Cm was carried out and the DNA was screened by PCR using various sets of primers to confirm the success of the excision of the *erm* cassette.

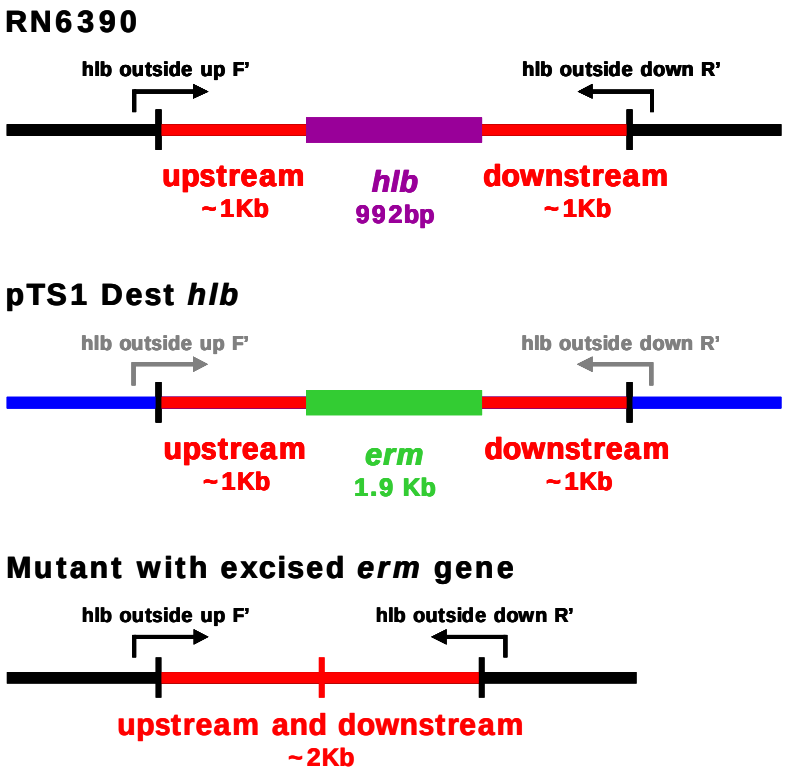

FIGURE 4.15: Schematic diagram showing the annealing sites for the hlb outside up F' and hlb outside down R' primers, of *S. aureus* RN6390, pTS1-Dest *hlb* and a ∆*hlb* with excised *erm* cassette. The black line represents the *S. aureus* RN6390 genome and the blue line represents the pTS1-Dest *hlb* backbone. Primers in grey text would not yield product due to lack of an annealing site.

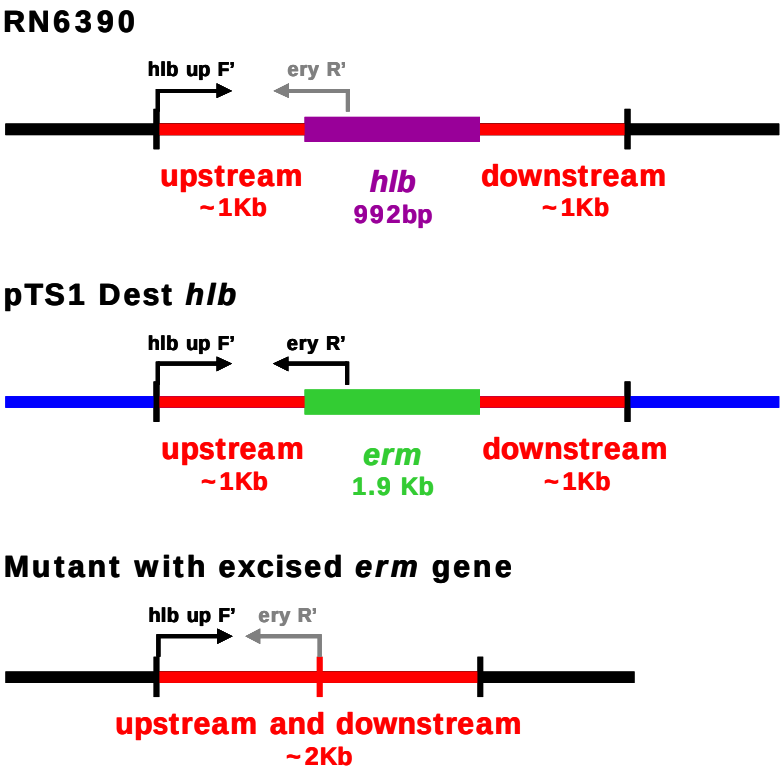

FIGURE 4.16: Schematic diagram showing the annealing sites for the hlb up F' and ery R' primers, of *S. aureus* RN6390, pTS1-Dest *hlb* and a Δ*hlb* with excised *erm* cassette. The black line represents the *S. aureus* RN6390 genome and the blue line represents the pTS1-Dest *hlb* backbone. Primers in grey text would not yield product due to lack of an annealing site.

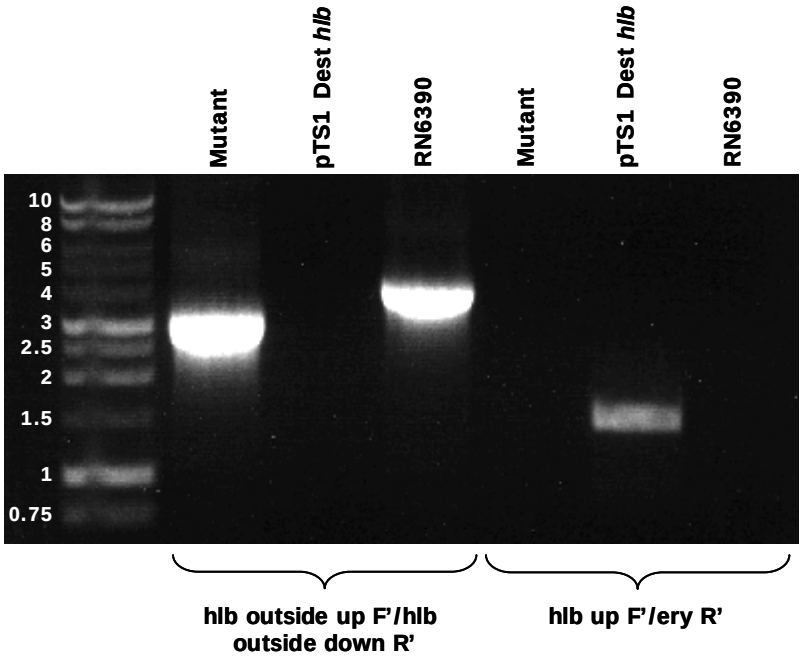

FIGURE 4.17: Agarose gel electrophoresis showing PCR products from PCR of genomic DNA from *S. aureus* RN6390 and the *S. aureus* RN6390 *hlb* mutant, and pTS1-Dest *hlb* plasmid DNA, using primers specific for regions outside of the regions used to construct the pTS1-Dest *hlb* plasmid and primers specific for regions outside of the *hlb* gene which were used to construct the pTS1-Dest *hlb* plasmid.

The two sets of primers used in Figure 4.17 demonstrate the loss of the *erm* cassette from the mutant. Primers specific for regions outside of the 1Kb upstream and downstream regions flanking the *hlb* gene yielded product from both the mutant and the wild type RN6390 suggesting outside regions of the *hlb* gene have remained intact. Furthermore, the PCR product from the mutant using these primers is approximately 1Kb smaller than that from *S. aureus* RN6390, due to the absence of both the *hlb* gene and the *erm* gene. No product was yielded from the pTS1-Dest *hlb* plasmid since these primers are specific for regions outside of the

regions incorporated into the plasmid. The hlb up F'/ery R' combination of primers again indicates loss of the *erm* gene, with product only present from the pTS1-Dest *hlb* plasmid as would be expected (Figure 4.15 and Figure 4.16).

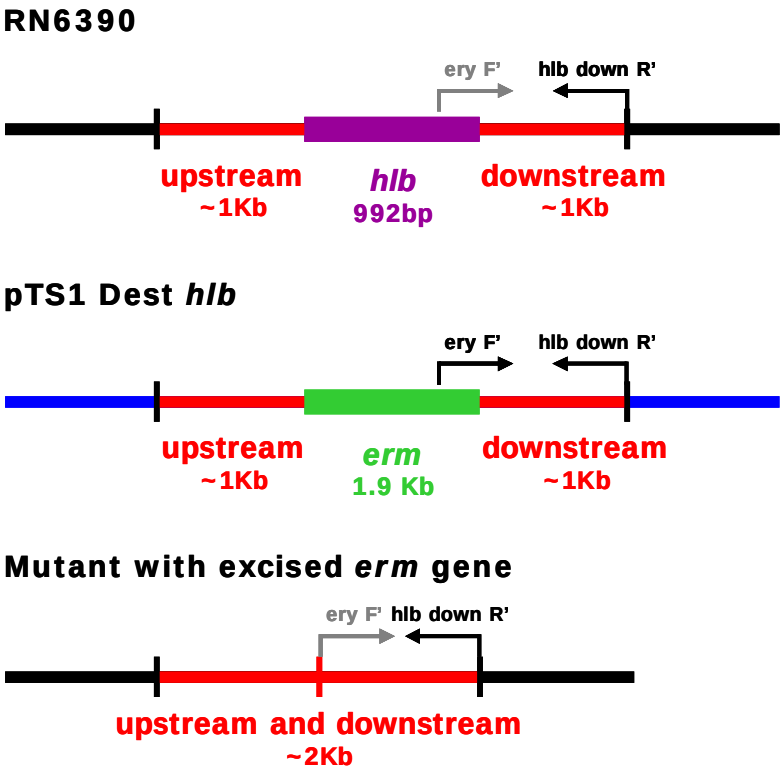

FIGURE 4.18: Schematic diagram showing the annealing sites for the ery F' and hlb down R' primers, of *S. aureus* RN6390, pTS1-Dest *hlb* and a Δ*hlb* with excised *erm* cassette. The black line represents the *S. aureus* RN6390 genome and the blue line represents the pTS1-Dest *hlb* backbone. Primers in grey text would not yield product due to lack of an annealing site.

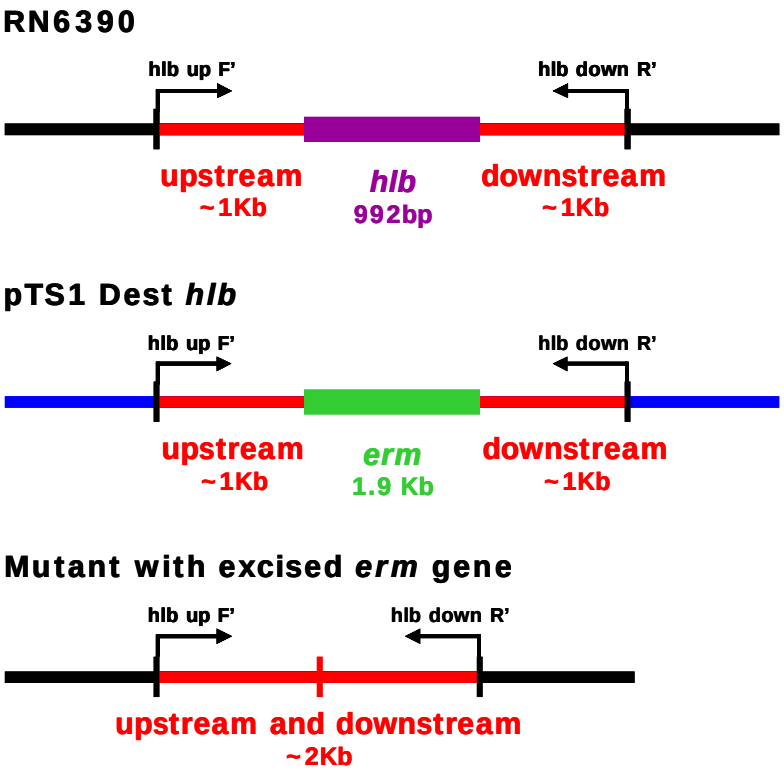

FIGURE 4.19: Schematic diagram showing the annealing sites for the hlb up F' and hlb down R' primers, of *S. aureus* RN6390, pTS1-Dest *hlb* and a Δ*hlb* with excised *erm* cassette. The black line represents the *S. aureus* RN6390 genome and the blue line represents the pTS1-Dest *hlb* backbone. Primers in grey text would not yield product due to lack of an annealing site.

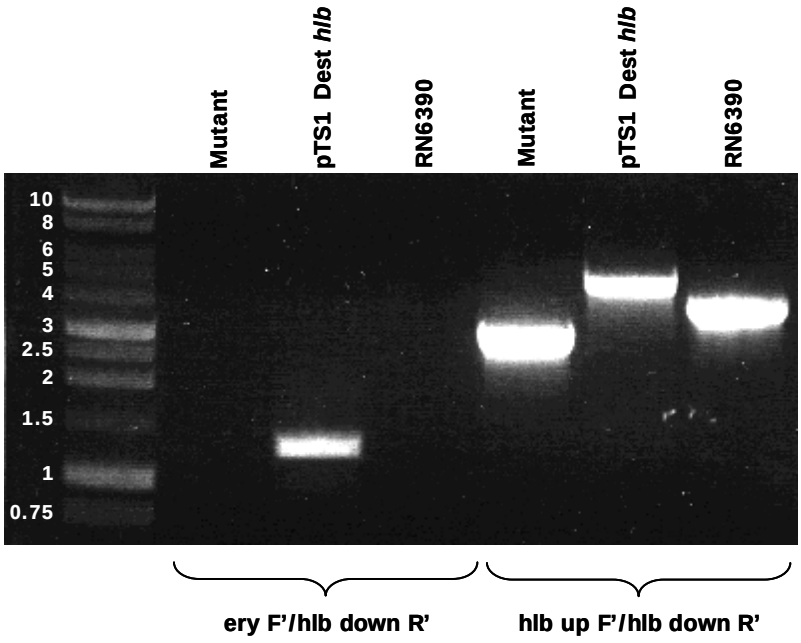

FIGURE 4.20: Agarose gel electrophoresis showing PCR products from PCR of genomic DNA from *S. aureus* RN6390 and the *S. aureus* RN6390 *hlb* mutant, and pTS1-Dest *hlb* plasmid DNA, using primers specific for regions outside of the *hlb* gene which were used to construct the pTS1-Dest *hlb* plasmid and primers specific for the *erm* cassette.

Similarly to the hlb up F'/ery R' primers, the ery F'/hlb down R' primers also only yield product from the pTS1-Dest *hlb* plasmid, indicating loss of the *erm* gene from the mutant. As would be expected, the hlb up F'/hlb down R' primers yield product from *S. aureus* RN6390 and the mutant since these primers are specific for the 1Kb regions upstream and downstream of the *hlb* gene. They also yield product from the pTS1-Dest *hlb* plasmid as these primers were used to construct this plasmid, causing it to also contain these *hlb* flanking regions. However, the product from the pTS1-Dest *hlb* PCR with these primers is larger than that from both *S.*

aureus RN6390 and the mutant due to the presence of the *erm* cassette. In fact, Figure 4.20 clearly shows how this PCR product is approximately 1Kb larger than that from *S. aureus* RN6390 as the *erm* gene is 1Kb larger than the *hlb* gene. In addition, the product yielded from *S. aureus* RN6390 is approximately 900bp larger than that from the mutant due to the fact that the mutant has neither the *hlb* gene nor the *erm* cassette present (Figure 4.18 and Figure 4.19).

PCR with the above illustrated four pairs of primers therefore confirms the loss of the *erm* gene in the *S. aureus* ∆*hlb*. The mutant also no longer demonstrated the phenotype of erythromycin resistance, indicating that the excision was successful.

4.3.4: Phenotypic Confirmation of α- and γ-Haemolysin Mutants

Mutants in *S. aureus* α- and δ-haemolysin had previously been constructed for use in endosomal escape research. In addition to this, a γ-haemolysin mutant was obtained from Tim Foster's laboratory in Dublin. The β-haemolysin mutant was made in this study to complete the complement of haemolysin mutants. However, problems were experienced transforming the *S. aureus* RN6390 ∆*hla* with any reporter plasmids, and it was decided that this may be due to point mutations elsewhere within the genome of this strain. To overcome this issue, the mutation was transduced from the *S. aureus* RN6390 ∆*hla* back into *S. aureus* RN6390. Additionally, the γ-haemolysin mutation was transduced into *S. aureus* RN6390 to ensure all mutations were within the same background strain.

While the β-haemolysin mutant was being constructed, the phenotypes of the newly transduced mutations were tested for haemolytic activity.

All strains were cultured in LB broth and normalised according to their OD_{600}. After centrifugation, bacterial supernatants were filter sterilised and added to specified quantities of haemolysin buffer and rabbit blood and mixed by inverting. After incubation, cultures were centrifuged and the OD_{543} of the supernatant was measured. These figures were then used to calculate the haemolysin activity of each sample.

TABLE 4.1: Haemolysin activity of *S. aureus* RN6390 Δ*hla* and two transduced putatives as compared to the wild-type *S. aureus* RN6390 strain. P-values indicated in relation to student's t-test used to analyse data.

	Haemolysin activity	**P-value**
RN6390	**1.58 ± 0.02**	
Δhla	**0.16 ± 0.27**	**$<3x10^{-4}$**
Putative 1	**0.12 ± 0.10**	**$<6x10^{-6}$**
Putative 2	**0.04 ± 0.05**	**$<3x10^{-7}$**

As illustrated above in Table 4.1, both the original *S. aureus* RN6390 Δ*hla* strain, and the two transduced putative Δ*hla* strains are significantly less haemolytic than *S. aureus* RN6390 in rabbit blood.

TABLE 4.2: Haemolysin activity of *S. aureus* 8325-4 Δ*hlg* and two transduced putatives in an *S. aureus* RN6390 background, as compared to the wild-type *S. aureus* 8325-4 strain. P-values indicated in relation to student's t-test used to analyse data.

	Haemolysin activity	P-value
8325-4	**1.48 ± 0.09**	
Δhlg	**0.00 ± 0.01**	**$<3x10^{-6}$**
Putative 1	**0.00 ± 0.00**	**$<6x10^{-6}$**
Putative 2	**0.00 ± 0.00**	**$<3x10^{-6}$**

Similarly, Table 4.2 shows that both the original *S. aureus* 8325-4 Δ*hlg* strain, and the two transduced putative Δ*hlg* strains are significantly less haemolytic than *S. aureus* RN6390 in rabbit blood. However, all three strains appear to show no haemolytic activity, as compared with the *S. aureus* RN6390 Δ*hla* strains, which still showed some haemolytic activity as compared with the wild-type. Although both β- and δ-haemolysin are not specifically active against rabbit erythrocytes, α-haemolysin is active against rabbit erythrocytes, and subsequently some lysis would be expected in a Δ*hlg* strain still capable of producing α-haemolysin. It was thought that this may be due to the growth phase of bacteria used for the assay, and so assays were repeated with stationary phase bacterial cultures (data not shown). However, the same effect was seen.

4.3.5: Invasion Assays

4.3.5.1: *agr* Expression and Growth of *S. aureus* within A549 Cells

Previous work has shown that *agr* expression precedes escape of internalised *S. aureus* from the host endosome (Qazi *et al.*, 2001), suggestive of a role for *agr* regulated gene products in the breaching of the host endosome.

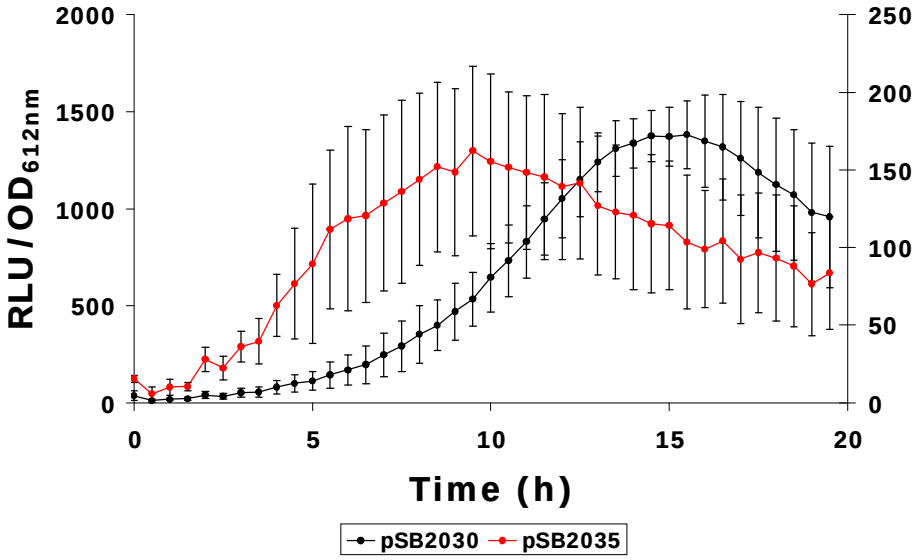

FIGURE 4.21: Cell Invasion Assay

Bioluminescence as relative light units (RLU) divided by optical density (OD) of *S. aureus* RN6390 harbouring pSB2030 *S. aureus* RN6390 harbouring pSB2035. For comparison, different scales are used to represent data relating to growth (left y axis) and *agr* expression (right y axis) to compensate for variations in promoter strength. Results represent the mean value of 6 data points for each reading.

Preliminary experimentation confirmed that *agr* is activated before replication of internalised *S. aureus* occurs (Figure 4.21). Invasion assays were carried out with both the existing *agr* reporter strain *S. aureus* RN6390 pSB2035 and the growth reporter strain *S. aureus* RN6390 pSB2030. Bioluminescence from *S. aureus* RN6390 pSB2035 peaked at 9.5 hours, whereas bioluminescence from *S. aureus* RN6390 pSB2030 was not at a maximum until approximately 15 hours, indicative of endosomal lysis due to production of *agr* controlled gene products, and consequent bacterial replication within the host cell cytoplasm.

In order to determine the involvement of *agr* regulated gene products, specifically haemolysins, in endosomal escape, this study aimed to use the haemolysin mutants in an *in vitro* invasion assay, with the intention of using the findings in conjunction with the MRI reporter system to design a specific disease model. Again, while the β-haemolysin mutant was under construction, initial experiments were carried out using the *S. aureus* RN6390 Δ*hla* mutant. *S. aureus* RN6390 and *S. aureus* RN6390 Δ*hla* were transduced with an expression vector, pMK4 P_{xylA}-gfp-term, which incorporated the P_{xylA} and the gfp gene. This plasmid was chosen for preliminary experiments due to its low metabolic demand in contrast with *lux* containing vectors.

Results indicate that the Δ*hla* is less able to replicate when internalised within A549 cells than the wildtype (Figure 4.22).

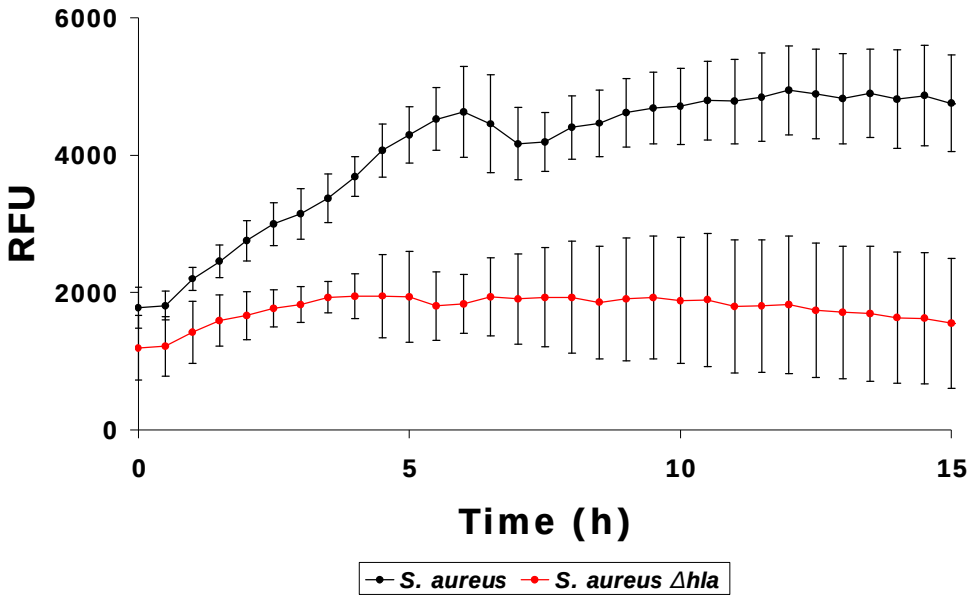

FIGURE 4.22: Cell Invasion Assay

Fluorescence normalised for growth of *S. aureus* RN6390 and *S. aureus* RN6390 Δ*hla*, both harbouring pMK4 P_{xylA}-gfp-term Results represent the mean value of 3 data points for each reading.

Unfortunately, during this work, Jarry *et al*. (2008) documented a major role for α-haemolysin in endosomal escape. Due to this fact, coupled with the time restrictions of the study, further work with the other haemolysin mutants, including the newly constructed β-haemolysin mutant, was halted in favour of other aspects of the project.

5.0: *IN VIVO* EVALUATION OF AN *S. AUREUS* MRI REPORTER IN MICE

5.1: Objectives

One of the main aims of this study was to develop an imaging modality which enables the non-invasive *in vivo* detection of bacterial reporter gene expression while offering detailed anatomical information. To accomplish this, an MRI bacterioferritin reporter gene for *S. aureus* was constructed and evaluated *in vitro* as described in Chapter 3. The next step was to use this system in pilot studies *in vivo* to confirm its potential for studying specific aspects of staphylococcal disease.

5.2: Introduction

Mice have been successfully used in bioluminescence optical imaging due to their relatively small size and therefore reduced light attenuation by tissue layers. The MRI reporter genes in this study were constructed with a downstream *lux* cassette for *in vitro* evaluation, making the mouse model ideal for the *in vivo* evaluation of the reporter system, since the bioluminescence can be utilised as a preliminary test of reporter gene function. Previous work with BFR MRI reporter genes in *E. coli* demonstrated the effective use of mouse thigh tumour models (Hill *et al*., manuscript in preparation). *E. coli* was shown to colonise the tumours in

high numbers allowing for a more dramatic contrast during MRI. In fact, a range of bacteria showing preferential accumulation in tumours have been studied (Kimura *et al*., 1980; Riedel *et al*., 2007; Stritzker *et al*., 2007; Brader *et* al., 2008). Specific colonisation of this nature by *S. aureus* would enable the relatively easy removal of the colonisation site for further *in vitro* analysis, making the mouse thigh tumour model an ideal candidate for experimental use in this study.

5.3: Results

5.3.1: Preliminary *in vivo* Evaluation of MRI Reporter Function

In order to determine functionality of the expression vectors *in vivo*, three groups of mice were inoculated in the tail vein with 1 x 10^9 *S. aureus* RN6390 harbouring either the MRI reporter plasmids, pUNK1 P_{S10}-bfr-luxterm and pUNK1 P_3-bfr-luxterm, or a control plasmid, pUNK1 P_{S10}-dual-term, which is approximately the same size as the MRI reporter plasmids. Each test group contained three mice which were monitored over a 3 day period using a Berthold NightOWL to visualise luminescence.

Colonisation of the initial inoculation site in the tail by *S. aureus* pUNK P_{S10}-dual-term can be seen after 1 day, with further colonisation of the tumours and also localisation in thoracic organs in the following 2 days (Figure 5.1). This indicates that the reporter gene in the recombinant *S. aureus* are expressed *in vivo*, and are maintained for at least 3 days.

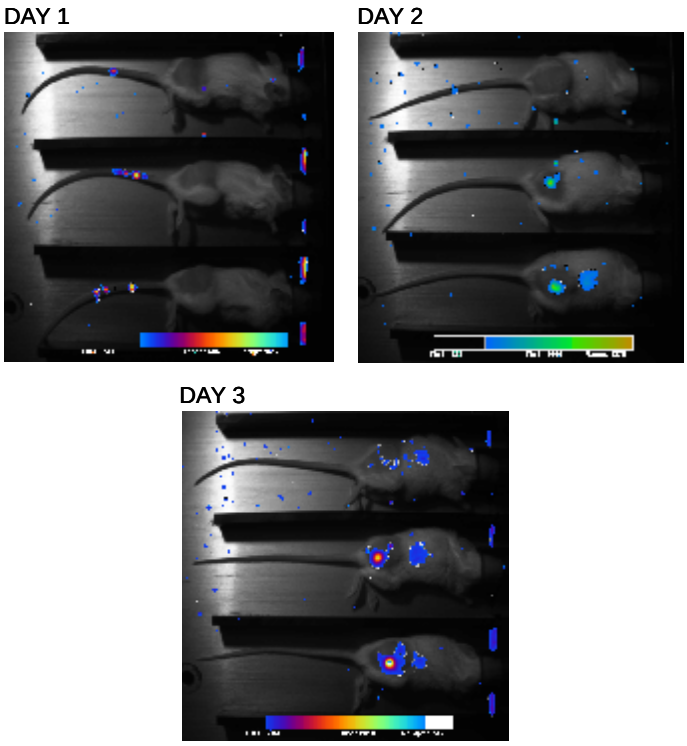

FIGURE 5.1: Photos overlaid with luminescence images of mice inoculated with *S. aureus* harbouring pUNK1 P_{S10}-dual-term. Images show luminescence 1, 2 and 3 days post-inoculation. Order of mice does not remain the same for each picture.

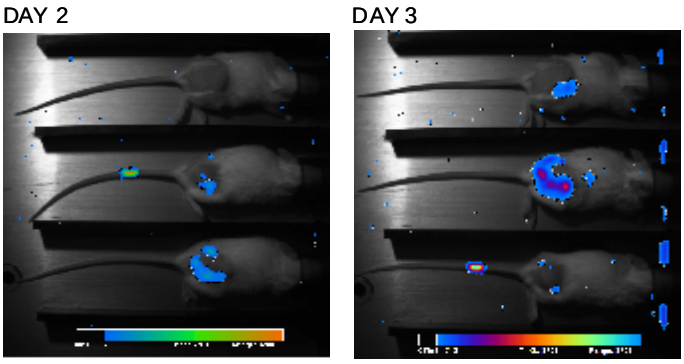

FIGURE 5.2: Photos overlaid with luminescence images of mice inoculated with *S. aureus* harbouring pUNK1 P_{S10}-bfr-luxterm. Images show luminescence 2 and 3 days post-inoculation. Order of mice does not remain the same for each picture.

DAY 1

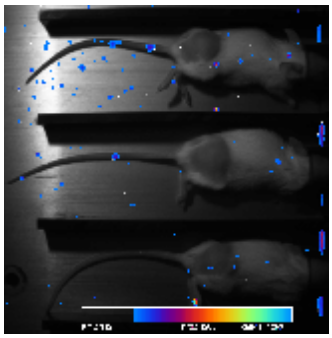

FIGURE 5.3: Photos overlaid with luminescence images of mice inoculated with *S. aureus* harbouring pUNK1 P_3-bfr-luxterm. Images show luminescence 1 day post-inoculation.

No bioluminescence was observed in mice inoculated with *S. aureus* pUNK1 P_{S10}-bfr-luxterm on day 1 (Figure 5.2). However, on days 2 and 3 the pattern of colonisation was similar to that of *S. aureus* pUNK1 P_{S10}-dual-term. Mice inoculated with *S. aureus* pUNK1 P_3-bfr-luxterm showed colonisation of the inoculation site in the tail after 1 day (Figure 5.3). Interestingly, no bioluminescence was observed on days 2 and 3. Despite this, bioluminescence detected at the inoculation site 1 day post-inoculation clearly demonstrates that like the other two plasmids, pUNK1 P_3-bfr-luxterm is also expressed *in vivo*. The lack of bioluminescence 2 and 3 days post-inoculation could be due to plasmid loss. However, the maintenance of plasmid in the other two test groups makes this unlikely, especially due to the fact that all expression vectors are approximately the same size. A more feasible cause is the nature of the P_3 promoter which, unlike the P_{S10} promoter, is not expressed constitutively, but rather in

relation to increased bacterial cell numbers, meaning that at the time the mice were imaged, the promoter may not have been expressed.

These images confirm expression of the reporters, suggesting that bacterioferritin should be successfully synthesised *in vivo*. MR imaging of the colonised tumours should therefore demonstrate contrast as a darkening of T_2-weighted images generated by the loading of iron onto the endogenous bacterioferritin.

Unfortunately, due to time restrictions, the mice used in the pilot study were not scanned using the MRI scanner. Consequently, the *S. aureus* haemolysin mutants could not be evaluated in conjunction with the MRI reporter system in vivo as the reporter genes first need to be fully evaluated prior to use in the animal model.

5.3.2: Evaluation of Colonisation

5.3.2.1: Viable Cell Counts

In order to confirm colonisation of the tumours with *S. aureus*, and to additionally determine localisation of other thoracic organs, the tumours, spleens and livers of one mouse from each of the three groups inoculated with either *S. aureus* pUNK1 P_{S10}-dual-term, *S. aureus* pUNK1 P_{S10}-bfr-luxterm or *S. aureus* pUNK1 P_3-bfr-luxterm were removed and weighed before being homogenised with 1ml PBS and plated at varying dilutions both with antibiotic selection (5µg ml^{-1} Erm) and without antibiotic

selection (LB) (Figure 5.4). Plates with between 10 and 300 colonies were included in the data. CFU g^{-1} were then calculated for each tissue.

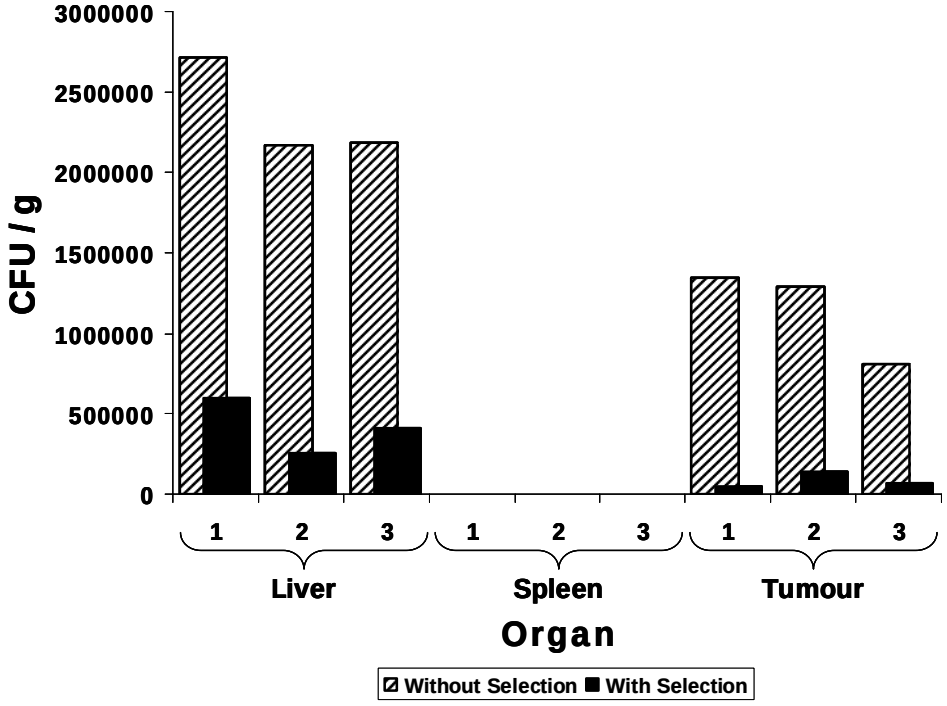

FIGURE 5.4: Viable cell counts from the livers, spleens and tumours of one mouse from each test group. Mice were inoculated with *S. aureus* pUNK1 P_{S10}-dual-term (1 on the graph), *S. aureus* pUNK1 P_{S10}-bfr-luxterm (2 on the graph) or *S. aureus* pUNK1 P_3-bfr-luxterm (3 on the graph).

Viable cell counts from the tumours support the suggestion in response to Figures 5.1 and 5.2, that the tumours are colonised by *S. aureus*. Although bioluminescence was not imaged 2 and 3 days post-inoculation in mice infected with *S. aureus* pUNK1 P_3-bfr-luxterm, the viable cell counts suggest that the tumours were colonised, giving strength to the theory that

perhaps lack of light was due to the nature of the promoter, which is not constitutively expressed. Both the tumours and livers of all 3 mice inoculated with *S. aureus* pUNK1 P_{S10}-dual-term contained bacteria, with no localisation in the spleens either with or without selection. Antibiotic selection to determine plasmid loss from recovered bacteria indicates that the plasmid is not very stable in the absence of antibiotics in the mice, with an average plasmid loss in the livers of 88% and the tumours of 92%. Despite this, Figures 5.1 and 5.2 show that plasmid loss has not reduced the signal from the expressed *lux* cassette to levels which are undetectable. For use in MRI, selection could be maintained in the mice to ensure maximum production of BFR. Another option would be to incorporate the plasmid into the *S. aureus* genome.

5.3.2.2: Histological Evaluation of Colonisation

This work was done in conjunction with Dr. Jochen Stritzker from the University of Würzburg in Germany. Histology was carried out on one of the removed tumours from a mouse in the test group inoculated with *S. aureus* pUNK1 P_{S10}-bfr-luxterm to determine the region of colonisation. As can be seen in Figure 5.5, *S. aureus* appears to colonise the necrotic region of the tumour, as is the case with *E. coli* (Hill *et* al., manuscript in preparation). However, the distribution of *S. aureus* within the tumour differs to that of *E. coli*, which forms a ring around the necrotic area. *S. aureus* appears to colonise in a patchy fashion, being much more widely distributed throughout the necrotic region.

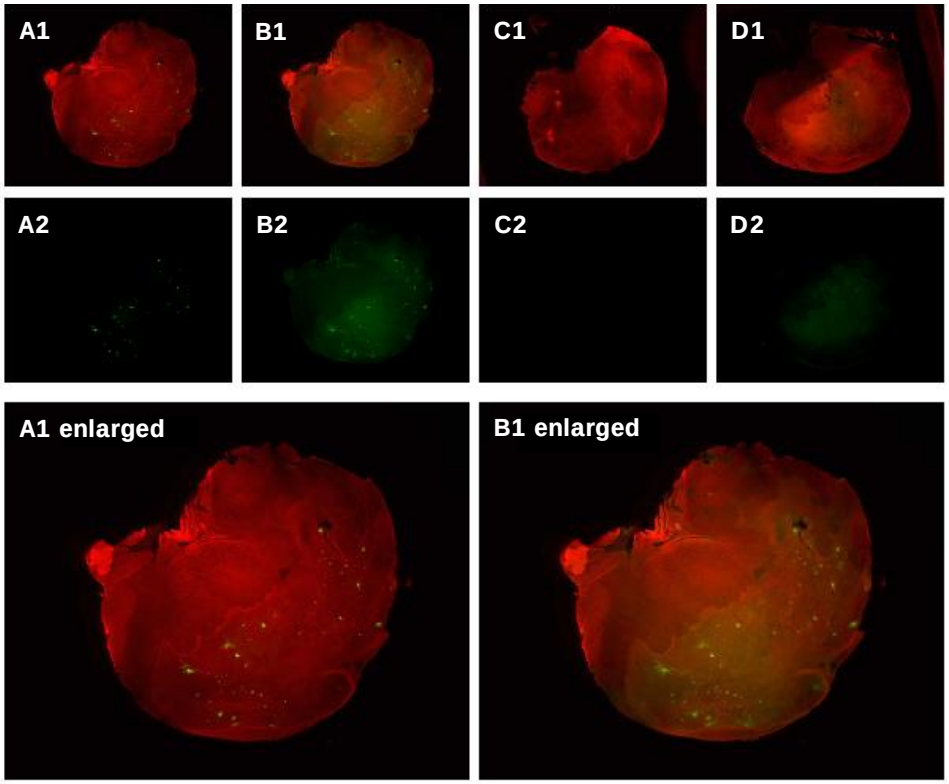

FIGURE 5.5: Confocal microscopy showing colonisation of a tumour removed from a mouse inoculated with *S. aureus* pUNK1 P_{S10}-bfr-luxterm. Actin was stained red to visualise tumours and *S. aureus* was labelled using FITC (A2, B2, C2 and D2). Images were then overlaid (A1, B1, C1 and D1). Labelled *S. aureus* can be seen with (A2) and without (B2) background correction. C1 shows the same tumour as in A1 and B1, but without anti-Protein A antibody. D1 shows a tumour from a mouse with no *S. aureus* inoculation.

6.0: DISCUSSION

6.1: Construction and *in vitro* Evaluation of an MRI Reporter in *S. aureus*

The development of MRI reporters for use in the non-invasive *in vivo* studies of bacterial infection, colonisation and transcription would be an invaluable tool in the future understanding of bacterial pathogenesis and host-microbe interactions during disease processes. The functional and anatomical data which could be achieved from such an imaging modality, coupled with the potential reduction in animal usage has made this an exciting area of research, with a range of MRI reporter gene systems currently being studied. Of particular interest is the increasing use of ferritins and ferritin-like proteins, which are ideal for use as MRI reporters due to their ferroxidase activity which converts stored iron from the Fe^{2+} form to the paramagnetic Fe^{3+} form, which is responsible for the T_2 contrast modification in MRI (Harrison *et al*., 1996). Previous studies have successfully used human ferritins as MRI reporters in eukaryotic cells (Cohen *et al*., 2005; Genove *et al*., 2005; Cohen *et al*., 2007). However, despite knowledge of the iron storage properties of bacterial ferritin-like proteins, there is no documented evidence of their use as MRI reporters. Recently, a range of bacterial ferritin-like genes were evaluated for their use as MRI reporters in prokaryotic studies (Hill *et al*., manuscript in preparation). The use of a murine thigh tumour model demonstrated both the success of the tumour model for imaging purposes due to bacterial tumour targeting, and also the functionality of bacterial ferritin-like proteins

as MRI reporters. This study implemented these findings in the development of an MRI reporter system for the tracking of *S. aureus* disease processes.

Expression vectors were constructed using both constitutive and inducible promoters upstream of the *E. coli bfr* gene. A *luxABCDE* cassette was also cloned downstream of the *bfr* for use in the *in vitro* and preliminary *in vivo* evaluation of the MRI reporter system. The constructs were evaluated *in vitro* and the best were taken forward for use in *in vivo* studies, namely the SaP_{S10} and P_3 constructs. Initial ICP-MS data suggested, however, that although it was apparent that BFR was successfully expressed in the transformed *S. aureus*, it did not affect the iron concentrations found in cell cultures, suggesting that the BFR was not functional. In its native background strain, *E. coli*, *bfr* is co-transcribed with the *bfd* gene, whose product, a [2Fe-2S] protein, forms a complex with BFR. Garg *et al*., (1996) suggested a role for this protein in the iron storage function of BFR. This would explain the lack of iron collection seen in this study in *S. aureus*, which does not have a *bfd* gene within its genome.

To test this hypothesis, new expression vectors were constructed containing the *bfd* gene upstream of the *bfr* gene. SDS-PAGE gels showed that *E. coli* harbouring the *bfd/bfr* construct appeared to express higher levels of BFR. One explanation for this could be translational enhancement of the downstream *bfr* gene due to presence of the *bfd* gene. Iron assays indicated that, as expected, the *E. coli* harbouring the

control plasmid still collected iron due to its native *bfr* gene and also other ferritin-like proteins including FtnA and FtnB (Chiancone *et al.*, 2004). The *E. coli* harbouring the *bfr* and *bfd/bfr* constructs both showed increased iron collection of a roughly equal scale, which supports previous documentation of the role of BFR as an iron storage protein (Bauminger *et al.*, 1980; Yariv *et al.*, 1981). This finding is also in line with those of Hill *et al*. (manuscript in preparation), that overexpression of the BFR protein in *E. coli* results in increased iron content of the bacteria. If the *bfd* gene product played a role in the functionality of the BFR then a higher level of iron collection would be expected in the *E. coli bfd/bfr* strain. However, this data can not confirm this role for *bfd* since the SDS-PAGE gels clearly showed an increased amount of BFR in this strain, which would also contribute to increased iron levels. Additionally, it is difficult to determine the effect of *bfd* in *E. coli* due to the native *bfd* expressed in *E. coli* harbouring the *bfr* construct. To address this issue a ∆*bfd E. coli* strain could be made.

For *S. aureus*, SDS-PAGE gels revealed that, unlike the BFR expression vectors which led to synthesis of BFR, *S. aureus* harbouring the new constructs containing the *bfd* gene did not express levels of BFR visible by SDS-PAGE analysis. This led to the consideration that the presence of the *bfd* gene was somehow affecting the transcription or translation of the *bfr* gene in *S. aureus*.

The presence of the *bfd* gene, regardless of a role in BFR functionality, was not expected to affect the amount of BFR expressed. A role in BFR functionality would only cause an increase in the amount of iron the BFR is able to load. Due to the fact that the *bfd* construct is causing a reduction in the amount of BFR synthesised, then any reduction seen in iron loading can not be attributed to the role of *bfd* in iron loading, but rather to the reduction in BFR expression.

Iron assays were carried out on these samples to correlate the amount of BFR produced to iron loading. Despite the initial ICP-MS data which suggested the BFR expressed in *S. aureus* was not functional, iron assays and ICP-MS data carried out on the new constructs showed iron collection in both the *bfr* and *bfd/bfr* constructs in *S. aureus*. As would be expected from the increased levels of BFR seen in the *S. aureus* harbouring the *bfr* constructs, this strain also showed the most iron collection. As described above, this can not rule out a role for *bfd* in iron loading due to the fact that there is more BFR present in the *bfr* construct samples. However, despite the low levels of BFR in the *bfd/bfr* construct, these data show that an increase in expression of BFR in *S. aureus* causes increased iron collection. Regardless of the mechanism behind this, and any possible role for *bfd*, this indicates that the BFR expression vectors are usable as a contrast agent for MRI imaging of *S. aureus* disease processes.

To determine if the incorporation of the *bfd* gene was affecting the transcription or translation of the *bfr* gene, bioluminescence assays were

carried out with both the *bfr* and *bfd/bfr* constructs. One finding from these bioluminescence assays was that, compared with the pUNK1 P_3-dual-term and pUNK1 P_{S10}-dual-term constructs, bioluminescence levels measured from the the *bfr* constructs were over 3 fold less. An explanation for this could be that the expression of iron storage proteins in *S. aureus* has somehow affected iron homeostasis within the bacteria. Ferritins within the *S. aureus* cytoplasm could cause low iron concentrations which could result in the upregulation of other iron synthesis or scavenging systems. If this is the case, the extra metabolic demand placed on the bacteria may decrease expression of the MRI reporter genes. Alternatively, the *bfr* gene could be affecting the translation of the *lux* operon. Another explanation could be that the *bfr* gene is reducing the half life of the mRNA from transcription of the operon, resulting in less opportunity for translation to occur. This could be investigated further by Northern Blot analysis.

With respect to the potential effects of the *bfd* gene on the transcription or translation of the *bfr* gene, if the *bfd* gene was terminating transcription of the expression vector, then no bioluminescence signal would be detected due to the failure of transcription of the *lux* cassette. However, if the *bfd* gene was affecting the translation of the *bfr* gene then light output would be maintained since the genes of the *lux* operon each has its own RBS. The bioluminescence assay results showed that the light output from both the *bfr* and *bfd/bfr* constructs was maintained, suggesting that the translation of the *bfr* gene was being interrupted by the presence of the *bfd*

gene. One cause for this could be the formation of stem loop structures within the mRNA.

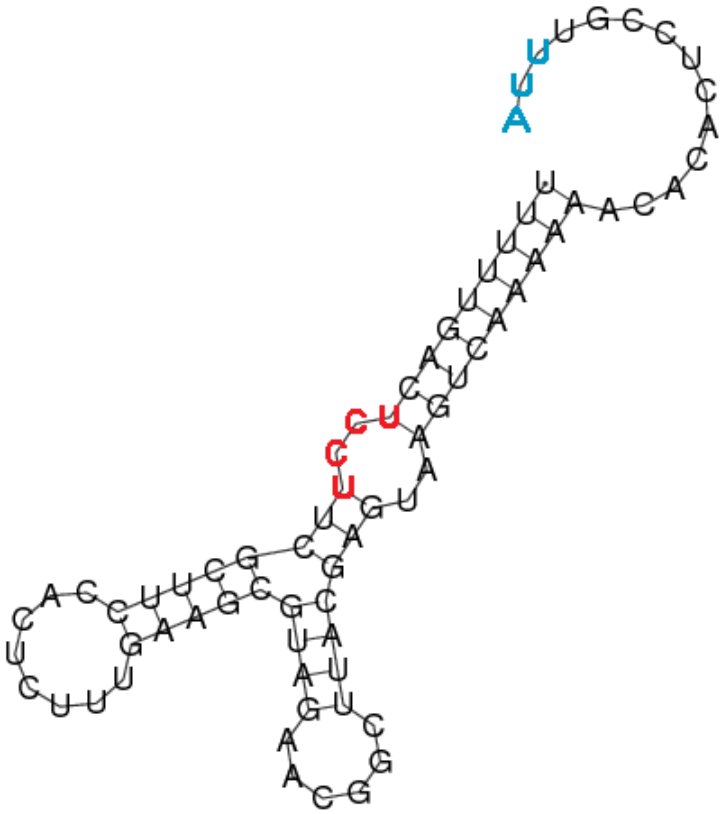

FIGURE 6.1: Diagram showing a potential stem loop in the mRNA sequence of the intergenic region between the *bfd* and *bfr* genes. The red highlights the RBS of the *bfr* gene and the blue highlights the end of the *bfd* gene.

If a stem loop such as the one depicted in Figure 6.1 formed between the 3' end of the *bfd* gene, the 5' end of the *bfr* gene and the intergenic region between the genes, this could potentially cause the decrease in translation of the *bfr* gene seen in *S. aureus* due to inaccessibility of ribosomes to the *bfr* RBS. It is possible that in *E. coli* the formation of an intergenic stem

loop has little effect on translation of the *bfr* gene due to a strong *bfd* RBS, whereby attached ribosomes can remove the stem loop during translation, effectively translationally coupling *bfd* and *bfr*. However, the *bfd* RBS may be relatively poor in *S. aureus*. The ensuing low levels of translation of the *bfd* gene may therefore not be sufficient to remove the stem loop thus leaving the *bfr* RBS occluded.

There are various ways in which this issue could be addressed. One option would be to change the codon usage within this region of DNA to prevent the formation of stem loops in *S. aureus*. Alternatively, the *bfd* gene could be incorporated in a separate transcriptional unit, or even in a separate vector. However, to justify such changes, an important role for *bfd* would firstly need to be established. Although this route of study is extremely interesting, with potential improvements to the MRI reporter system should a role for *bfd* in BFR functionality be discovered, the bfd/bfr constructs were developed to address the problem of non-functional BFR in response to the initial ICP-MS data. Since repetition of this investigation with additional iron assays appears to indicate that the BFR expressed by *S. aureus* harbouring the *bfr* construct does in fact collect iron, the *bfd/bfr* construct at this stage does not need to be further evaluated until the *bfr* construct is established as a successful MRI reporter. To this end, the *bfr* construct needs to be made more stable. Experiments analysing plasmid loss indicated the need for selection to be maintained during *in vivo* experiments to ensure maximum production of BFR. However, introduction of the expression vector into the chromosome of the *S. aureus* would allow

for use of the MRI reporter system in different animal models without the need for unnecessary invasive procedures to administer the antibiotics.

6.2: Construction and Characterisation of a *hlb* Mutant and Characterisation of Existing Haemolysin Mutants in *S. aureus*

Internalised *S. aureus* enclosed within a host membrane-bound endosome has been shown to have the ability to escape this endosome, residing and potentially replicating in the host cell cytoplasm (Bayles *et al*., 1998; Wesson *et al*., 1998). However, at the commencement of the current study, the mechanisms via which this escape occurred were not well understood. Wesson *et al*. (1998) suggested a model describing a role for *agr*-regulated quorum sensing in *S. aureus* internalisation and endosomal escape, yet it is not fully clear which genes specifically are important. This study aimed to investigate the role of haemolysins, products of genes under the control of the *agr* system which disrupt eukaryotic cell membranes, in endosomal escape of internalised *S. aureus*, and as such, several *S. aureus* haemolysin mutants were characterised and a *S. aureus hlb* mutant was constructed.

PCR indicated that the bacterial mutagenesis of *S. aureus* using pTS1-Dest *hlb* constructed using Gateway® technology was successful. Additionally, it would appear that excision of the *erm* marker was also achieved using the pTS1 intC expression vector. This technology was developed by Qazi *et al*. (manuscript in preparation), to enable the construction of mutants without the bioburden of resistance gene

expression, and also the production of double or triple mutants without the need for multiple resistance genes. This is achieved by using allelic replacement cassettes during the mutagenesis process in which resistance genes are flanked with *Streptomyces lividans* ϕC31 *attB* and *attP* sites. Excision of the resistance gene can then be achieved by expression of site-specific recombinase, ϕC31 integrase (IntC), in the *S. aureus* mutants. The successful use of this technology in this study supports the development of this technology by Qazi *et al*. (manuscript in preparation). However, Western blots would need to be carried out for formal confirmation of a β-haemolysin negative phenotype.

In addition to the construction of a new *S. aureus* Δ*hlb* strain, an existing *S. aureus* RN6390 mutant in α-haemolysin was transduced back into the RN6390 background strain in an attempt to overcome problems with the transformation of this strain. An *S. aureus* 8325-4 γ-haemolysin mutant was obtained from Tim Foster's laboratory in Dublin and the mutation was also transduced into the RN6390 background strain. Phenotypic analysis of the newly transduced strains revealed that the two transduced putative *S. aureus* Δ*hla* strains were significantly less haemolytic than *S. aureus* RN6390 in rabbit blood. However, the two transduced putative *S. aureus* Δ*hlg* demonstrated no haemolytic activity, indicating that they were not expressing α-haemolysin which is specifically active against rabbit erythrocytes. Further experiments revealed that the growth phase of the bacteria was not the cause of this apparent lack of α-haemolysin production, indicating that other mutations within the genome of this strain

may be present. This requires further attention by way of PCR, SDS-PAGE protein gels, Western blots and Southern blots before this strain can be used.

Preliminary work using a cell invasion assay and *S. aureus* harbouring growth and *agr* expression reporter plasmids, confirmed that *agr* is activated before replication of internalised *S. aureus* occurs. This supports work carried out previously by Qazi *et al*. (2001) and Shompole *et al*. (2003) indicating the occurrence of endosomal lysis due to production of *agr* controlled gene products, before bacterial replication within the host cell cytoplasm. However, to ensure that the increase in bioluminescence seen with the *agr* expression reporter plasmid was, in fact, due to expression of the *agr* operon and not because of bacterial replication, a microscopic study would have to be done. In the case of this study, however, this preliminary work served the purpose of establishing a functional assay, and the fact that the data matches that of the previous work carried out by Qazi *et al*. (2001) indicates that the bacteria are behaving in a similar way.

A further invasion assay using the *S. aureus* Δ*hla* strain indicated a role for α-haemolysin in endosomal escape, since the *S. aureus* Δ*hla* showed reduced growth levels as compared with the *S. aureus* RN6390 wildtype strain. Unfortunately, during this work, Jarry *et al*. (2008) documented a major role for α-haemolysin in endosomal escape. Due to this fact, coupled with the time restrictions of the study, the other mutants, including

the newly constructed β-haemolysin mutant, were not used in the cell invasion assay. However, the haemolysin mutants could hopefully be used in conjunction with the MRI reporter gene system in *in vivo* experiments to determine patterns of colonisation during infection within the mutants.

6.3: *In vivo* Evaluation of an *S. aureus* MRI Reporter in Mice

Preliminary *in vivo* experiments tracking bioluminescence demonstrated expression of the MRI reporter genes, suggesting that bacterioferritin should be successfully synthesised *in vivo*. MR imaging of the colonised tumours should therefore demonstrate contrast generated by the loading of iron onto the endogenous bacterioferritin. Bioluminescence was only detected from the *S. aureus* pUNK1 P_3-bfr-luxterm strain, however, on day 1, with light only being emittied from the inoculation site. It was thought that this could be due to the temporal nature of the expression of the P_3 promoter which, unlike the P_{S10} promoter, is not expressed constitutively, but rather in relation to bacterial cell numbers. This would be in line with observations made by Wright *et al*. (2005), who noted that a P_3-*lux* construct in *S. aureus* used *in vivo* in a mouse model demonstrated periods of expression and subsequent bioluminescence, followed by periods of reduced bioluminescence. This was attributed to the entry of the bacteria into stationary phase. Some 48-72 hours later, bioluminescence signals were recorded again, which were explained as a result of renewed bacterial growth.

Evaluation of the stability of the MRI reporter gene *in vivo* indicated that although plasmid loss occurred to quite a high level, it was obviously not significant enough to reduce the bioluminescence output to undetectable levels. However, for use in MRI, plasmid stability is vital to ensure maximal synthesis of BFR for optimal contrast.

As seen with other bacterial species including *E. coli*, *Listeria monocytogenes* and *Salmonella* species, *S. aureus* preferentially colonised the tumour, with bacteria also found in the liver (Riedel *et al*., 2007; Stritzker *et al*., 2007; Brader *et al*., 2008). The presence of bacteria in the liver could be due to failure of bacterial clearance by the liver. Colonisation of mice livers and spleens by a variety of pathogenic tumour targeting bacteria was observed by Stritzker *et al*. (2007), but reduction of bacterial load of *E. coli* Nissle 1917 in the spleen was achieved at lower bacterial loading levels. Different loading levels of *S. aureus* could therefore be trialed to determine an innoculum load which can achieve tumour colonisation without excessive liver colonisation.

Due to the relatively low levels of iron present in *S. aureus* samples as determined by ICP-MS, the tumours in this study were not scanned by MRI due to cost implications. However, colonisation of tumours by *S. aureus* seen in this study makes the mouse thigh tumour model ideal for development of this MRI reporter system since a specific area can be imaged using MRI, and parameters changed with relative reproducibility of the colonisation pattern in order to determine optimal conditions to achieve

MRI contrast. Once the MRI reporter system has be optimised for iron collection in *S. aureus*, MR imaging can be carried out to confirm the efficacy of this MRI reporter system for use in the monitoring of *S. aureus* disease processes.

Histology of one of the tumours from a mouse inoculated with *S. aureus* pUNK1 P_{S10}-bfr-luxterm revealed interesting information regarding the colonisation pattern of *S. aureus* within the tumour. This type of *ex vivo* technique is currently required for such detailed anatomical information to be gained. However, development of the MRI reporter system would abolish such a necessity, providing such information without the need for experimental animals to be sacrificed.

REFERENCES

Abdelnour, A., Arvidson, S., Bremell, T., Ryden, C., and Tarkowski, A. (1993) The accessory gene regulator (*agr*) controls *Staphylococcus aureus* virulence in a murine arthritis model. *Infect Immun* **61**: 3879-3885.

Ahmed, S., Meghji, S., Williams, R.J., Henderson, B., Brock, J.H. and Nair, S.P. (2001) *Staphylococcus aureus* fibronectin binding proteins are essential for internalization by osteoblasts but do not account for differences in intracellular levels of bacteria. *Infection and Immunity* **69**(5): 2872-2877.

Alexander, E.H., and Hudson, M.C. (2001) Factors influencing the internalization of *Staphylococcus aureus* and impacts on the course of infections in humans. *Appl Microbiol Biotechnol* **56**: 361-366.

Andrews, S.C., Arosio, P., Bottke, W., Briat, J.F., von Darl, M., Harrison, P.M., Laulhère, J.P., Levi, S., Lobreaux, S. and Yewdall, S.J. (1992) Structure, function and evolution of ferritins. *J Inorg Biochem* **47**(3-4): 161-174.

Armstrong-Buisseret, L., Cole, M.B. and Stewart, G.S.A.B. (1995) A homologue to the *Escherichia coli* alkyl hydroperoxide reductase AhpC is induced by osmotic upshock in *Staphylococcus aureus*. *Microbiology* **141**: 1655-1661.

Ausubel, F.M., Kingston, R.E., Moore, D.D., Seidman, J.G., Smith, J.A. and Struhl, K. (2000) *Current Protocols in Molecular Biology*: John Wiley & Sons, Inc.

Bauminger, E.R., Cohen, S.G., Dickson, D.P., Levy, A., Ofer, S. and Yariv, J. (1980) Mössbauer spectroscopy of *Escherichia coli* and its iron-storage protein. *Biochem Biophys Acta* **623**(2): 237-242.

Bayles, K.W., Wesson, C.A., Liou, L.E., Fox, L.K., Bohach, G.A., and Trumble, W.R. (1998) Intracellular *Staphylococcus aureus* escapes the endosome and induces apoptosis in epithelial cells. *Infect Immun* **66**: 336-342.

Berger-Bachi, B., and Rohrer, S. (2002) Factors influencing methicillin resistance in staphylococci. *Arch Microbiol* **178**: 165-171.

Bettegowda, C., Foss, C.A., Cheong, I., Wang, Y., Diaz, L., Agrawal, N., Fox, J., Dick, J., Dang, L.H., Zhou, S., Kinzler, K.W., Vogelstein, B. and Pomper, M.G. (2005) Imaging bacterial infections with radiolabeled 1-(2'-deoxy-2'-fluoro-β-D-arabinofuranosyl)-5-iodouracil. *PNAS* **102**(4): 1145-1150.

Bhakdi, S., and Tranum-Jensen, J. (1991) Alpha-toxin of *Staphylococcus aureus*. *Microbiol Rev* **55**: 733-751.

Blasberg, R. (2002) PET imaging of gene expression. *European Journal of Cancer* **38**(16): 2137-2146.

Brader, P., Stritzker, J., Riedl, C.C., Zanzonico, P., Cai, S., Burnazi, E.M., Ghani, E.R., Hricak, H., Szalay, A.A., Fong, Y. and Blasberg, R. (2008) *Escherichia coli* Nissle 1917 facilitates tumor detection by positron emission tomography and optical imaging. *Clin Cancer Res* **14**(8): 2295-2302.

Carrondo, M.A. (2003) Ferritins, iron uptake and storage from the bacterioferritin viewpoint. *EMBO* **22**(9): 1959-1968.

Chan, W.C., Coyle, B.J., and Williams, P. (2004) Virulence regulation and quorum sensing in staphylococcal infections: competitive AgrC antagonists as quorum sensing inhibitors. *J Med Chem* **47**: 4633-4641.

Chiancone, E., Ceci, P., Ilari, A., Ribacchi, F. And Stefanini, S. (2004) Iron and proteins for iron storage and detoxification. *Biometals* **17**: 197-202.

Clement, S., Vaudaux, P., Francois, P., Schrenzel, J., Huggler, E., Kampf, S., Chaponnier, C., Lew, D., and Lacroix, J.S. (2005) Evidence of an intracellular reservoir in the nasal mucosa of patients with recurrent *Staphylococcus aureus* rhinosinusitis. *J Infect Dis* **192**: 1023-1028.

Cohen, B., Dafni, H., Meir, G., Harmelin, A. and Neeman, M. (2005) Ferritin as an endogenous MRI reporter for noninvasive imaging of gene expression in C6 glioma tumors. *Neoplasia* **7**(2): 109-117.

Cohen, B., Ziv, K., Plaks, V., Israely, T., Kalchenko, V., Harmelin, A., Benjamin, L.E. and Neeman, M. (2007) MRI detection of transcriptional regulation of gene expression in transgenic mice. *Nature Medicine* **13**: 498-503.

Cooney, J., Kienle, Z., Foster, T.J., and O'Toole, P.W. (1993) The gamma-hemolysin locus of *Staphylococcus aureus* comprises three linked genes, two of which are identical to the genes for the F and S components of leukocidin. *Infect Immun* **61**: 768-771.

Courvalin, P. (2006) Vancomycin resistance in gram-positive cocci. *Clin Infect Dis* **42**(1): S25-34.

de Jonge, B.L., and Tomasz, A. (1993) Abnormal peptidoglycan produced in a methicillin-resistant strain of *Staphylococcus aureus* grown in the presence of methicillin: functional role for penicillin-binding protein 2A in cell wall synthesis. *Antimicrob Agents Chemother* **37**: 342-346.

Dinges, M.M., Orwin, P.M., and Schlievert, P.M. (2000) Exotoxins of *Staphylococcus aureus*. *Clin Microbiol Rev* **13**: 16-34.

Ellington, J.K., Reilly, S.S., Ramp, W.K., Smeltzer, M.S., Kellam, J.F., and Hudson, M.C. (1999) Mechanisms of *Staphylococcus aureus* invasion of cultured osteoblasts. *Microb Pathog* **26**: 317-323.

Fournier, B., and Philpott, D.J. (2005) Recognition of *Staphylococcus aureus* by the innate immune system. *Clin Microbiol Rev* **18**: 521-540.

Francis, K.P., Joh, D., Bellinger-Kawahara, C., Hawkinson, M.J., Purchio, T.F. and Contag, P.R. (2000) Monitoring bioluminescent *Staphylococcus aureus* infections in living mice using a novel *luxABCDE* construct. *Infection and Immunity* **68**(6): 3594-3600.

Garg, R.P., Vargo, C.J., Cui, X. and Kurtz Jr., D.M. (1996) A [2Fe-2S] protein encoded by an open reading frame upstream of the *Escherichia coli* bacterioferritin gene. *Biochemistry* **35**: 6297-6301.

Genove, G., DeMarco, U., Xu, H., Goins, W.F. and Ahrens, E.T. (2005) A new transgene reporter for *in vivo* magnetic resonance imaging. *Nature Medicine* **11**: 450-454.

Gilad, A.A., McMahon, M.T., Walczak P, Winnard, P.T. Jr., Raman, V., van Laarhoven, H.W., Skoglund, C.M., Bulte, J.W. and van Zijl, P.C.

(2007) Artificial reporter gene providing MRI contrast based on proton exchange. *Nat Biotechnol* **25**(2): 217-219.

Gillaspy, A.F., Hickmon, S.G., Skinner, R.A., Thomas, J.R., Nelson, C.L., and Smeltzer, M.S. (1995) Role of the accessory gene regulator (*agr*) in pathogenesis of staphylococcal osteomyelitis. *Infect Immun* **63**: 3373-3380.

Gossuin, Y., Muller, R.N. and Gillis, P. (2004) Relaxation induced by ferritin: a better understanding for an improved MRI iron quantification. *NMR Biomed* **17**: 427-432.

Grigg, J.C., Ukpabi, G., Gaudin, C.F.M. and Murphy, M.E.P. (2010) Structural biology of heme binding in the *Staphylococcus aureus* Isd system. *Journal of Inorganic Biochemistry* **104**(3): 341-348.

Haggar, A., Hussain, M., Lo¨nnies, H., Herrmann, M., Norrby-Teglund, A. and Flock, J. (2003) Extracellular adherence protein from *staphylococcus aureus* enhances internalization into eukaryotic cells. *Infection and Immunity* **71**(5): 2310-2317.

Hardy, J., Francis, K., DeBoer, M., Chu, P., Gibbs, K., and Contag, C. (2004) Extracellular replication of *Listeria monocytogenes* in the murine gall bladder. *Science* **303**: 851-853.

Harrison, P.M. and Arosio, P. (1996) The ferritins: molecular properties, iron storage function and cellular regulation. *Biochem Biophys Acta* **1275**(3): 161-203.

Hauck, C.R. and Ohlsen, K. (2006) Sticky connections: extracellular matrix protein recognition and integrin-mediated cellular invasion by *Staphylococcus aureus*. *Current Opinion in Microbiology* **9**(1): 5-11.

Herschman, H.R. (2003) Micro-PET imaging and small animal models of disease. *Current Opinion in Immunology* **15**: 378-384

Hickson, J. (2009) In vivo optical imaging: Preclinical applications and considerations. *Urologic Oncology* **27**: 295–297.

Hill, P.J., Stritzker, J., Scadeng, M., Haddad, D., Gburek, U., Jakob, P. and Szalay, A.A. *In vivo* transcriptional reporter genes for MRI. (Manuscript in preparation).

Hiramatsu, K., Cui, L., Kuroda, M., and Ito, T. (2001) The emergence and evolution of methicillin-resistant *Staphylococcus aureus*. *Trends Microbiol* **9**: 486-493.

Horsburgh, M.J., Clements, M.O., Crossley, H., Ingham, E. and Foster, S.J. (2001) PerR controls oxidative stress resistance and iron storage proteins and is required for virulence in *Staphylococcus aureus*. *Infect Immun* **69**(6): 3744–3754.

Hutchens, M. and Luker, G.D. (2007) Applications of bioluminescence imaging to the study of infectious diseases. *Cell Microbiol* **9**(10): 2315-2322.

Ilari, A., Stefanini, S., Chiancone, E. and Tsernoglou, D. (2000) The dodecameric ferritin from *Listeria innocua* contains a novel intersubunit iron-binding site. *Nature Structural Biology* **7**: 38-43.

Invitrogen MultiSite Gateway® Three-Fragment Vector Construction Kit Using Gateway® Technology to simultaneously clone multiple DNA fragments. *Invitrogen*.

Janzon, L., Lofdahl, S., and Arvidson, S. (1989) Identification and nucleotide sequence of the delta-lysin gene, *hld*, adjacent to the

accessory gene regulator (*agr*) of *Staphylococcus aureus*. *Mol Gen Genet* **219**: 480-485.

Jarry, T.M., Memmi, G. and Cheung, A.L. (2008) The expression of alpha-haemolysin is required for *Staphylococcus aureus* phagosomal escape after internalization in CFT-1 cells. *Cellular Microbiology* **10**(9): 1801-1814.

Jevon, M., Guo, C., Ma, B., Mordan, N., Nair, S.P., Harris, M., Henderson, B., Bentley, G., and Meghji, S. (1999) Mechanisms of internalization of *Staphylococcus aureus* by cultured human osteoblasts. *Infect Immun* **67**: 2677-2681.

Kahl, B.C., Goulian, M., van Wamel, W., Herrmann, M., Simon, S.M., Kaplan, G., Peters, G., and Cheung, A.L. (2000) *Staphylococcus aureus* RN6390 replicates and induces apoptosis in a pulmonary epithelial cell line. *Infect Immun* **68**: 5385-5392.

Kimura, N.T., Taniguchi, S., Aoki, K. and Baba, T. (1980) Selective localization and growth of *Bifidobacterium bifidum* in mouse tumours following intravenous administration. *Cancer Res* **40**: 2061-2068.

Kintarak, S., Whawell, S.A., Speight, P.M., Packer, S., and Nair, S.P. (2004) Internalization of *Staphylococcus aureus* by human keratinocytes. *Infect Immun* **72**: 5668-5675.

Kluytmans, J., van Belkum, A., and Verbrugh, H. (1997) Nasal carriage of *Staphylococcus aureus*: epidemiology, underlying mechanisms, and associated risks. *Clin Microbiol Rev* **10**: 505-520.

Kreiswirth, B.N., Lofdahl, S., Betley, M.J., O'Reilly, M., Schlievert, P.M., Bergdoll, M.S., and Novick, R.P. (1983) The toxic shock syndrome exotoxin structural gene is not detectably transmitted by a prophage. *Nature* **305**: 709-712.

Lammersa, A., Nuijtena, P.J.M. and H.E. Smitha, H.E. (1999) The fibronectin binding proteins of *Staphylococcus aureus* are required for adhesion to and invasion of bovine mammary gland cells. *FEMS Microbiol Letters* **180**(1): 103-109.

Li, X., Lindahl, L., Sha, Y. and Zengel, J.M. (1997) Analysis of the *Bacillus subtilis* S10 ribosomal protein gene cluster identifies two promoters that may be responsible for transcription of the entire 15-kilobase S10-*spc*-α cluster. *Journal of Bacteriology* **179**(22): 7046-7054.

Louie, A.Y., Hüber, M.M., Ahrens, E.T., Rothbächer, U., Moats, R., Jacobs, R.E., Fraser, S.E. and Meade, T.J. (2000) *In vivo* visualization of gene expression using magnetic resonance imaging. *Nature Biotechnology* **18**: 321-325.

Lyons, S.K. (2005) Advances in imaging mouse tumour models *in vivo*. *Journal of Pathology* **205**: 194-205.

Ma, H., Qi, X., Maitani, Y. and Nagai, T. (2007) Preparation and characterization of superparamagnetic iron oxide nanoparticles stabilized by alginate. *International Journal of Pharmaceutics* **333**: 177–186.

Maltezou, H.C., and Giamarellou, H. (2006) Community-acquired methicillin-resistant *Staphylococcus aureus* infections. *Int J Antimicrob Agents* **27**: 87-96.

McDowell, P., Affas, Z., Reynolds, C., Holden, M.T., Wood, S.J., Saint, S., Cockayne, A., Hill, P.J., Dodd, C.E., Bycroft, B.W., Chan, W.C., and Williams, P. (2001) Structure, activity and evolution of the group I thiolactone peptide quorum-sensing system of *Staphylococcus aureus*. *Mol Microbiol* **41**: 503-512.

Menzies, B.E., and Kourteva, I. (1998) Internalization of *Staphylococcus aureus* by endothelial cells induces apoptosis. *Infect Immun* **66**: 5994-5998.

Novick, R. (1967) Properties of a cryptic high-frequency transducing phage in *Staphylococcus aureus*. *Virology* **33**: 155-166.

Novick, R.P. (2003) Autoinduction and signal transduction in the regulation of staphylococcal virulence. *Molecular Microbiology* **48**(6): 1429-1449.

Novick, R.P. and Jiang, D. (2003) The staphylococcal saeRS system coordinates environmental signals with agr quorum sensing. *Microbiology* **149**: 2709-2717.

Peng, H.L., Novick, R.P., Kreiswirth, B., Kornblum, J., and Schlievert, P. (1988) Cloning, characterization, and sequencing of an accessory gene regulator (*agr*) in *Staphylococcus aureus*. *J Bacteriol* **170**: 4365-4372.

Perehinec, T.M., Qazi, S.N., Gaddipati, S.R., Salisbury, V., Rees, C.E.D. and Hill, P.J. (2007) Construction and evaluation of multisite recombinatorial (Gateway) cloning vectors for Gram-positive bacteria. *BMC Mol Biol* **8**: 80-91.

Qazi, S.N., Counil, E., Morrissey, J., Rees, C.E., Cockayne, A., Winzer, K., Chan, W.C., Williams, P., and Hill, P.J. (2001) *agr* expression precedes escape of internalized *Staphylococcus aureus* from the host endosome. *Infect Immun* **69**: 7074-7082.

Qazi, S.N., Harrison, S.E., Self, T., Williams, P., and Hill, P.J. (2004) Real-time monitoring of intracellular *Staphylococcus aureus* replication. *J Bacteriol* **186**: 1065-1077.

Qazi, S.N., Perehinec, T.M., Fray, R.G., Williams, P. and Hill, P.J. Mutagenesis using multisite recombination and irreversible marker excision with PhiC31 integrase to investigate the intracellular lifestyle of *Staphylococcus aureus*. (Manuscript in preparation).

Ray, P., De, A., Min, J.J., Tsien, R.Y. and Gambhir, S.S. (2004) Imaging tri-fusion multimodality reporter gene expression in living subjects. *Cancer Res* **64**: 1323-1330.

Reilly, S.S., Hudson, M.C., Kellam, J.F., and Ramp, W.K. (2000) *In vivo* internalization of *Staphylococcus aureus* by embryonic chick osteoblasts. *Bone* **26**: 63-70.

Riedel, C.U., Monk, I.R., Casey, P.G., Morrissey, D., O'Sullivan, G.C., Tangney, M., Hill, C. and Gahan, C.G.M. (2007) Improved luciferase tagging system for *Listeria moncytogenes* allows real-time monitoring *in vivo* and *in vitro*. *Appl Environ Microbiol* **73**: 3091-3094.

Rygus, T., Scheler, A., Allmansberger, R. and Hillen, W. (1991) Molecular cloning, structure, promoters and regulatory elements for

transcription of the *Bacillus megaterium* encoded regulon for xylose utilization. *Arch Microbiol* **155**: 535-542.

Schito, G.C. (2006) The importance of the development of antibiotic resistance in *Staphylococcus aureus*. *Clin Microbiol Infect* **12**(1): 3-8.

Serganova, I. and Blasberg, R.G. (2006) Multi-modality molecular imaging of tumours. *Hematol Oncol Clin N Am* **20**(6): 1215-1248.

Shallcross, L.J., Williams, K., Hopkins, S., Aldridge, R.W., Johnson, A.M. and Hayward, A.C. (2009) Panton Valentine Leukocidin associated Staphylococcal Disease: A Cross Sectional Study at a London Hospital, England. *Clin. Microbiol. Infect.* [Epub ahead of print].

Shompole, S., Henon, K.T., Liou, L.E., Dziewanowska, K., Bohach, G.A., and Bayles, K.W. (2003) Biphasic intracellular expression of *Staphylococcus aureus* virulence factors and evidence for Agr-mediated diffusion sensing. *Mol Microbiol* **49**: 919-927.

Shu, X., Royant, A., Lin, M.Z., Aguilera, T.A., Lev-Ram, V., Steinbach, P.A. and Tsien, R.Y. (2009) Mammalian expression of infrared fluorescent proteins engineered from a bacterial phytochrome. *Science* **324**(5928): 804-807.

Smith, R.S., and Iglewski, B.H. (2003) *Pseudomonas aeruginosa* quorum sensing as a potential antimicrobial target. *J Clin Invest* **112**: 1460-1465.

Stillman, T.J., Hempstead, P.D., Artymiuk, P.J., Andrews, S.C., Hudson, A.J., Treffry, A., Gues, J.R. and Harrison, P.M. (2001) The high-resolution X-ray crystallographic structure of the ferritin (EcFtnA) of

Escherichia coli; comparison with human H ferritin (HuHF) and the structures of the Fe^{3+} and Zn^{2+} derivatives. *J Mol Biol* **307**(2): 587-603.

Stritzker, J., Weibel, S., Hill, P.J., Oelschlager, T.A., Goebel, W. and Szalay, A.A. (2007) Tumour-specific colonization, tissue distribution, and gene induction by probiotic *Escherichia coli* Nissle 1917 in live mice. *International Journal of Medical Microbiology* **297**(3): 151-162.

Taylor, A.G., and Bernheimer, A.W. (1974) Further characterization of staphylococcal gamma-hemolysin. *Infect Immun* **10**: 54-59.

Vymazal, J., Brooks, R.A., Bulte, J.W.M., Gordon, D. and Aisen, P. (1998) Iron uptake by ferritin: NMR relaxometry studies at low iron loads. *J Inorg Biochem* **71**(3-4): 153-157.

Ward, K.M., Aletras, A.H. and Balaban, R.S. (2000) A new class of contrast agents for MRI based on proton chemical exchange dependent saturation transfer (CEST). *Journal of Magnetic Resonance* **143**: 79–87.

Wesson, C.A., Liou, L.E., Todd, K.M., Bohach, G.A., Trumble, W.R., and Bayles, K.W. (1998) *Staphylococcus aureus* Agr and Sar global regulators influence internalization and induction of apoptosis. *Infect Immun* **66**: 5238-5243.

Wiles, S., Clare, S., Harker, J., Huett, A., Young, D., Dougan, G., and Frankel, G. (2004) Organ specificity, colonization and clearance dynamics *in vivo* following oral challenges with the murine pathogen citrobacter rodentium. *Cell Microbiol* **6:** 963-972.

Wright, J.S., Jin, R. and Novick, R.P. (2005) Transient interference with staphylococcal quorum sensing blocks abscess formation. *PNAS* **102**(5): 1691-1696.

Yang, M., Baranov, E., Moossa, A.R., Penman, S. and Hoffman, R.M. (2000) Visualizing gene expression by whole-body fluorescence imaging. *Proc Natl Acad Sci USA* **97**: 12278-12282.

Yariv, J., Kalb, A.J., Sperling, R., Bauminger, E.R., Cohen, S.G. and Ofer, S. (1981) The composition and the structure of bacterioferritin of *Escherichia coli*. *Biochem J* **197**: 171-175.

Yarwood, J.M., and Schlievert, P.M. (2003) Quorum sensing in *Staphylococcus* infections. *J Clin Invest* **112**: 1620-1625.

Zhao, M., Yang, M., Baranov, E., Wang, X., Penman, S., Moossa, A.R. and Hoffman, R.M. (2001) Spatial–temporal imaging of bacterial infection and antibiotic response in intact animals. *PNAS* **98**(17): 9814-9818.

Zurkiya, O., Chan, A.W.S. and Hu, X. (2008) MagA is sufficient for producing magnetic nanoparticles in mammalian cells, making it an MRI reporter. *Magnetic Resonance in Medicine* **59**: 1225-1231.